2 p(mix)

NASA CR-122382

DEVELOPMENT OF IMPROVED PYROELECTRIC DETECTORS

Measurements of pyroelectric material characteristics and FET characteristics

(NASA-CR-122382) DEVELOPMENT OF IMPROVED PYROELECTRIC DETECTORS. MEASUREMENTS OF PYROELECTRIC MATERIAL CHARACTERISTICS AND FET S. Weiner, et al (Barnes Engineering Co.) 29 Feb. 1971 87 p CSCL 14B G3/14

N72-21427

Unclas 24395

Seymour Weiner, Henry P. Beerman, and Frank Schwarz

Barnes Engineering Company, Inc.

30 Commerce Road

Stamford, Conn. 06904

February 29, 1971

Quarterly Technical Report for Period November 1971 - February 1972

Prepared for

GODDARD SPACE FLIGHT CENTER

Greenbelt, Maryland 20771

NATIONAL AERONAUTICS AND SPACE ADMINISTRATION

CAT 14

1. Report No.	2. Government Accession No.	3. Recipient's Catalog No.
4. Title and Subtitle Development of Improved Pyroelectric Detectors		5. Report Date Feb. 29, 1972 6. Performing Organization Code
7. Author(s) Seymour Weiner, Henry Beerman, Frank Schwarz		8. Performing Organization Report No. BEC 2064QR2
9. Performing Organization Name and Address Barnes Engineering Company 30 Commerce Rd. Stamford, Conn. 06904		10. Work Unit No. 11. Contract or Grant No. NAS5-21655
12. Sponsoring Agency Name and Address National Aeronautics & Space Administration Goddard Space Flight Center Greenbelt, Maryland 20771		13. Type of Report and Period Covered Quarterly Technical Nov. 23, 1971 to Feb. 22, 1972 14. Sponsoring Agency Code

15. Supplementary Notes

Andrew W. McCulloch, Code 652, Tech. Monitor

16. Abstract

The object of this program is to improve the detectivity of the pyroelectric detector with the ultimate goal of operation at or near the temperature-noise limit. Two general areas of investigation are undertaken. The first is to improve responsivity through the use of new materials. The second is directed toward reduction of noise and will be effected with improved field effect transistor characteristics, and improved electroding of the pyroelectric material.

The review of the literature on pyroelectric materials continues. From this, several materials have already been selected for investigation, and several were tested.

FET's are being obtained from various manufacturers, evaluated, and selected units tested for evaluation of characteristics critical to their use as preamplifiers with pyroelectric detectors.

17. Key Words (Selected by Author(s))	18. Distribution Statement
Infrared Detectors Pyroelectricity Ferroelectricity	

19. Security Classif. (of this report)	20. Security Classif. (of this page)	21. No. of Pages	22. Price*
Unclassified	Unclassified	75	

*For sale by the Clearinghouse for Federal Scientific and Technical Information, Springfield, Virginia 22151.

PREFACE

The object of this program is to improve the detectivity of the pyroelectric detector with the ultimate goal of operation at or near the temperature-noise limit.

During the second phase of this program the literature search for new pyroelectric detector materials has been continued and all new data has been included in the table of pyroelectric materials characteristics.

Equipment for the determination of dielectric constant, loss tangent, and pyroelectric coefficient has been completed, and measurements of these parameters as functions of temperature have been started. The use of gamma irradiation from a cobalt 60 source on TGS and DTGS appears as a promising method to obtain "locked in" polarization (i.e., no repoling required after having gone through the Curie point).

Transmittance and reflectance measurements have been continued over a range of 0.25μ to 40μ.

Crystal growth from aqueous solution is continuously proceeding on such materials as DTGS, doped TGS, $NaNO_2$, and glucuronolactone.

Measurement of current noise, short circuit noise, transconductance, and input capacitance proceeded on eight different FET types in order to select a type with the lowest possible gate leakage (I_{GSS}) and short circuit noise, thus leading to an improvement in the sensitivity of the detector-preamplifier system.

Project accomplishments to date are consistant with the objectives of the program.

TABLE OF CONTENTS

LIST OF ILLUSTRATIONS

LIST OF TABLES

Section 1.0 INTRODUCTION

The second phase of this program has been carried out over a three month period beginning Nov. 23, 1971 and ending February 22, 1972.

The goals of the second phase were as follows:

1. Continue the literature search for new pyroelectric materials, and update the compiled data on pyroelectric materials characteristics started in the first phase.
2. Continue the transmittance and reflectance measurements of 1 mm and 0.1mm thick pyroelectric materials not previously measured.
3. Complete the test equipment for the measurement of dielectric constant and loss tangent as functions of frequency and temperature. The equipment that would permit determination of the pyroelectric coefficient was also to be completed and the measurements made. If time permitted, actual detector elements were to be processed from the most promising detector materials, and responsivity, noise, detectivity, and spectral response measurements were to be carried out.
4. Determine the effect of gamma and U-V irradiation on TGS and DTGS as well as the effects of Cu^{++} and Cr^{+++} doping. These techniques were to lead to "locked-in" polarization of single domains.
5. Measurements of sample FET's were to be started.

Most of the goals were achieved and each is discussed in turn in the remainder of this report. Any difficulties that arose causing delays in some goals are also mentioned.

Search 2.0 LITERATURE SEARCH

Since the first quarter's efforts were concentrated largely on a literature search pertaining to pyroelectric detector materials, very few additional materials were encountered during the second quarter. The new ferroelectric materials are lead titanate, lanthanum-doped lead zirconate titanate (PLZT), α -alanine doped TGS, lithium formate and polyvinyl fluoride. Data commensurate with the data headings in Table A-1 in the first quarterly report were found only for $PbTiO_3$ and PLZT and are shown in the updated Table A-1.

Yamaka et al (Y4) claim a D* (500°K, 10Hz, 1) of $\sim 8 \times 10^8$ cm cps $^{1/2}$ w $^{-1}$ for $PbTiO_3$. The figure of merit for responsivity of $PbTiO_3$ appears to be down a factor of five from DTGS. For $PbTiO_3$ to have a figure of merit for detectivity $(d P_s/dT)\rho^{1/2} c^{-1}$ even equivalent to that for TGS or DTGS, the A-C shunt resistance ρ at 1 KHz would have to be $\sim 1 \times 10^{10}$ ohms, which is equivalent to a loss tangent of $\sim 1 \times 10^{-3}$ at 1 KHz. Until such values for ρ and tan δ are actually measured, it appears questionable whether the indicated D* is valid. An attempt will be made to obtain single crystal $PbTiO_3$. However, according to Dr. A. M. Glass of Bell Laboratories, $PbTiO_3$ is not commercially available, is generally only grown in approximately 3 x 3 x 1 mm twinned crystals from a flux, and must be detwinned by observing under a microscope while annealing and applying pressure.

Lock (L5) has shown that "locked in" polarization in TGS (and therefore presumably also in DTGS) may be obtained by doping the crystal with 1% α-alanine during growth from aqueous solution (ATGS hereafter). The loss tangent is apparently reduced since the conductivity of ATGS is reported an order of magnitude lower than the conductivity of TGS. Dielectric constant of ATGS is also reduced. A D* of 2×10^9 cm cps $^{1/2}$ w $^{-1}$ is claimed for a 0.5 x 0.5 mm detector below 10 Hz.

Liu et al (L4) claim a D* (500°K, 10Hz, 1) of ~3 x 10^8 cm cps $^{1/2}$ w^{-1} for PLZT 6.5/65/35. Some material samples will be requested from Honeywell.

Phelan et at (P4) have reported polyvinyl fluoride as being a promising low cost, large area pyroelectric detector material. Additional data on pyroelectric polymer films are discussed by Furukawa et at (F3).

Samples of lithium formate and polyvinyl fluoride were obtained, and the results of measurements are discussed in the following sections.

Additional publications on previously known pyroelectric materials were examined but yielded no new parameters.

Section 3.0 MATERIALS UNDER INVESTIGATION

In the first quarterly report it was stated that the following materials were on hand:

1. Triglycine sulfate (TGS).
2. Deuterated triglycine sulfate (DTGS).

   DTGS is TGS whose hydrogen atoms (except in the CH_2 group) are replaced by deuterium. Only 11 out of 17 hydrogen atoms can be substituted by deuterium and a crystal of DTGS made from three or more recrystallizations of TGS in D_2O will be considered 100% or fully deuterated (B3).
3. Lithium sulfate ($Li_2SO_4 \cdot H_2O$).
4. TGS with approximately 15% Se.

Putley (P2) originally designated such a crystal as "TGS/Se(~15% Se)". A single crystal was grown from a solution containing $TGS_{0.85} \cdot TGSe_{0.15}$. The resulting crystal was analyzed* for selenium (0.39%), and from these results the composition of the solid crystal was calculated as $TGS_{0.98} \cdot TGSe_{0.02}$.

Analogous to the results for TGS-TGFB discussed by Brezina et al (B6), the composition of the starting solution must be $TGS_{0.5}\ TGSe_{0.5}$ in order to arrive at a solid with the approximate composition $TGS_{0.85} \cdot TGSe_{0.15}$. A new crystal will be grown.

5. $TGS_{0.88} \cdot TGFB_{0.12}$.

This crystal was originally started from a liquid composition $TGS_{0.5} \cdot TGFB_{0.5}$. The resulting crystal was analyzed* for fluorine. On the basis of 2.72%F one obtains $TGS_{0.885} \cdot TGFB_{0.115}$ which is in agreement with the results of Brezina et al (B6).

6. Strontium barium niobate, SBN, $(Sr_{1-x}\ Ba_xNb_2O_6)$.

The material on hand was $(Sr_{0.75}Ba_{0.25}Nb_2O_6)$. After making trans-

*Bridgeport Testing Laboratory, Bridgeport, Ct.

mittance and reflectance measurements, on the original thickness (1.5 mm) material, the crystal slice was accidentally ruined while attempting to lap to 0.1 mm. A new slice has been ordered from Crystal Technology, Inc.

7. Lithium tantalate ($LiTa_2O_3$).
8. Polyvinylidene fluoride, 19μ thick.

Additional materials obtained for investigation during the second quarter were:

9. TGS and DTGS slices irradiated with 1Mr* and 2Mr gamma rays from a cobalt-60 source at NASA, Greenbelt, Md., after poling the electroded slices. Yurin et at (Y2), Yurin & Zheludev (Y3) and Chynoweth (C8) have previously shown that the spontaneous polarization could be stabilized (i.e., locked in) by gamma irradiation.
10. Lithium formate.
11. Polyvinyl fluoride film, Dupont "Tedlar", 50μ thick.
12. Attempted to grow sodium nitrite ($NaNO_2$) crystal from an aqueous solution. After one month's effort, only a polycrystalline mass resulted whose individual rhombic single crystals turned cloudy overnight. Apparently, a hydrate had been grown from solution and the crystal subsequently dehydrated. An order had been previously placed with Isomet, Inc. to supply a single crystal $NaNO_2$, grown from the melt, but it has not yet been received.
13. A communication with Dr. Putley of the Royal Radar Establishment, England, provided more information on glucuronolactone, so that this material (in powder form) has been ordered from Eastman Kodak and will subsequently be grown from aqueous solution at Barnes Engineering Co.
14. α -Alanine is on order so that ATGS crystal growth may be started shortly.

*Megaroentgen

Section 4 MEASUREMENTS

4.1 TRANSMITTANCE AND REFLECTANCE

All 1 mm thick pyroelectric materials for which transmittance and reflectance data had been reported in the first report were to be lapped down to 0.1mm and the transmittance measurements from 0.2 to 40μ repeated. Difficulty was encountered in handling the unsupported thin crystalline material of sufficient area to fill the beam dimension of the spectrometer. Transmittance for 0.1 mm thick TGS and DTGS from 0.2 to 40μ is in Appendix B, and may be compared with 1 mm transmittance data in the first report. A slight reduction (rather than increase) seen in the maximum transmittance from 0.25 to 0.40 is probably due to some scattering off the front surface. The 0.1 mm thick samples of $Li_2SO_4.H_2O$ and TGFB cracked repeatedly during handling, and the data below 1.5μ for the resulting small areas were unsatisfactory. Time permitting, the measurements on 0.1 mm thick $Li_2SO_4.H_2O$ and TGFB will be repeated. It will require the design of a single fixture that holds the sample both during lapping and insertion into the spectrometer. Transmittance and reflectance for 1 mm thick $LiTaO_3$, 1.5mm $Sr_{0.75}Ba_{0.25}Nb_2O_6$ and 15μ thick polyvinyl fluoride are also in Appendix B.

Since the spectral characteristics of 1 mm thick $TGS_{0.88}TGFB_{0.12}$ did not seem to vary from that of 1 mm thick TGS (first quarter report) it was felt that the additional transmittance measurements for 0.1mm $TGS_{0.88}$. $TGFB_{0.12}$ were not warranted.

On attempting to record spectral data for the new sample of lithium formate, it was noted that the portion of the crystal traversed by the beam of the spectrometer turned cloudy. The measurement was therefore considered invalid. Only if some further preliminary data on lithium formate from the supplier (Lasermetrics, Inc.) or the literature is found that might be encourag-

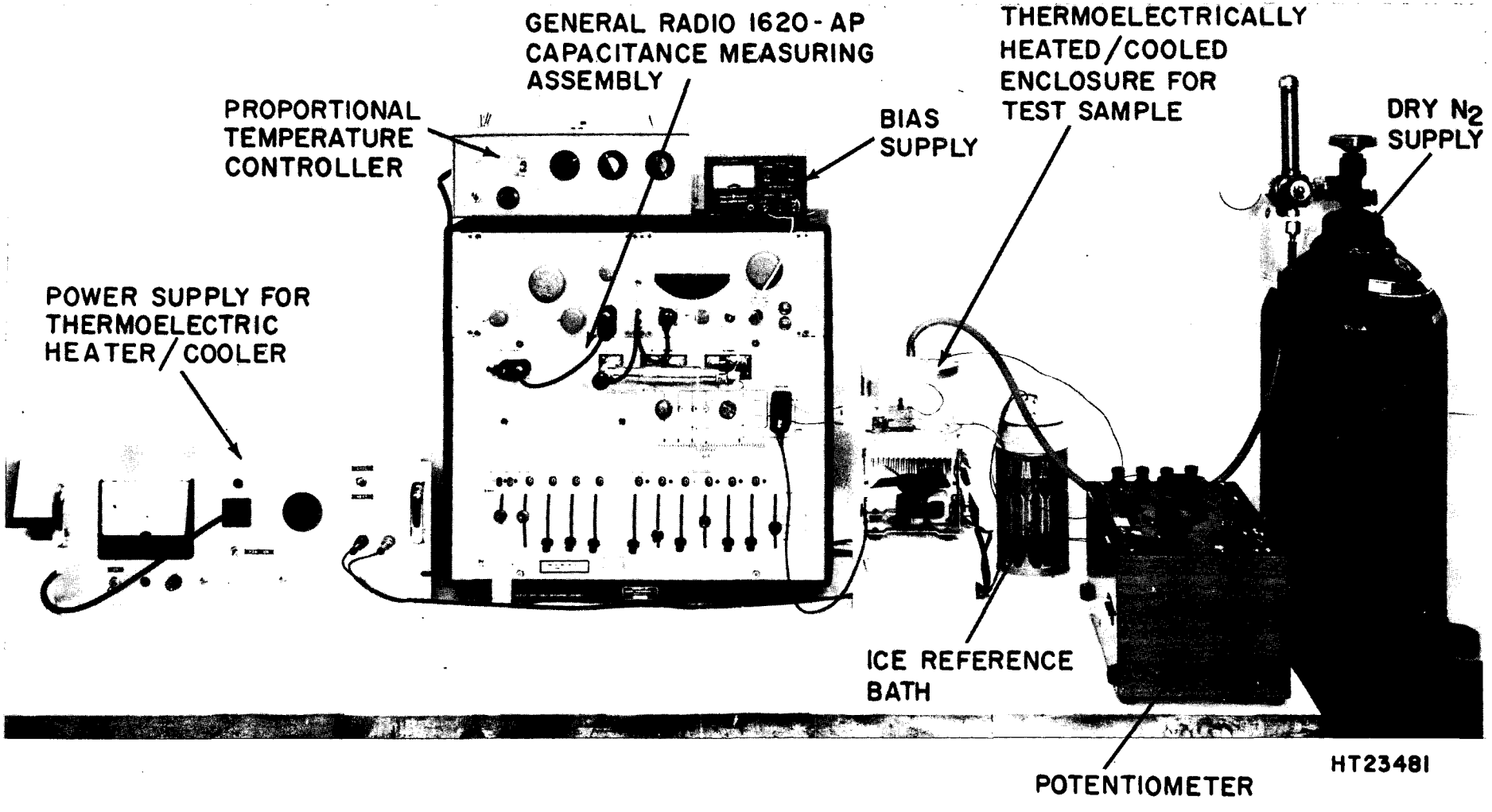

Figure 4.1 TEST EQUIPMENT FOR DETERMINATION OF CAPACITANCE AND LOSS TANGENT AS FUNCTIONS OF TEMPERATURE AND FREQUENCY

ing will it be further considered as a possible I-R detector.

4.2 DIELECTRIC CONSTANT AND LOSS TANGENT

4.2.1 Equipment (Figure 4-1)

The equipment consists of a General Radio Type 1620-AP capacitance measuring assembly whose oscillator and detector permit capacitance and loss tangent measurements from 20Hz to 100KHz. In addition there is a Hewlett-Packard 0-50 VDC power supply that proved insufficient to maintain a suitable field strength (5KV/cm) for the 1mm thick samples, so that it became necessary to assemble a battery supply. A thermoelectrically heated or cooled copper block into which the test sample is inserted was automatically controlled by a YSI* Type 72 proportional temperature controller between 0° C and approximately 80° C. Below 0° C only a fixed current was supplied to the thermoelectric cooler until a steady state was achieved. The temperature was monitored in all cases with an Iron/Constantan thermocouple. Below ambient temperature the thermoelectrically cooled test sample was flushed with dry nitrogen to prevent moisture condensation.

4.2.2 Measurement of Dielectric Constant and Loss Tangent

The dielectric constant and loss tangent of TGS, DTGS, gamma irradiated TGS and DTGS, and $Li_2SO_4.H_2O$ have been measured over a temperature range from approximately -30° C to 80° C for frequencies of 50Hz, 100Hz, 1 KHz, 10KHz and 100KHz, and are plotted in Figures 4-2 through 4-10 for generally 100, 1K and 10KHz. While the original intent was to measure the dielectric constant and loss tangent down to 20Hz, the capacitance bridge proved to be rather insensitive below 100Hz.

Since all apparent loss tangent readings on the capacitance bridge have to be multiplied by the frequency in kilohertz in order to arrive at the true loss tangent, one is limited to a maximum loss tangent reading of

*Yellow Springs Instrument Co.

0.11 at 100Hz, 0.055 at 50Hz, and 0.022 at 20Hz. Even at 50Hz it proved somewhat difficult to achieve balance of the capacitance bridge. The results at 50Hz generally duplicated the measurement obtained at 100Hz but with lower precision. Therefore, the lowest frequency for which results were plotted is 100Hz. The results for 100KHz were actually outside of the scope of this program. Only in the case of $Li_2SO_4.H_2O$, where the results at 100KHz differed materially from those at lower frequencies, have they been plotted. The electroded samples were always 5 x 5 mm in area and approximately 1 mm thick. For non-irradiated TGS and DTGS, a 5 KV/cm external bias was arbitrarily applied during the measurements to keep the samples poled. This corresponds to about 12V for a typical pyroelectric detector element. The dielectric constant and loss tangent are functions of the poling voltage, and the dielectric constant is also a function of sample thickness - especially at the Curie point (Sekido and Mitsui (S12) and Chynoweth (C5)). The actual Curie point is also shifted slightly to higher temperatures with increasing bias.

Each material will be discussed in turn; the following comments pertain to all the measured materials.

While the use of relatively large (5 x 5 x 1 mm) samples leads to smaller errors as far as the determination of their physical size is concerned (used to calculate the dielectric constant from the measured capacitance), it nevertheless leads to other difficulties. In the case of materials with a low dielectric constant (≤ 30), the entire capacitance for a 5 x 5 x 1mm sample is only ≤ 6.6 pf, which is small compared to the 7.7 pf of the leads and shielded input of the capacitance bridge. Great care had to be taken to obtain proper balance of the bridge whenever a low capacitance with a low loss tangent was measured, particularly at frequencies of 100Hz and below.

The rate of changing the temperature (dT/dt) of the sample being measured - to arrive at a new and constant temperature - materially affects the rate at which one can measure the new capacitance and loss tangent.

A large dT/dt causes a sufficiently high charge which can partially depole the sample. Particularly as one drops further and further below the Curie point, T_C, the 5KV/cm becomes less and less sufficient to repole the sample to the maximum for that field strength. Thus, above T_C and down to T_C-5°C, capacitance and loss tangent measurements are made immediately. At T_C-25°C it may take 1-2 hours to obtain the maximum possible poling due to the 5 KV/cm bias, while at T_C-75°C (approximately -25°C for TGS) it may take overnight. Maximum poling has been achieved when the capacitance and loss tangent reach minimum values for that temperature.

Conversely, it is expected that materials like $LiTeO_3$ (T_C=660°C) and $PbTiO_3$ (T_C = 492°C) should not depole in the temperature range -30° to 80°C due to a rapid change in temperature since they were originally poled at a much higher temperature, and it would take considerably higher field strength to switch these ferroelectrics several hundred degrees below their Curie point.

It was noted that measurements of the loss tangent at 100KHz proved to be a much more sensitive indicator of the degree of poling than lower frequency measurements. Only when a minimum tanδ was obtained could one be sure of having achieved full poling (i.e., minimum capacitance).

Another source of trouble: when using 1 mm thick material that has been directly attached to the steel header with the feed-through pins (Figure 4-3 of the first quarterly report), cracking of the sample can occur easily if the entire specimen is heated or cooled too rapidly. To minimize the effect due to the difference in thermal expansion between the steel header and the pyroelectric materials, 1/2 mil mylar has been interposed between them in some of the more recent samples. While not eliminating the problem of cracking if the sample temperature is changed too rapidly, it reduces the likelihood of breakage.

4.2.2.1 TGS

The dielectric constant of TGS as a function of temperature is plotted in Figure 4-2A, and the loss tangent as a function of temperature

TGS, DIELECTRIC CONSTANT (ϵ_b) AT 1KHz VS. TEMPERATURE. (A) 5 KV/cm BIAS DURING MEASUREMENT, (B) TGS POLED WITH 9 KV/cm, IRRADIATED WITH 2 Mr GAMMA RAYS. NO BIAS DURING MEASUREMENT.

Figure 4.2

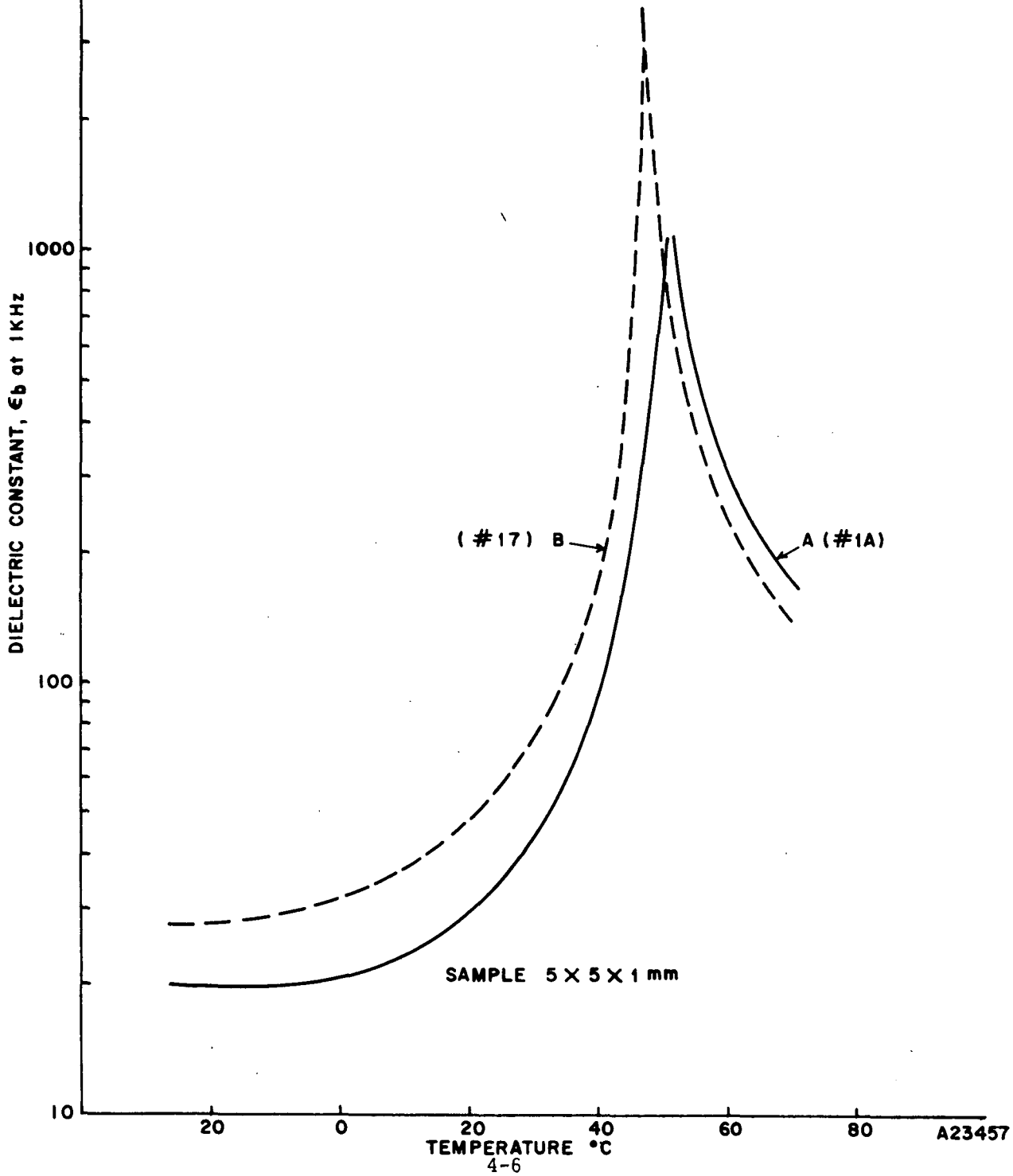

in Figure 4-3. At 5Kv/cm bias the Curie point T_c for TGS was found to be 51°C.

TGS that had originally been poled with 9KV/cm (above 900V for a 1mm sample, arcing occurred in air) and then irradiated with 2Mr of cobalt-60 gamma radiation has its dielectric constant as a function of temperature shown in Figure 4-2B. No bias was used during measurement. T_c was found to be 46.5°C. Loss tangent for irradiated TGS is shown in Figure 4-4.

Deviations of the dielectric constant at 100Hz and 10KHz from that shown at 1 KHz was always less than ±3%, with the maximum deviation occurring at T_c and at the minimum temperatures shown. The loss tangent for the irradiated TGS was approximately twice that for non-irradiated but biased TGS at ambient temperature. This seems to indicate that the irradiated TGS had been insufficiently poled prior to irradiation. Since 1mm thick TGS samples cannot be fully poled at ambient temperature without arcing in air, subsequent samples will have to be thinner to allow full poling with the required 15 KV/cm field. Alternatively, the thick sample will have to be immersed in an oil bath during poling (as is done with PZT ceramic discs).

The irradiated TGS clearly showed its "locked-in" polarization in that after exceeding T_c it reverted at once to the ferroelectric mode below T_c with the original values for dielectric constant and loss tangent without additional poling.

4.2.2.2 DTGS

Deuterated TGS has its dielectric constant vs. temperature plotted in Figure 4-5. (Somewhat lower values were obtained for a 0.36 mm thick sample (No. 18B) than for a 1 mm thick sample (No. 18). The Curie point was found to be 62.4°C for a 5 KV/cm bias.

Since Itoh and Mitsui (I4) have claimed that the dielectric constant of TGS did not decrease monotonically but would show a peak below 0°C,

LOSS TANGENT OF TGS (# 1A) VS. TEMPERATURE. 5KV/cm BIAS.
SAMPLE 5×5×1mm

Figure 4.3

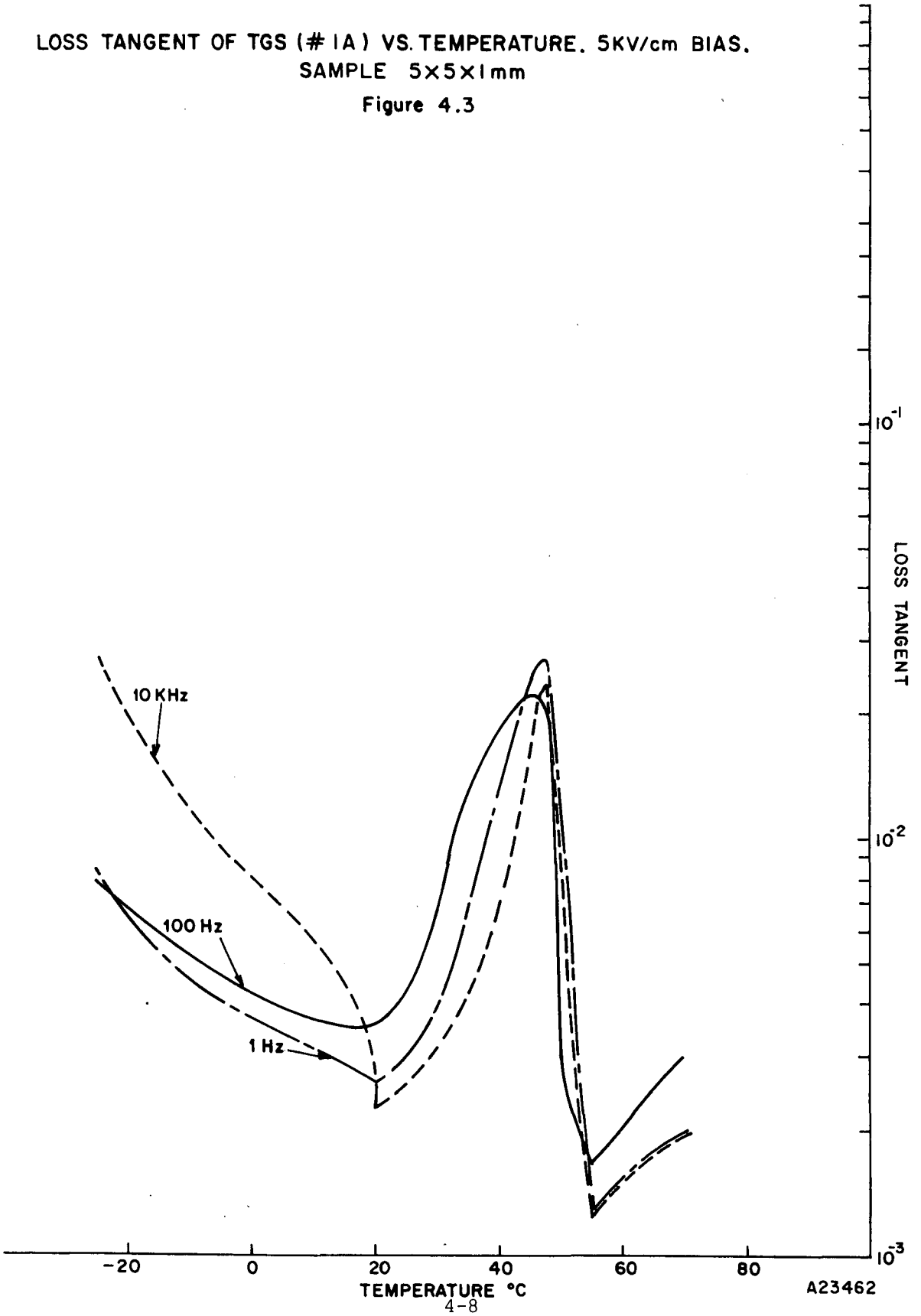

LOSS TANGENT OF 9KV/cm POLED PLUS 2 Mr GAMMA IRRADIATED TGS (#17) VS. TEMPERATURE. NO BIAS DURING MEASUREMENT. SAMPLE 5X5X1mm

Figure 4.4

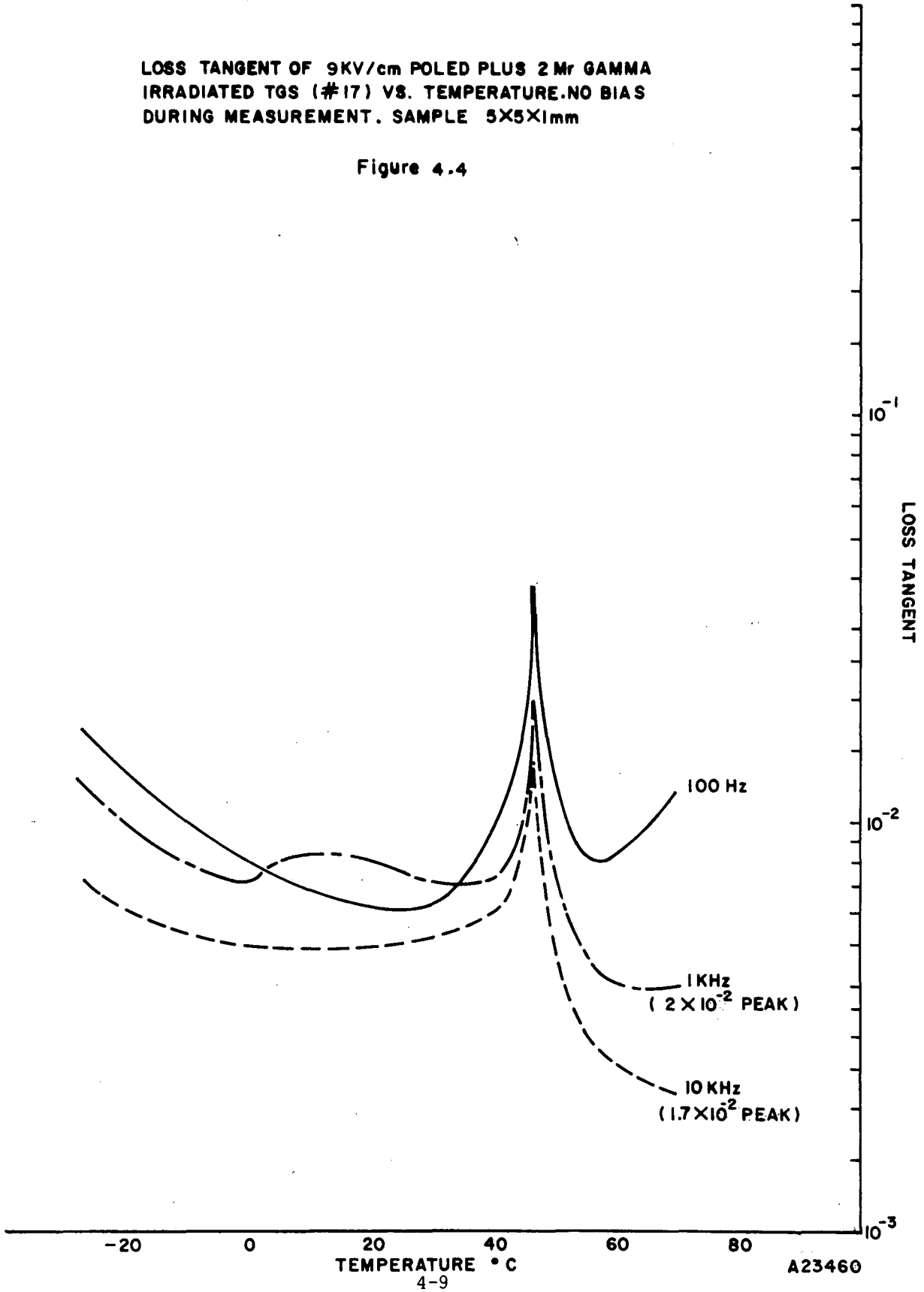

DTGS; DIELECTRIC CONSTANT (ϵ_b) AT 1KHz VS. TEMPERATURE

Figure 4.5

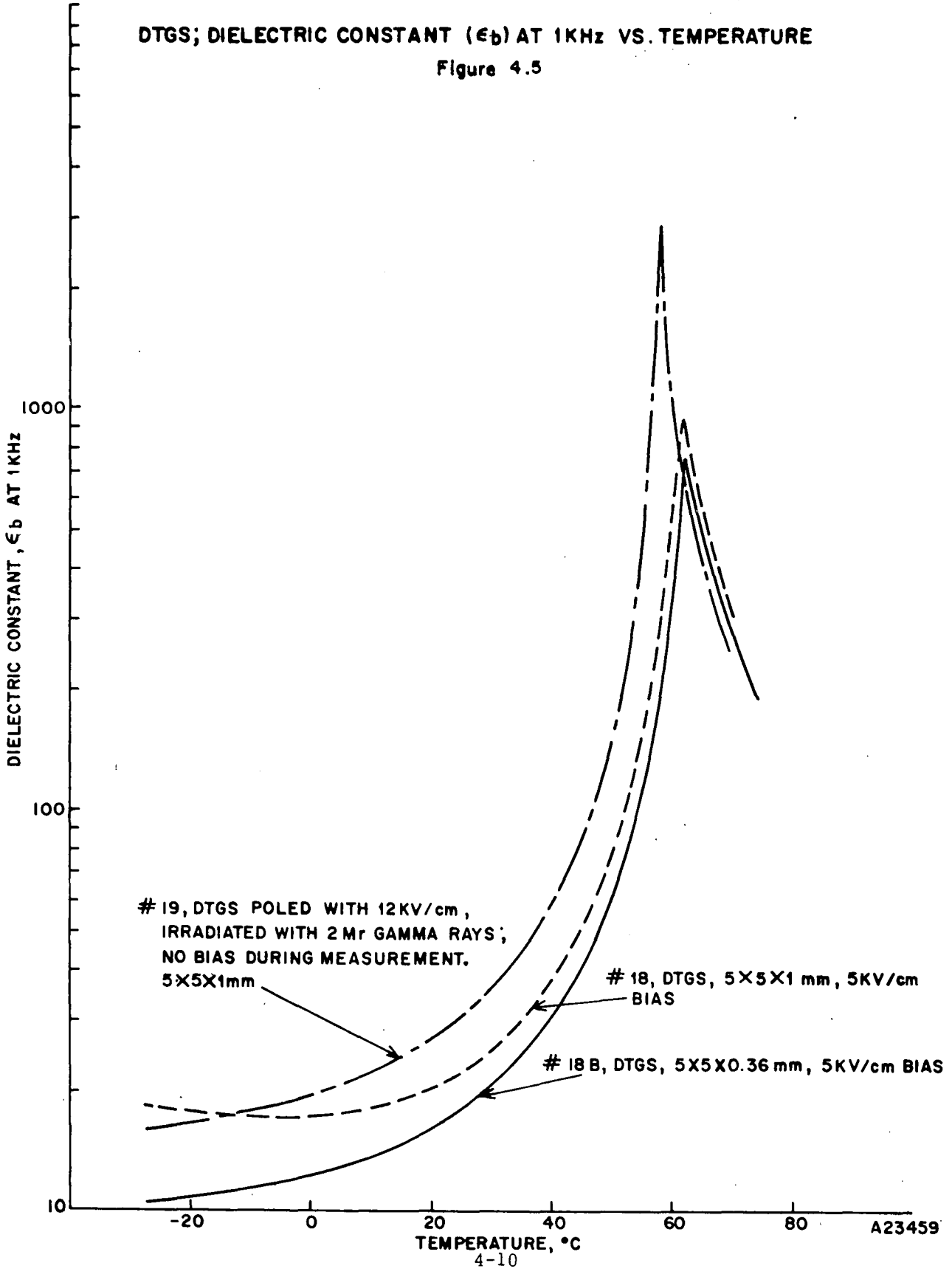

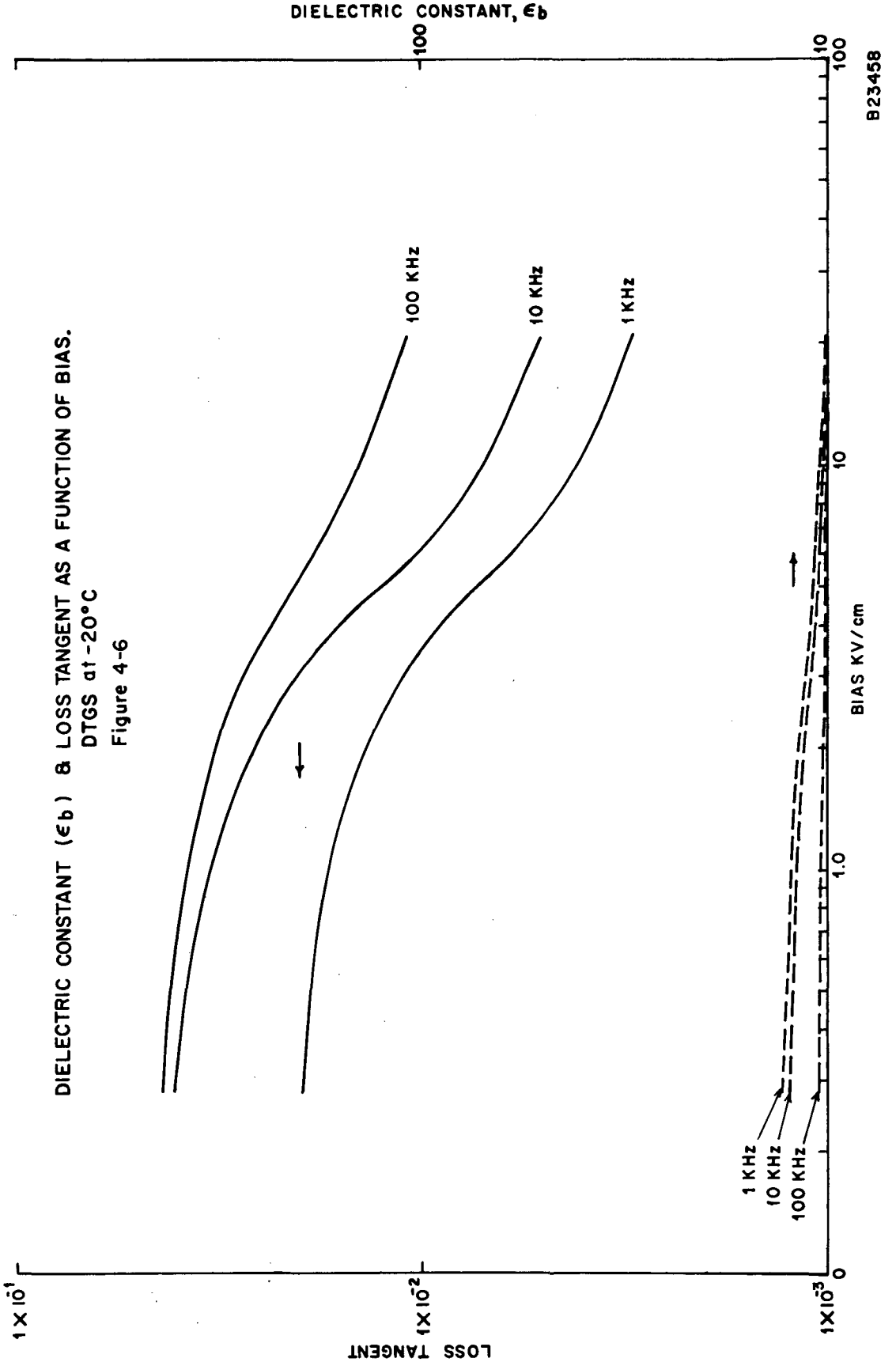

DIELECTRIC CONSTANT (ϵ_b) & LOSS TANGENT AS A FUNCTION OF BIAS.
DTGS at -20°C
Figure 4-6

LOSS TANGENT OF DTGS (#18B) VS. TEMPERATURE. 5 KV/cm BIAS. SAMPLE 5×5×0.36mm

Figure 4.7

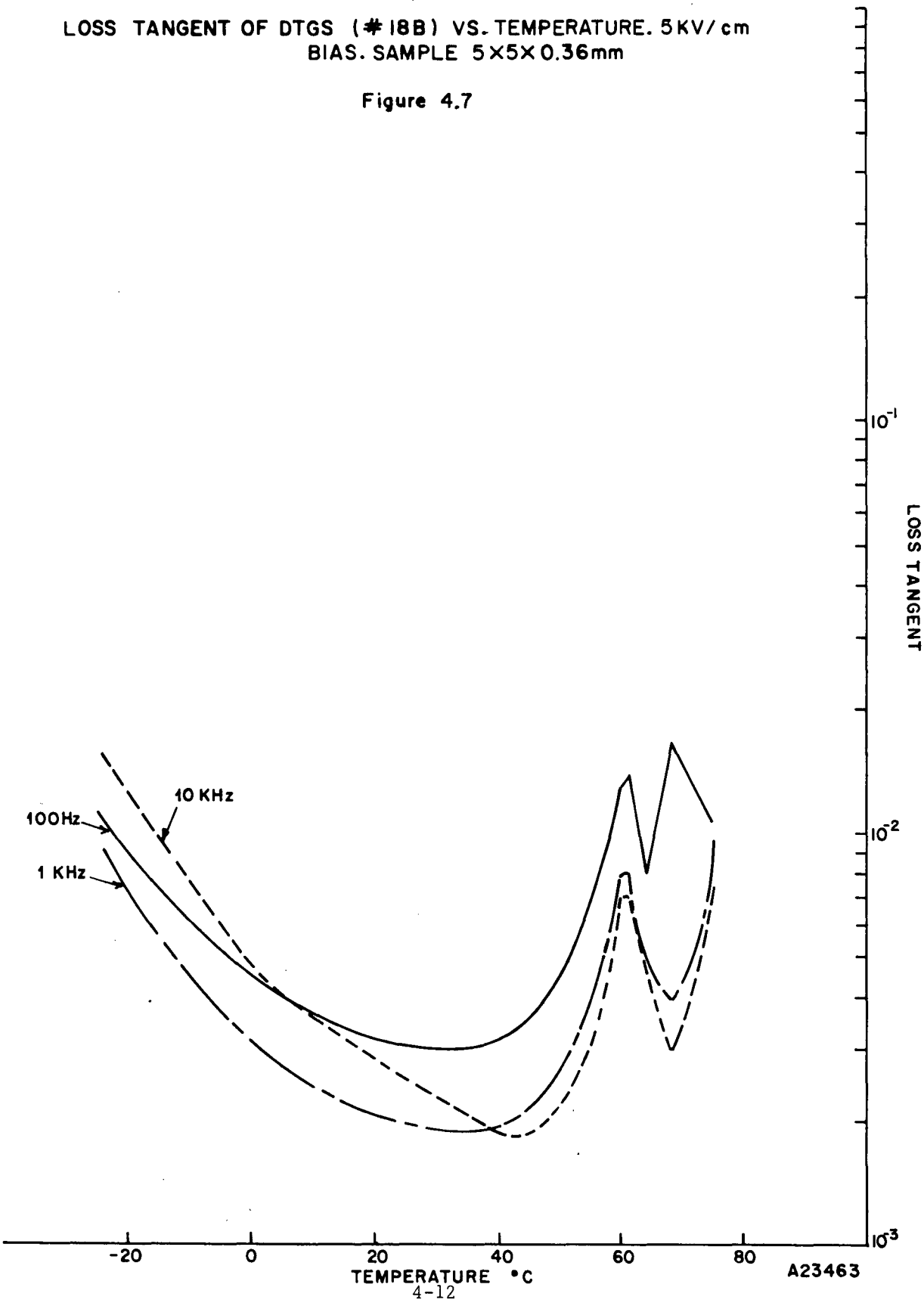

LOSS TANGENT OF 12 KV/cm POLED PLUS 2 Mr GAMMA IRRADIATED DTGS (#19) VS. TEMPERATURE. NO BIAS DURING MEASUREMENT. SAMPLE 5×5×1 mm.

Figure 4.8

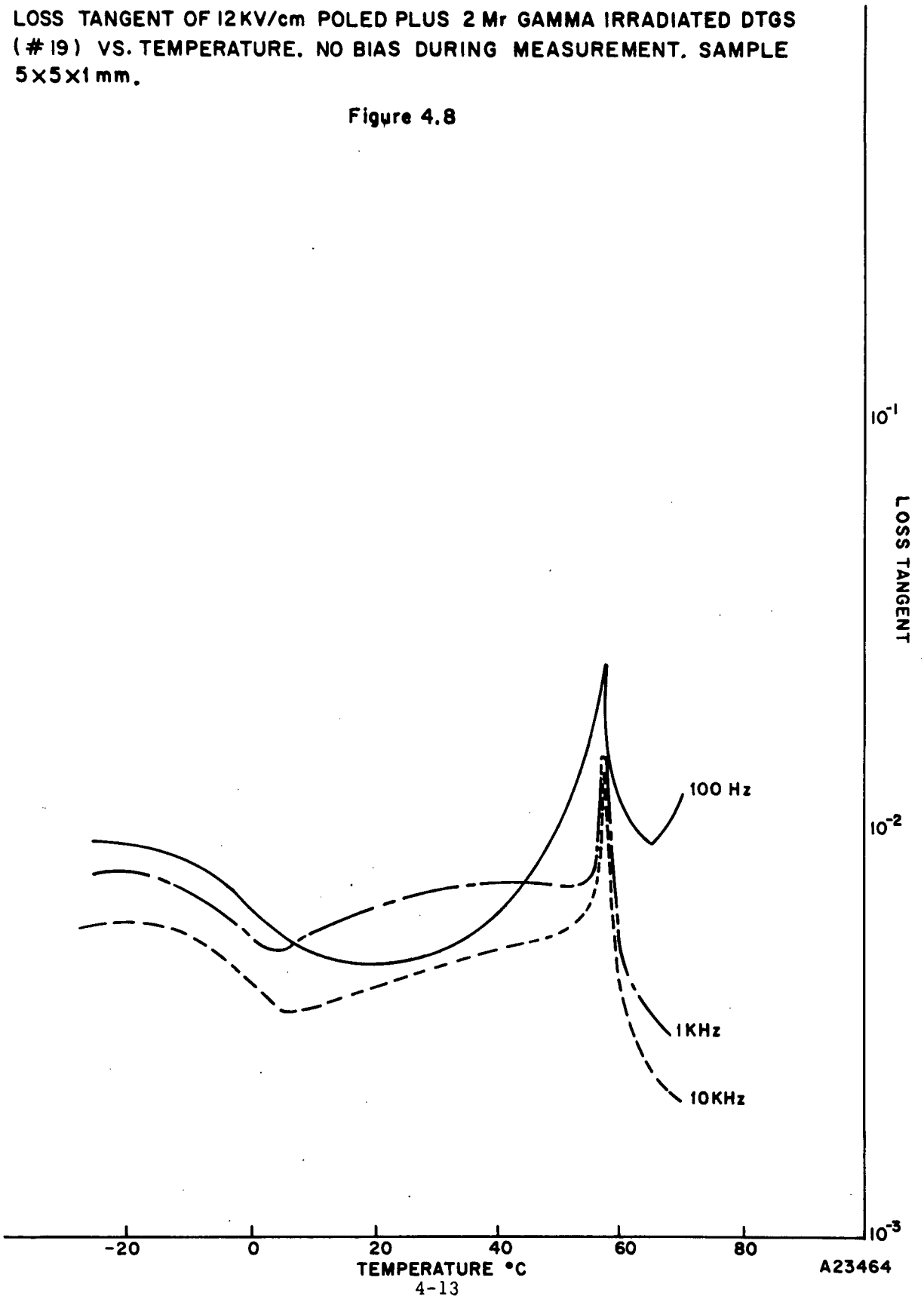

it was considered of interest whether DTGS at -20°C (some 82.4°C below T_c) could be even further poled with an increasing bias voltage, as indicated by a further reduction in the dielectric constant and loss tangent. The bias was varied from 2.8 KV/cm to 21 KV/cm and the results are shown in Figure 4-6. The loss tangent as a function of temperature for DTGS is shown in Figure 4-7.

Deuterated TGS that had originaly been poled with 12 KV/cm (for a 1 mm thick sample, arcing occurred above 1200 V in air) and then irradiated with 2Mr of cobalt-60 gamma radiation has its dielectric constant as a function of temperature shown in Figure 4-5, sample No. 19. The Curie point was found to be 57.7°C. Loss tangent for irradiated DTGS is shown in Figure 4-8. The loss tangent for the irradiated DTGS was (like irradiated TGS) approximately twice that of non-irradiated DTGS at ambient temperature. This also indicates that the irradiated DTGS had not been fully poled prior to irradiation.

As a preliminary check on the responsivity of the irradiated DTGS material, a detector element 1.5 x 1.5 x 0.04 mm with a transparent top electrode (opaque on reverse) was fabricated and supported on a 0.5 mil mylar substrate. With a KRS-5 window, the evacuated element (connected to a Siliconix type 1662 FET and a 1×10^{12} shunt resistor) yielded a responsivity $\mathcal{R}$(1000°K, 15Hz) of 1150 v/w at ambient temperature. A typical DTGS element, non-irradiated by gamma irradiation but fully poled, yields a responsivity of 1450 v/w under the same conditions. This confirms that the irradiated DTGS in all probability had not been fully poled prior to irradiation since the pyroelectric coefficient of TGS (and in all likelihood, also DTGS) is not affected at ambient temperature by gamma irradiation up to at least 4 Mr, according to Yurin and Zheludev (Y3).

4.2.2.3 $Li_2SO_2.H2O$

$Li_2SO_4.H_2O$, as grown, needs no bias to operate as a pyroelectric detector material. $Li_2SO_4.H_2O$ whose prior history since crystal growth has

$Li_2 So_4 . H_2o$; DIELECTRIC CONSTANT & LOSS TANGENT AS A FUNCTION OF TEMPERATURE AND FREQUENCY. NO BIAS. SAMPLE 5×5×0.72mm.

Figure 4.9

NOTE: SAMPLE HAD NOT BEEN HEATED ABOVE 50°C PRIOR TO MEASUREMENT.

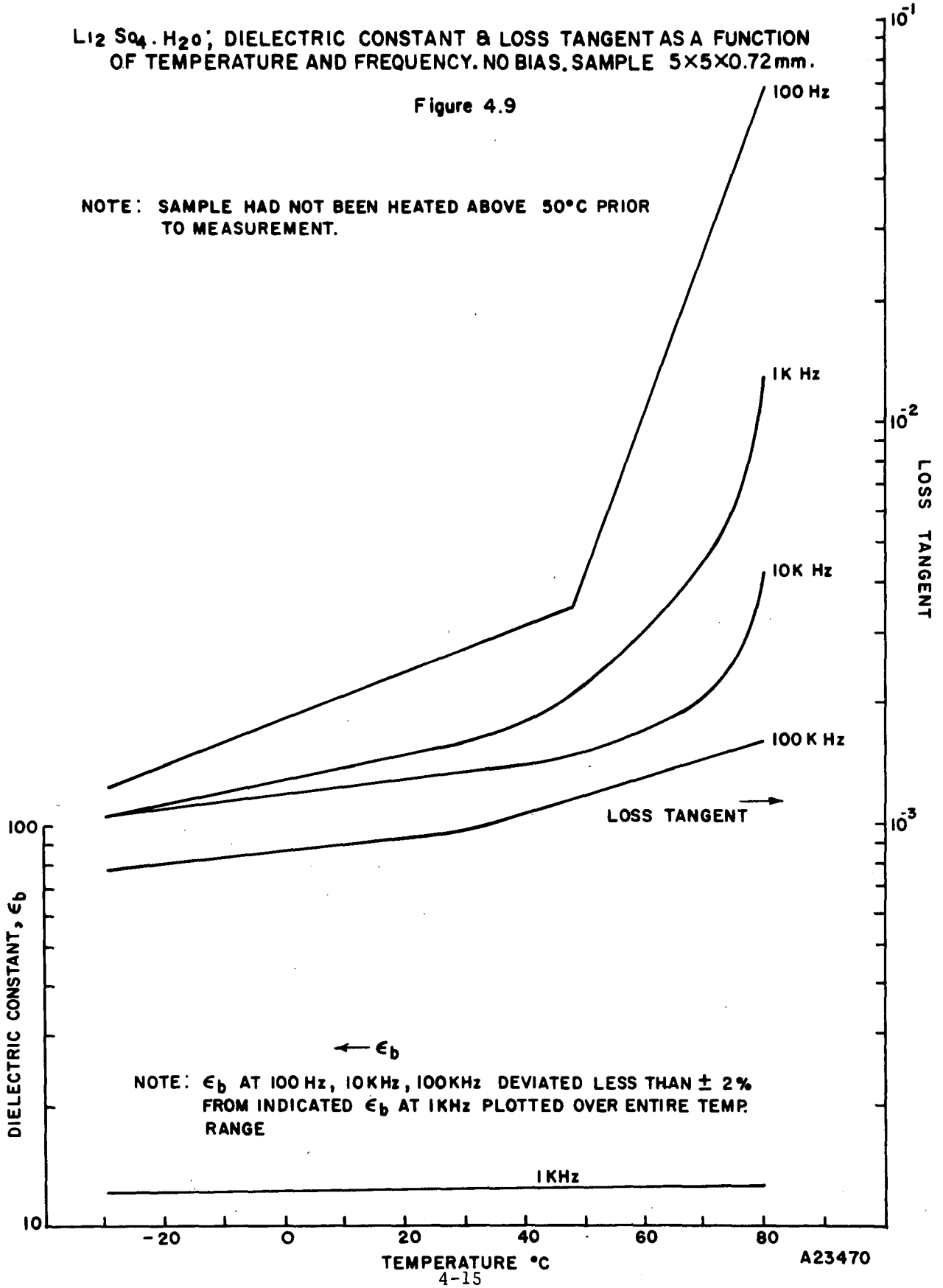

$Li_2 SO_4 \cdot H_2O$; DIELECTRIC CONSTANT & LOSS TANGENT AS A FUNCTION OF TEMPERATURE AND FREQUENCY, NO BIAS

Figure 4.10

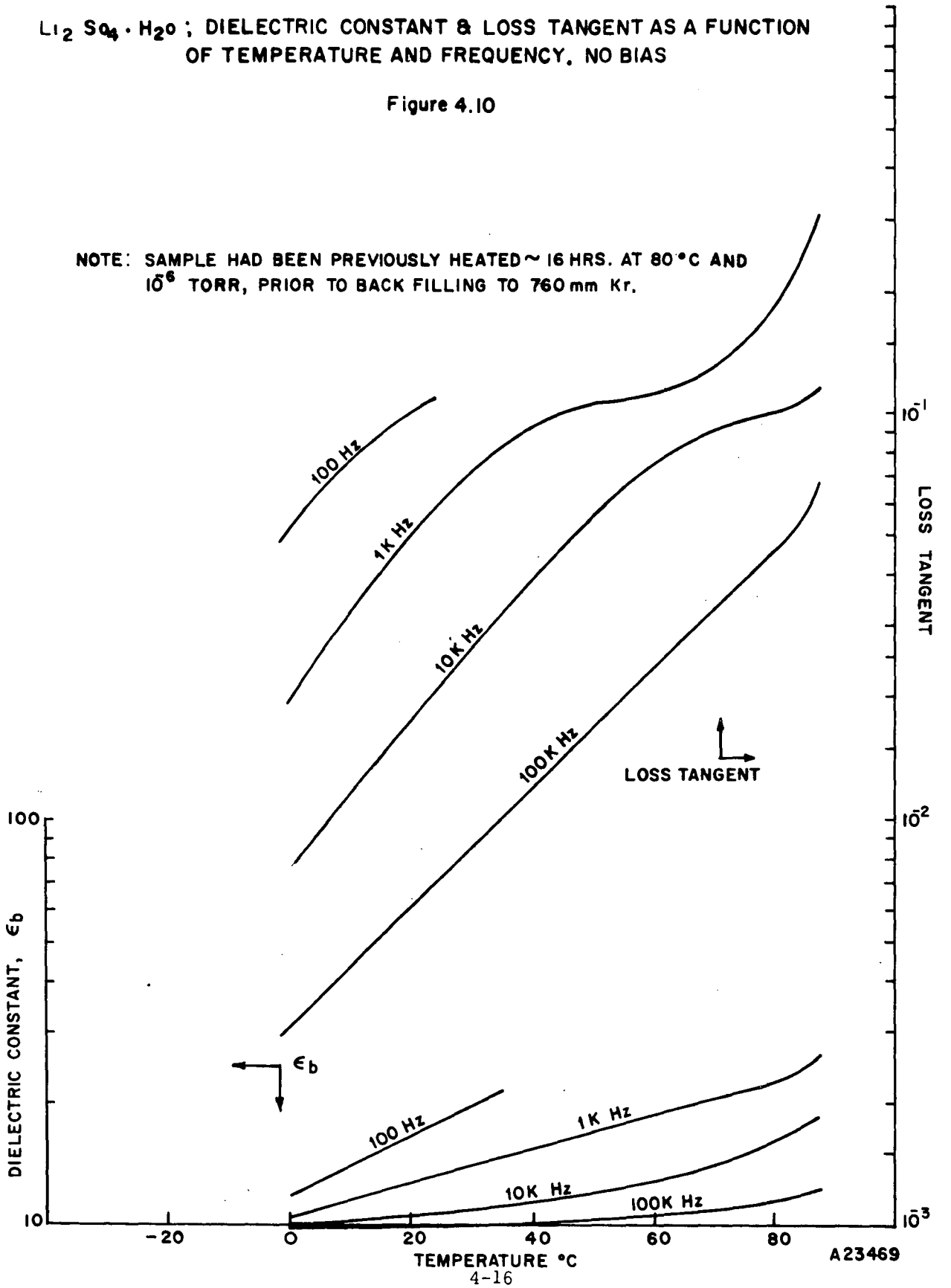

not exceeded 50° C, yielded a plot of dielectric constant and loss tangent as shown in Figure 4-9. As long as 75° C was not exceeded, the results could be duplicated. Having exceeded 75° C, the loss tangent and dielectric constant over the entire temperature span increased and were highly frequency dependent. This change is both a function of temperature above 75° C and dwell time. A sample that had originally been baked out at 80° C for approximately 16 hours during evacuation was then backfilled with 1 atmosphere of Kr. Its dielectric constant and loss tangent as functions of temperature are shown in Figure 4-10. After exceeding 75° C once more, the loss tangent and dielectric increased further over the entire temperature span.

Whether this effect above 75° C is a chemical decomposition or the equivalent of "depoling" has not been established. If $Li_2SO_4 \cdot H_2O$ cannot be baked out to at least 80° C during evacuation of the detector assembly, it would appear as a poorer candidate than had been previously anticipated. This also explains why sample $Li_2SO_4 \cdot H_2O$ detectors previously checked out at BEC, never performed as the figures of merit, based on published parameters, would lead one to expect.

4.3 PYROELECTRIC COEFFICIENT

4.3.1 Equipment

The equipment that permits the determination of the change in electrical charge (dQ) as a function of a change in temperature (dT) has been previously described on pages 4-2 and 4-3 of the first quarterly report. This equipment (Figure 4-11) has just been completed, calibrated, and tested on a sample of TGS. Use of the 40mv/cm gain position of the Y scale on the X-Y plotter corresponds to 2.47×10^{-9} Coulombs/cm. The slope dQ/dT of the trace divided by the area of the test specimen yields the pyroelectric coefficient (P_s, Coulombs $-cm^{-2} \circ K^{-1}$) at the corresponding temperature. Figure 4-12 is an initial plot of P_s vs temperature for TGS. The thermoelectrically heated or cooled specimen is first allowed to

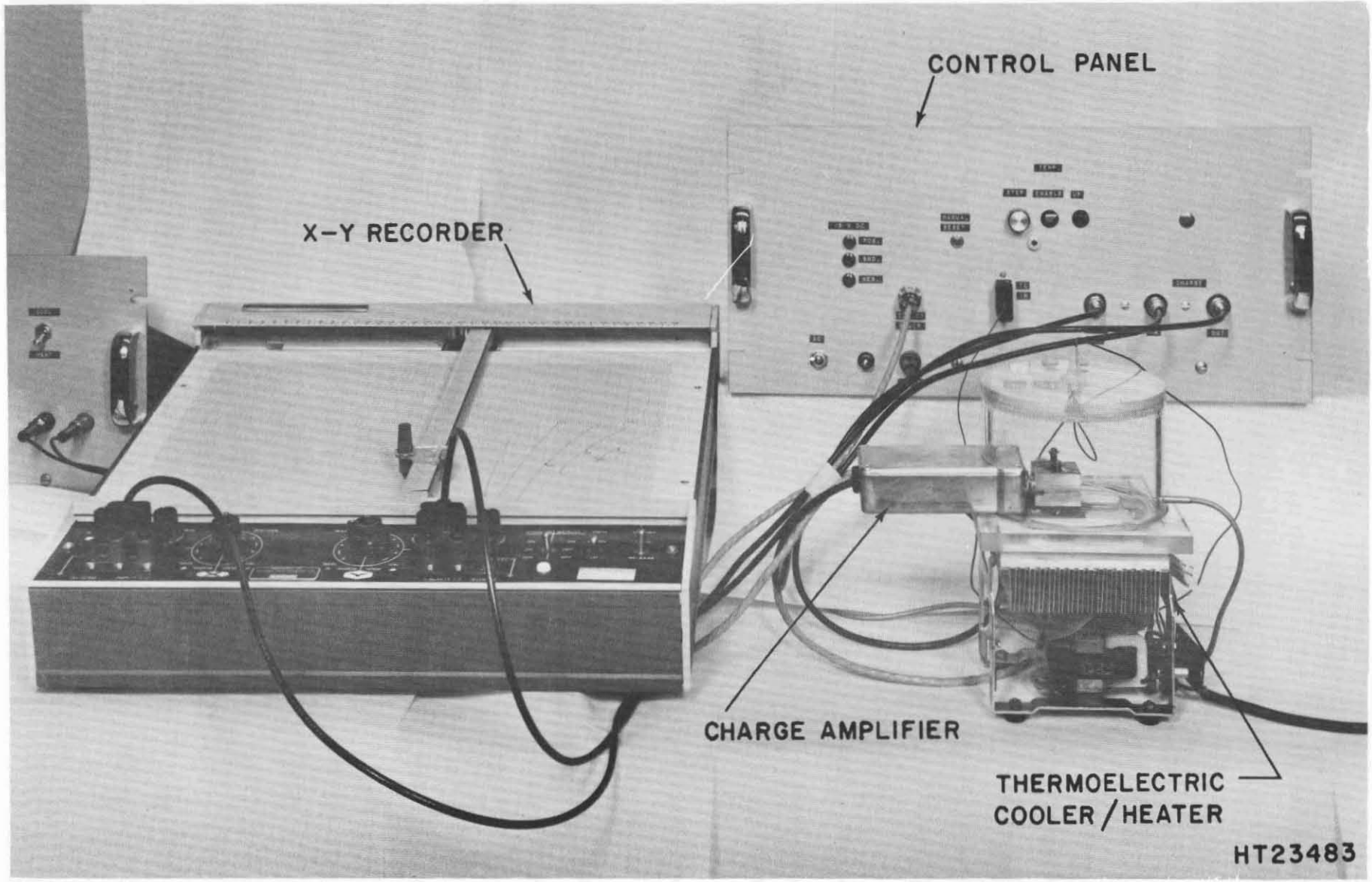

Figure 4-11 PYROELECTRIC COEFFICIENT DETERMINATION APPARATUS

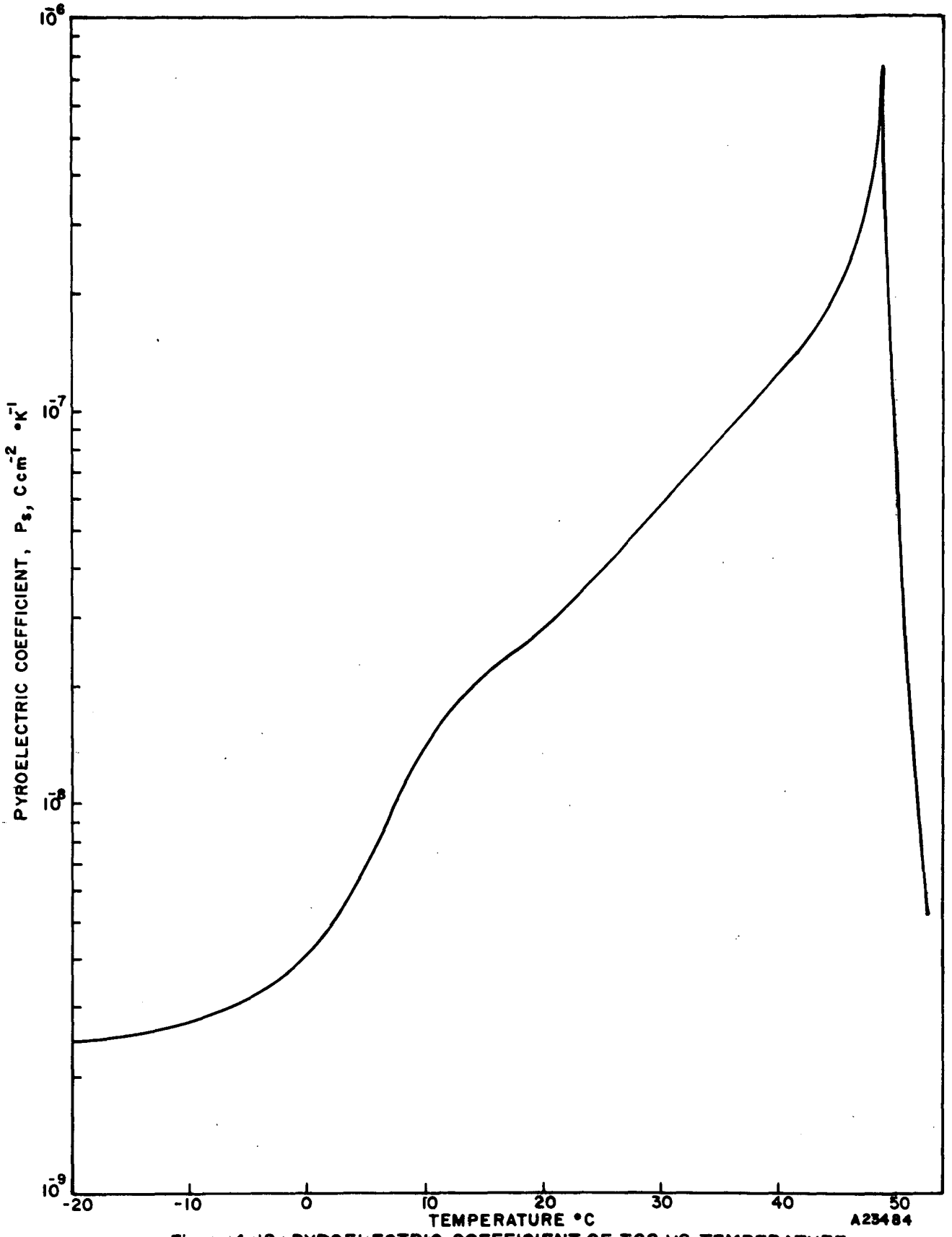

Figure 4-12 PYROELECTRIC COEFFICIENT OF TGS VS. TEMPERATURE. SAMPLE POLED, BUT NO EXTERNAL BIAS DURING MEASUREMENT.

reach a steady-state temperature, as set by the proportional temperature controller. The controller is then reset to a new temperature 1° or 2° C higher and the charge is integrated over that temperature interval. While provision for an eventual automatic charge dumping system at regular intervals was made, it now appears that the use of the present manual discharge system is sufficient.

A high-voltage supply will be added shortly to permit complete external poling (where required) of the thermoelectrically heated or cooled test sample prior to each run, but before the charge integrating amplifier is turned on. In the vicinity of the Curie point (T_c), charge integration can only be accomplished on the heating cycle since dQ/dT approaches zero beyond T_c and the sample would require repoling in going through T_c on the cooling cycle.

4.4 FET CHARACTERISTICS

As described in the First Quarterly Report, measurements were planned of various characteristics of FET's that would lead to a clear definition of all the critical requirements leading to an improvement in sensitivity of a detector-preamplifier system. The principal FET characteristics to be investigated were: leakage current, current (shot) noise, transconductance, and input capacitance.

The attempt to sort out and establish the magnitude of the various sources of noise in a pyroelectric detector FET preamplifier package is based on the assumption that the total noise measured can be expressed as

$$V_{n\ tot} = (V_{sh}^2 + V_J^2 + V_\delta^2 + V_{nsc}^2)^{1/2}$$

in which the significant contributors are shot noise, Johnson noise, loss resistance and amplifier short circuit noise, respectively. Using standard

symbols this can be written

$$V_{n\,tot} = \left[\frac{2\,q\,I_{GSS}\,R_L^{\,2}}{1 + \omega^2 \tau_e^{\,2}} + \frac{4\,KT\,R_L}{1 + \omega^2 \tau_e^{\,2}} + \frac{4\,KT \tan\delta}{\omega\,C_D} + V_{n\,sc}^{\,2} \right]^{1/2}$$

I_{GSS} = FET gate leakage current
(assumed to be the principal source of shot noise)

R_L = FET gate biasing resistor,

C_D = detector capacitance

$\tan\delta$ = loss tangent of detector = $\omega C_D R_{loss}$

$\tau_e = R_L C_D$ = electrical time constant of input circuit

(This assumes the input circuit and FET gate capacitance are negligible in comparison with the detector capacitance.)

There may be other sources of noise that are not thought to be dominant in the context of the present study. There may be Barkhausen noise, detector swish noise (if it is not in a vacuum), detector background thermal noise, etc. But these have not been clearly identified and are therefore omitted. When the identified and measured sources of noise are substantially reduced, the next echelon of noise source will have to be determined.

Fixtures and test instrumentation were assembled to perform those tests. Orders were placed for small numbers of a variety of FET's that represent the best available types for the intended application, based on the data available from the various manufacturers.

The following FET types were used in tests, the results of which are reported below:

E1600, VX9305 (Texas Instruments Ltd., British);
2N4119, 2N4867, U251A, FN2182A (Siliconix),
2N4117, 2N5196 (Intersil).

Table 4-1. Gate Leakage Current and Input Capacitance of FET's

No.	Designation	Manufacturer	Manufacturer Data		Measured Data	
			I_{GSS}**	C_{iss}	I_{GSS}	C_{iss}
			pA	pf	pA	pf
1	E1600	T.I. Ltd. (UK)	0.5	*	0.6	2.8
2	E1600	T.I. Ltd. (UK)	0.5	*	0.6	2.8
3	E1600	T.I. Ltd. (UK)	0.5	*	0.5	2.7
4	U251/a	Siliconix	1	3	0.75	3.3
5	U251/b	Siliconix	1	3	0.7	3.3
6	U251/a	Siliconix	1	3	0.65	3.2
7	U251/b	Siliconix	1	3	0.65	3.2
8	U251/a	Siliconix	1	3	1.25	3.4
9	U251/b	Siliconix	1	3	1.25	3.5
10	2N5196/a	Intersil	2.5	6	3.2	3.5
11	2N5196/b	Intersil	2.5	6	3.2	3.5
12	2N5186/a	Intersil	2.5	6	4.1	3.5
13	2N5196/b	Intersil	2.5	6	4.0	3.5
14	FN2182A	Siliconix	2	3	4.1	3.2
15	2N4119A	Siliconix	1	3	0.5	3.1
16	2N4117	Intersil	1	3	0.15	2.5
17	2N4117	Intersil	1	3	0.18	2.5
18	2N4117	Intersil	1	3	0.18	2.5
19	2N4117	Intersil	1	3	0.18	2.5
20	FN2182A	Siliconix	2	3	0.15	4
21	VX9305	T.I. Ltd. (UK)	100	10	50	9.5
22	VX9305	T.I. Ltd. (UK)	100	10	14	8

* Not given.

**Usually specified at 25°C, V_{DS} = 10 V.

4.4.1 Gate Leakage Current

It was recognized for some time that the FET to be used in conjunction with a pyroelectric detector as a charge amplifier or impedance converter must have an extremely low leakage current. This permits use of a large-valued gate-biasing resistor with operation over a reasonably large range of ambient temperatures without drifitng into cutoff or saturation. Presumably, this will also yield a low shot noise output.

As pointed out in the first quarterly report, it was necessary to mount the FET's in a special chamber that is evacuated during measurements to prevent surface leakage effects due to humidity and other contaminants. The equipment was checked out without an FET being installed, and it was found that the remnant leakage current was less than 0.01 pA. It was thus possible to measure FET leakage currents reliably to less than 0.1 pA.

The results of the gate leakage current measurements on the various samples tested are shown in Table 4-1, along with the values specified by the manufacturers. The table also includes the values of capacitance of the gate circuit as reported by the manufacturer and as measured (see Section 4.4.5).

There is ample evidence that FET's with gate leakage currents of 0.1-0.2pA at room temperature are within the state of the art and can be commercially obtained either by selection or by specifying a maximum value to which the manufacturer can hold.

4.4.2 Current Noise in FET's

In recent measurements of pyroelectric detector-preamplifier combinations the evidence has pointed to the prevalence of current as the dominant source of noise that limits the sensitivity of these detectors in the low frequency domain (e.g., 1 to 100Hz). Measurements made in the past did not show clearly and directly the composition of the noise measured. It was therefore not possible to properly

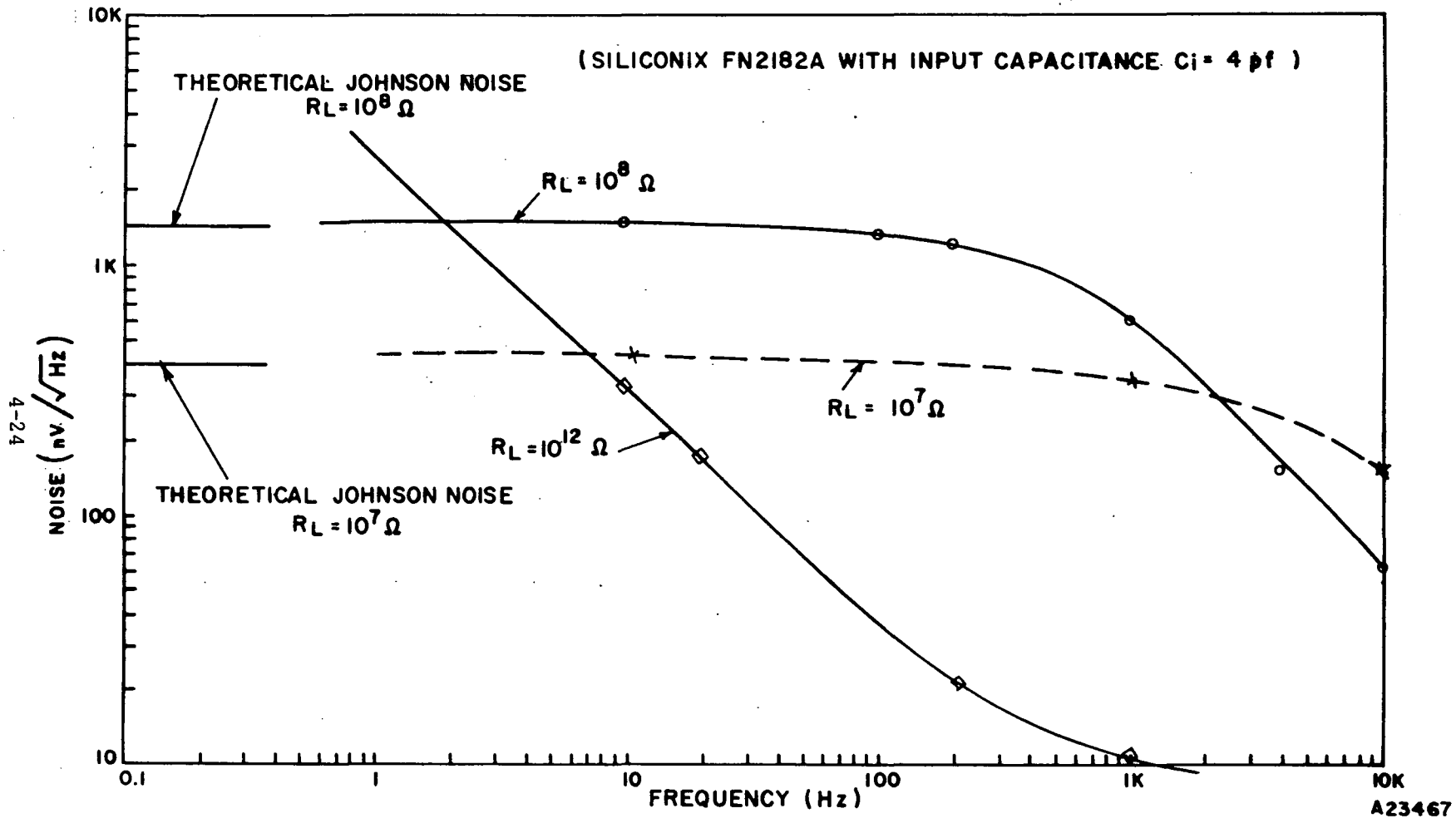

Figure 4-13 NOISE OF FET WITH VARIOUS INPUT RESISTORS

apportion the noise contributors: shot noise, Johnson noise, loss resistance noise, FET short circuit noise, etc. It was planned to single out current (shot) noise and Johnson noise by making noise measurements as a function of frequency with various values of gate resistance (R_L) as a running parameter, and also to make measurements of low frequency noise at several temperatures. If the measured noise is shot noise, a function of the gate leakage current, then an increase in temperature by 20° C (increasing leakage current by a factor of four) would double the shot noise ($I_S = (2q\, I_o\, \Delta f)^{1/2}$).

The measurements, while they do not clearly permit precise predetermination of shot noise based on a knowledge of the gate leakage current of FET's, do show correlation of noise and gate leakage current of various devices qualitatively if not quantitatively. The measured noise increases at high temperatures approximately in conformance with the shot noise equation and not the more modest increase associated with Johnson noise; $\frac{V_{JT1}}{V_{JT2}} \alpha \sqrt{\frac{T_1}{T_2}}$, where the temperatures are in Kelvin units.

The figures show the measured results.

Figure 4-13 shows that for $R_L = 1 \times 10^7$ and 1×10^8 ohms one measured the predicted Johnson noise (at all frequencies). For $R_L = 1 \times 10^{12}$ ohms the noise measured is in excess of the calculated Johnson noise and indicative of the presence of shot noise in approximately the level to be expected with a current of 0.2 pA generating this noise. For $R_L = 10^{12}$ ohms the electrical time constant is, of course, much larger.

Figure 4-14 lends further strength to the argument identifying the noise as being due to gate leakage current. As the temperature of the FET is raised there is a substantial increase in this noise. A rule

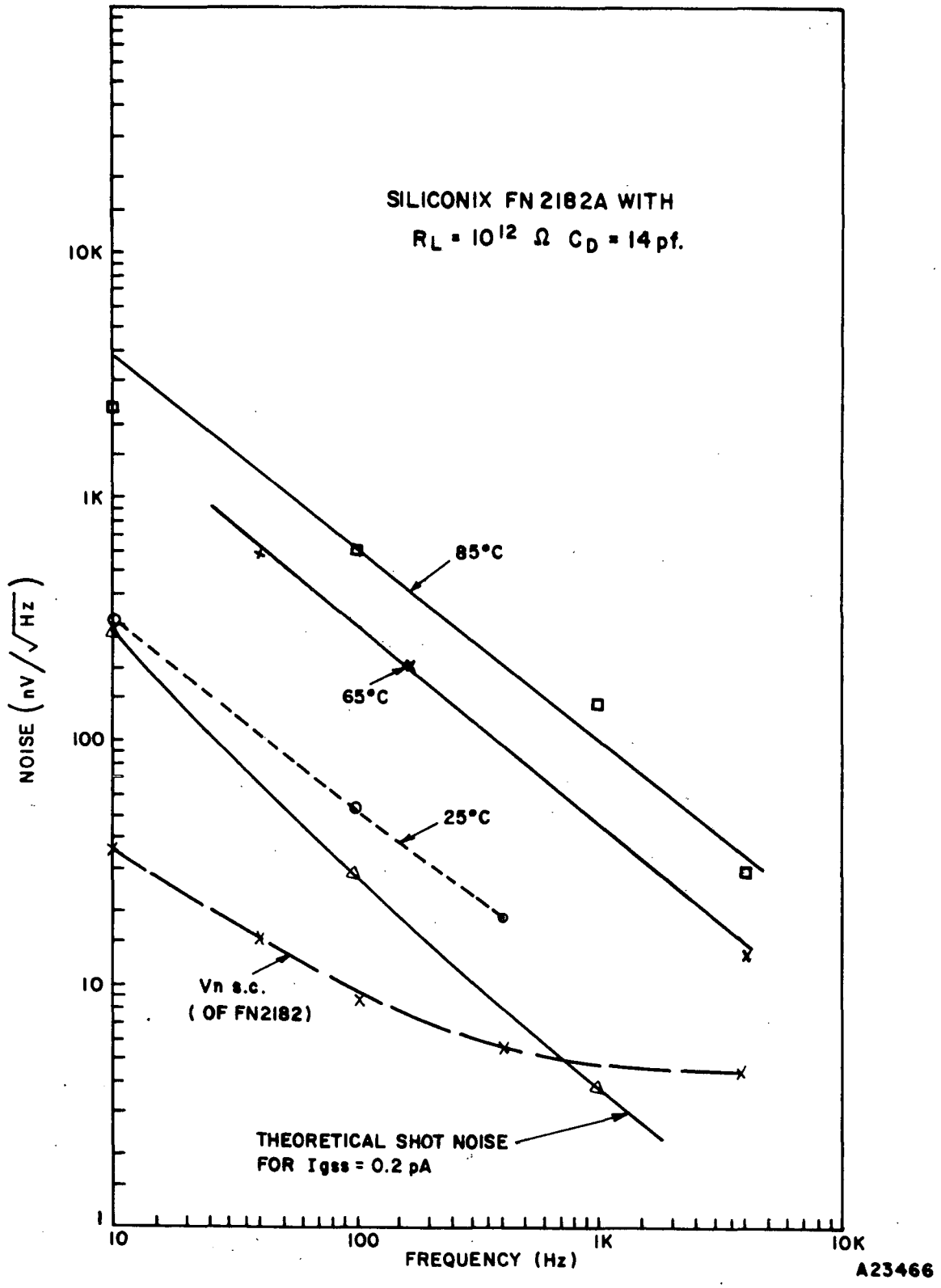

Figure 4-14 CURRENT NOISE VS. FREQUENCY AT VARIOUS TEMPERATURES

of thumb approximation is that leakage current doubles for a 10°C increment in temperature. Also, the current noise should increase by the square of the increase in current; therefore, at 65C one could expect a four-fold increase in shot noise, which is in evidence in Figure 4-14. The Johnson noise increase is only

$$\frac{V_{J65}}{V_{J25}} \alpha \sqrt{\frac{338}{298}} \cong 1.06$$

which would be barely measurable.

Figure 4-15 shows the measured noise for an FET (FN2182A) along with the calculated value based on contributions that include shot noise, Johnson noise and short circuit noise.

Figure 4-16 shows the shot and short circuit noise of an FET (VS9305) that has one of the lowest short circuit noise characteristics of any measured. Unfortunately, it has too much leakage current (14pA), and this results in a higher shot noise than for devices with lower values of leakage current.

It is evident that the measured current noise is related to the gate leakage noise of the FET. It may be useful to determine the load resistor for which the shot noise equals the Johnson noise.

Thus, $(2q\, I_o \Delta f)^{1/2} R_L = (4KTR_L \Delta f)^{1/2}$, whence $R_L = \frac{4KT\Delta f}{2qI_o\Delta f}$.
For T = 300°K and $I_o = 1 \times 10^{-13}$ amps, $R_L \cong 5 \times 10^{11}$ ohms.

This is a value near that which we commonly use. The total RMS noise at DC would be $V_{ntot} = (V_{sh}^2 + V_J^2)^{1/2} = 140\mu V\ Hz^{-1/2}$.

With this low leakage current and possibly with a cooled temperature-controlled FET one could go to even higher load resistors and thereby increase the electrical time constant, with a resultant reduction in noise at frequencies of 1-100 Hz.

Note that the capacitors used in the measurements above, unlike many pyroelectric detectors, had extremely low loss resistance, generally as low as tan $\delta = 0.0005$.

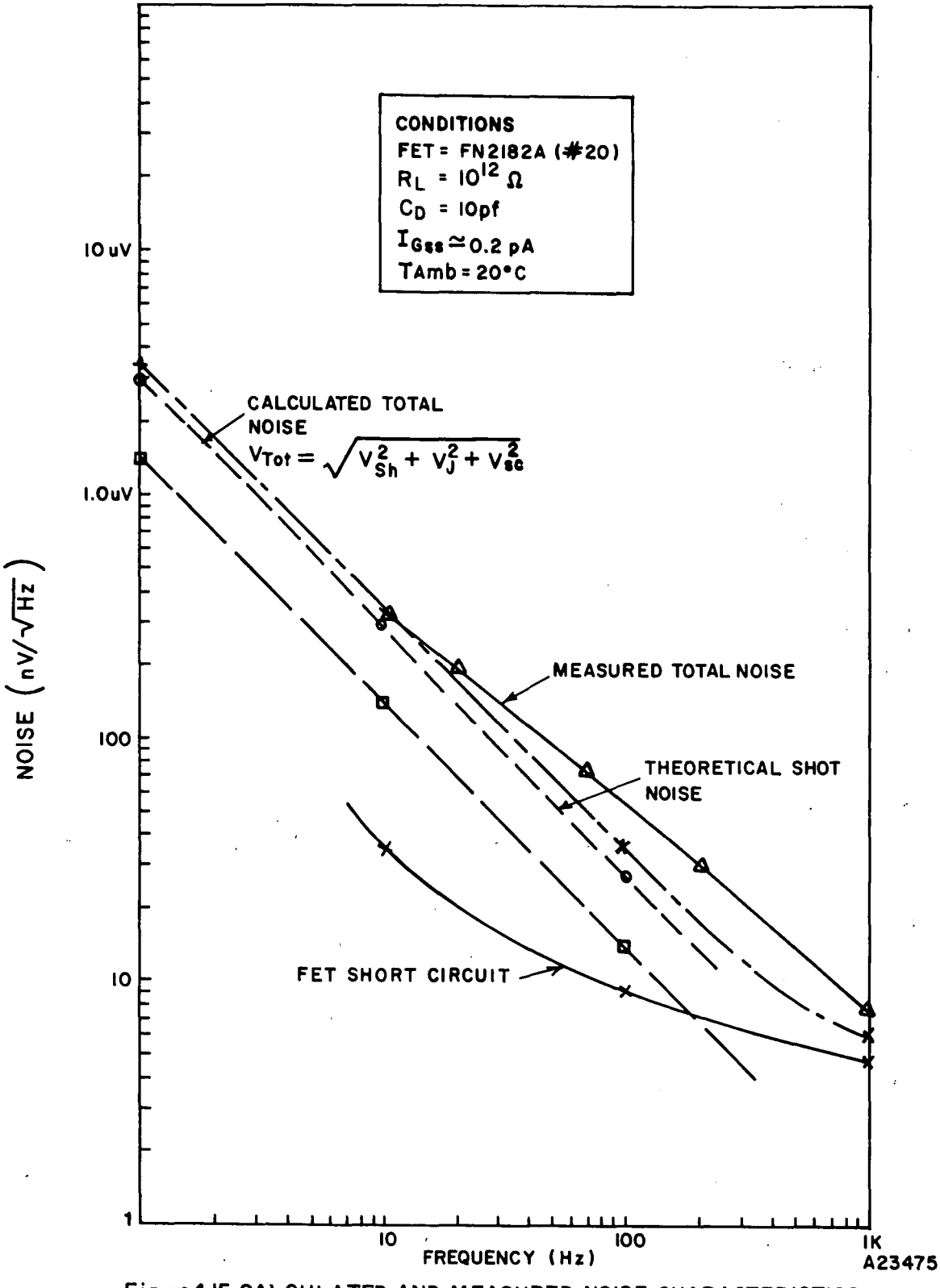

Figure 4-15 CALCULATED AND MEASURED NOISE CHARACTERISTICS OF TYPE FN 2182A FET

4.4.3 Short Circuit Noise

The short circuit noise of FET's is of particular concern at high frequencies or when they are used in conjunction with pyroelectric detectors of relatively high capacitance (large detectors, thin detectors or detectors having a high dielectric constant). In these cases the detector preamplifier combination may show a sensitivity that is limited by amplifier short circuit noise, a condition always to be avoided. Fairly large variations in short circuit noise between different types of FET's have been measured. Unhappily, the short circuit noise for FET's having low gate leakage current (one of the prerequisites for a good FET in the present application) is, as a rule, higher than for some devices having higher leakage current. This is a result of the geometry of the FET design that is chosen specifically to yield the desired (and unfortunately conflicting) characteristics. Figures 4-17, 4-18, and 4-19 show the results of the measurements.

Figures 4-17 and 4-18 show the short circuit (voltage) noise of several FET's. The post-amplifier's short circuit noise is seen to be sufficiently low to permit neglecting its contribution in reporting the noise of the FET whose gate may be shunted by a capacitor or at some future time may be connected to a pyroelectric detector. For detectors with a capacitance of 10-20 pf, the short circuit noise of most of these FET's will be the limiting noise at frequencies of 1 KHz and higher.

Figure 4-16 shows the short circuit noise of the T. I., Ltd. VX9305 to be considerably lower than that of other FET's like the SN2182A. It is therefore more suitable for applications requiring operations above 1 KHz. Unfortunately the low short circuit noise of this device goes with a higher gate leakage current and shot noise and thus makes the device less satisfactory for lower frequency operation. This is the dilemma referred to earlier, that the favorable properties of low leakage current and low short circuit noise do not normally coexist in one FET

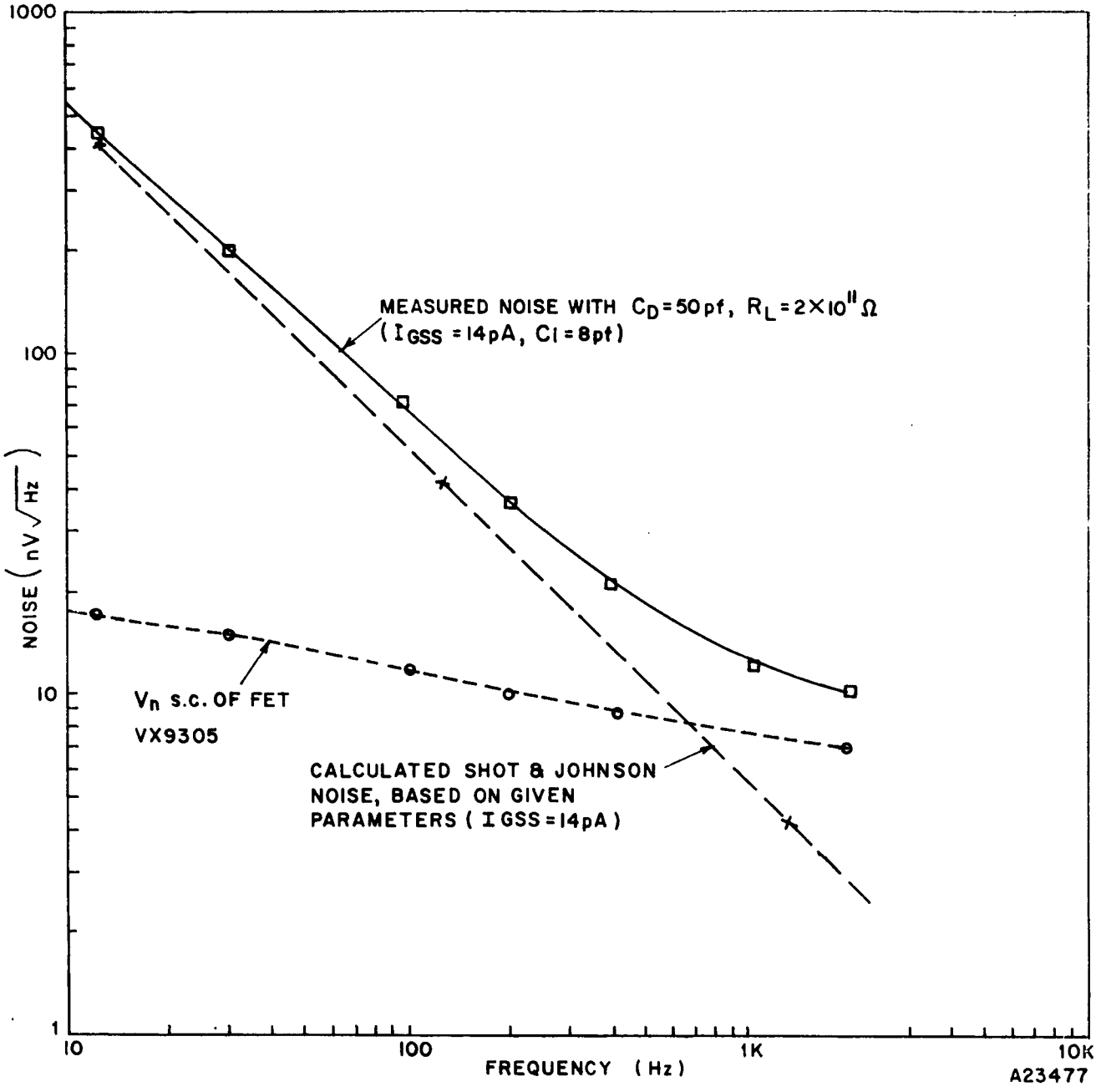

Figure 4-16 CURRENT NOISE AND SHORT CIRCUIT NOISE OF FET VX9305 (#22)

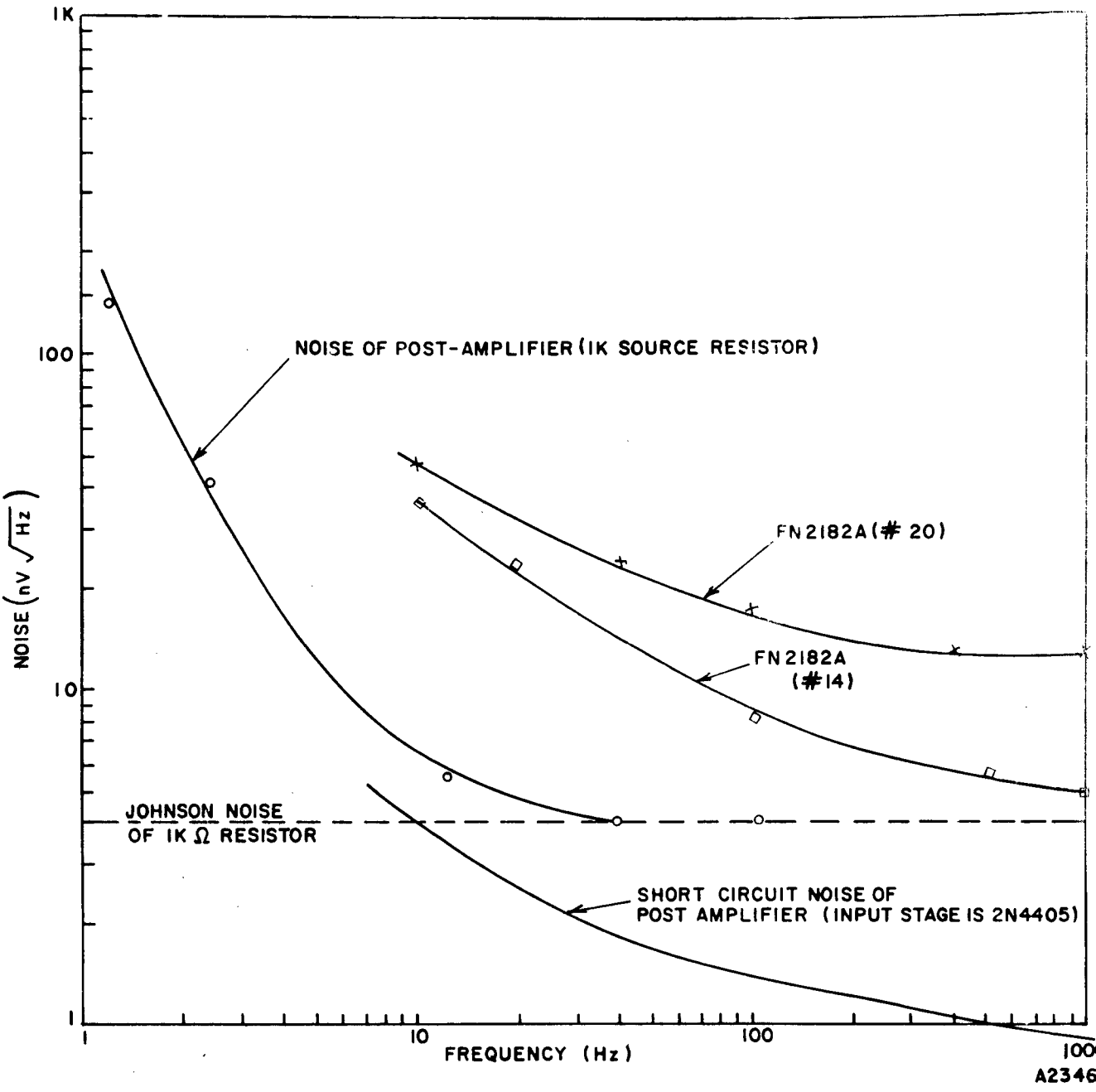

Figure 4-17 SHORT CIRCUIT NOISE OF SEVERAL FET'S AND OF POST-AMPLIFIER.

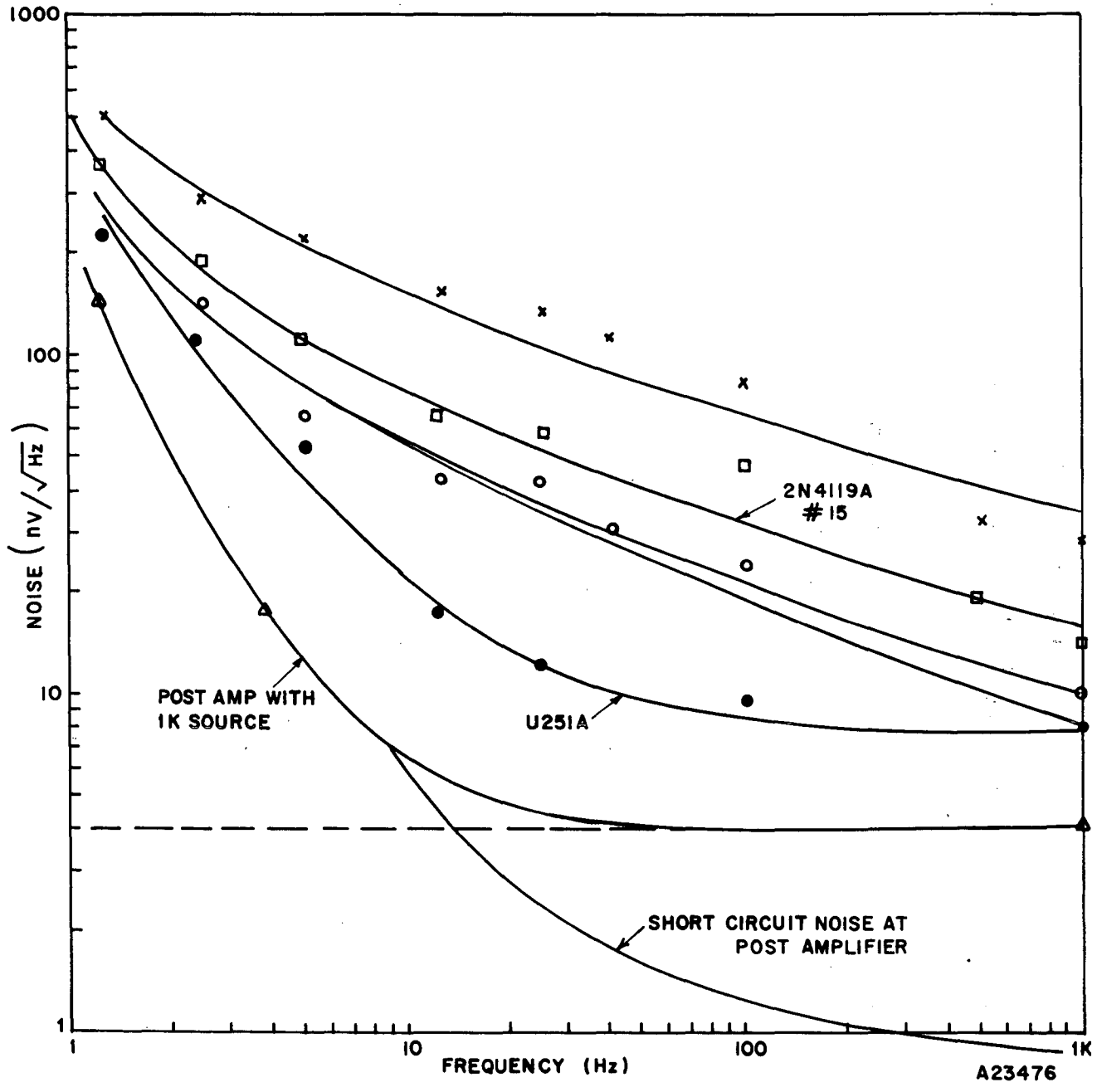

Figure 4-18 SHORT CIRCUIT NOISE OF VARIOUS FET's

device. Hence one may have to select the type of FET most suitable for a particular application.

A surprising exception to this common characteristic of FET's appeared to be the case of the T. I., Ltd. E1600. This device has a low leakage current ($I_{GSS} \simeq 0.6$pA for No. 1) and yet the short circuit noise is quite low. This is shown in Figure 4-19. The shot noise for this device compares with the best, and the short circuit noise is nearly as low as it is for the VX9305.

4.4.4 Transconductance

In order to produce the desired results, the FET must have gain, whether this be in the form of voltage gain or current gain or impedance conversion. FET's were used here as impedance converters (source follower mode); this is not very demanding in terms of gm, the transconductance. Provided the post-amplifier does not contribute measurably to the detector-FET noise, the gain of the impedance converter is not critical. The amplifier at the output of the FET source follower used a 2N4405 low noise bipolar transistor as the input stage. Its noise contribution is considerably below the short circuit noise of all the FET's tested and could therefore be ignored. (See Figure 4-17.) The voltage transfer ratio of the impedance coupler (usually about 0.9) was noted, but the output impedance or current gain was not checked to obtain a measurement of transconductance. All the devices tested had sufficient power gain to be useable in any ultimate system.

4.4.5 Input Capacitance

The FET gate circuit capacitance is particularly significant in the case of small or low-dielectric pyroelectric detectors. When used in conjunction with detectors having a capacitance of 5-10 pf the gate input capacitance represents a load that attenuates the signal generated by the detector.

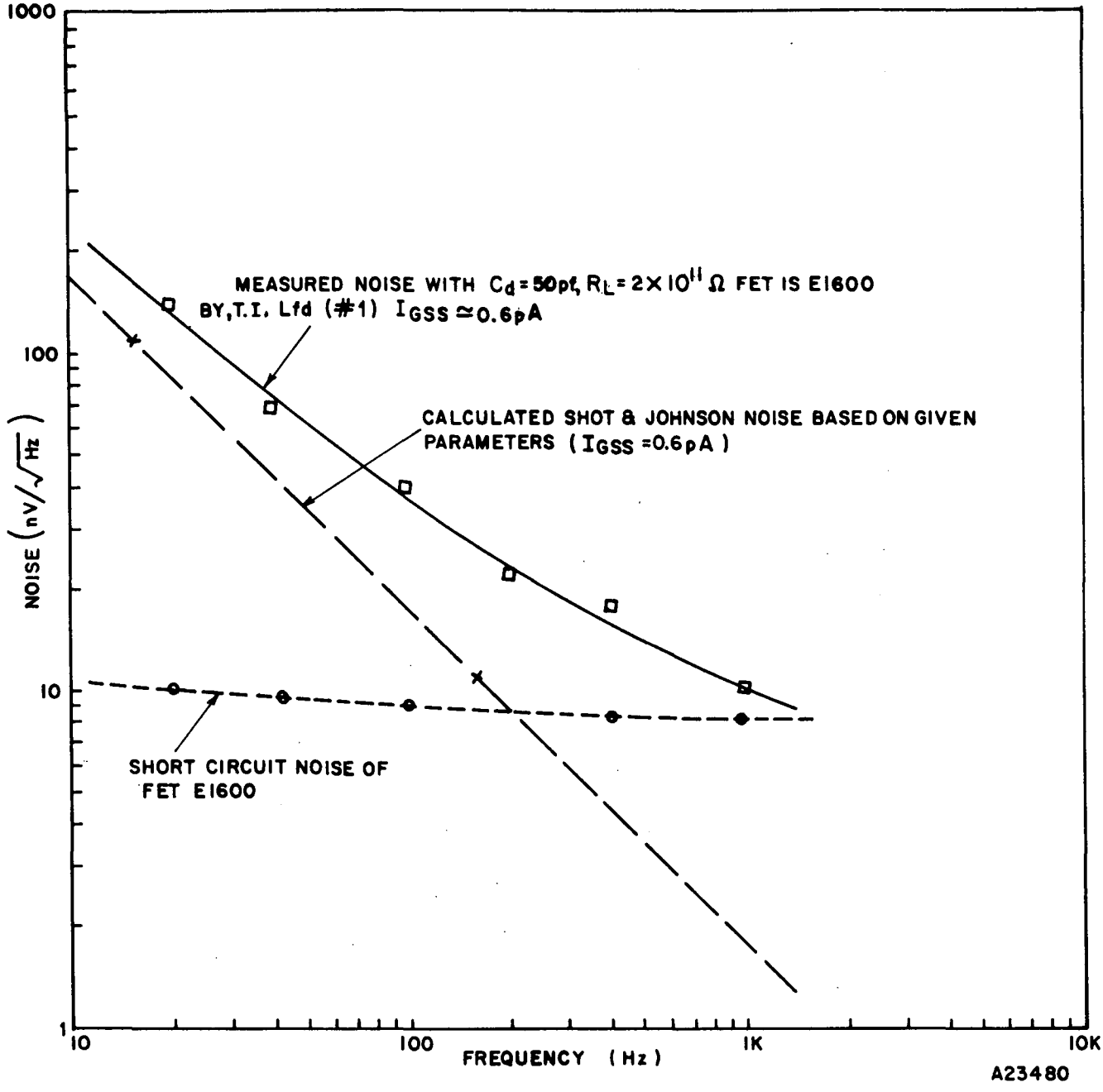

Figure 4-19 SHOT NOISE AND SHORT CIRCUIT NOISE OF BEST FET, E1600

To measure the gate circuit capacitance a sinusoidal signal was fed to the FET gate in series with a fixed resistor of 1×10^7 ohms and the source follower output voltage was measured to determine the high-frequency cut-off point. This established the gate circuit impedance. The results are shown in Table 4-1. The input capacitance does not appear to vary greatly from one FET type to another, being normally in the range of 2.5 to 4 pf. Very likely the value is determined largely by the leads and feedthrough terminals rather than by intrinsic device characteristics.

5.0 New Technology

During this report period there were no technical developments reportable under the New Technology Clause of the subject contract.

6.0 PLANNED FOR NEXT REPORTING PERIOD

The search for more pyroelectric materials for improved IR detection will continue and the table of material parameters continuously updated.

Transmittance and reflectance measurements will continue on those samples not previously measured.

Dielectric constant and loss tangent measurements as functions of temperature (-30° C to approx. 100° C) and frequency (50 Hz to 10 KHz), will continue. The pyroelectric coefficient as a function of temperature will also be determined for all samples on hand.

Gamma irradiation of deuterated TGS and doping of TGS and DTGS with α -alanine appear most promising for achieving locked-in polarization. These materials will take precedence over all others.

Detector elements 1.5 x 1.5 x 0.04mm will be fabricated from the most promising detector materials and mated to the best available transistors. Responsivity, noise, detectivity, and spectral response measurements will be carried out on these evacuated devices as functions of temperature and frequency.

A crystal of glucuronolactone will be grown from aqueous solution.

Time permitting the effect of U-V irradiation on TGS and DTGS will be examined.

The search for improved FETs and a determination of their characteristics will continue along with the best mode of operation of the detector-amplifier package. These measurements should permit determination of other possible sources of noise such as loss-resistance noise.

Detectors, such as those of SBN, will also be operated in the dielectric mode and performance data will be recorded.

Section 7.0 CONCLUSIONS AND RECOMMENDATIONS

The project accomplishments during the reporting period are consistant with the objectives of the program.

Determination of pyroelectric material parameters, (i.e., dielectric constant, loss tangent, and pyroelectric constant) as functions of temperature and frequency are proceeding satisfactorily.

Irradiation of TGS and DTGS with cobalt 60 gamma rays indeed serves to lock-in polarization. Complete poling prior to irradiation is a necessity. Since doping with Cu^{++}, Cr^{+++}, or α-alanine is also reported as leading to "locked-in" polarization. This could ultimately lead to an improved device. Doped or gamma irradiated TGS and DTGS should take precedence over less promising materials.

An explanation has been found for the previously poor performance of $Li_2SO_4.H_2O$, below the calculated Figures of Merit. In all cases 75°C had been exceeded during evacuation and bake out, leading irreversably to markedly increased noise at ambient temperature.

The following preliminary statements may be made with regard to the measurements made so far on transistors.

a. There is evidence that the FET in combintation with load resistors in the range of $1 \times 10^{11} - 10^{12}$ ohms and capacitors or detectors of 10-50 pf is shot-noise limited at frequencies to about 1 KHz.

b. There is a strong correlation between the measured gate leakage current (I_{GSS}) of an FET and the measured noise with gate terminations referred to in (a).

c. The shot noise is temperature dependent; i.e., it increases with temperature apparently as a result of leakage current increase with temperature.

d. As a rule, FET's with the lowest gate leakage (I_{GSS}) have higher short circuit noise than high I_{GSS} devices. This is believed due to the larger intrinsic resistance of the channel as produced by the geometry used in producing low leakage devices. An exception seems to have been found in the Type T. I., Ltd. E1600, which combines low leakage with low short-circuit noise.

e. It is now possible to specify or select devices with I_{GSS} of less than 0.2 pA at 25°C, V_{DS} = 10 V. With the above preliminary test results one can project some possible improvements, not yet checked out. It appears that by proper choice of FET's and possibly by cooling the FET (not the detector) one can hold the leakage current to below 0.1 pA. It may be that when these low values of gate leakage current are obtained, one will discover other sources of leakage, possibly in the detector crystal or the wiring, etc.

With parameters optimized according to guidelines set forth above, one can estimate the performance of a detector-FET package based, for example, on ITPR-type detectors operated at 37°C. Detector capacitance is 50 pf and the electrical time constant RC is $50 \times 10^{-12} \times 5 \times 10^{11}$ or 25 sec. If one could realize the theoretical noise (shot and Johnson noise) one should measure a total noise of $\sim 0.07 \mu V\ Hz^{-1/2}$ at 15 Hz. This is about four times lower than that normally reported for the ITPR detectors. In practice one may not achieve ideal performance. However, one should obtain a considerable improvement over the present detectivity.

APPENDIX A - COMPILATION OF PYROELECTRIC MATERIALS AND THEIR CHARACTERISTICS AS DERIVED FROM A SURVEY OF THE LITERATURE.

TABLE A-1. PYROELECTRIC MATERIALS CHARACTERISTICS

MATERIAL	Curie Temperature T_c °C	Temperature of Measurement T °C	Dielectric Constant ϵ	Frequency of ϵ Measurement F Hz	Spontaneous Polarization P_s C cm^{-2} x 10^{-6}	Pyroelectric Constant dP_s/dT C cm^{-2} °K^{-1} x 10^{-8}	Specific Heat c J cm^{-3} °K^{-1}	Density s g cm^{-3}	A.C. Resistivity (1 KHz) ρ Ω - cm	$(dP_s/dT)\,\epsilon^{-1}$ x 10^{-10}	$(dP_s/dT)\,(\epsilon\ c)^{-1}$ x 10^{-10}	$(dP_s/dT)\,\rho^{1/2}\,c^{-1}$ x 10^{-4}	Reference	COMMENTS
$LiNbO_3$	1200 ± 10	27	30	1K, 100K	50	0.4	2.8	4.65	9.8 x 10^{10}	1.3	0.46	4.5	N1, P1,	T_c depends on crystal composition; varies from 1150° - 1240°C. Transmits 0.4-5.0μ.
		100	30	100 K	49.5	0.5				1.7	0.61		S1	
		200	30	100 K	49	0.7				2.3	0.82			
		450	40	100 K	46									
$LiTaO_3$	660,	25	47	1 K	50	1.9	3.16	7.45	~1 x 10^{10}	4.0	1.3	6	G1, G2	T_c depends on crystal composition, varies from 660° -560°C. Transmits 0.5 to 5μ (3μ absorption).
	618 for	250	70	10 K	45	2.1	3.72			3.0	0.81		M1, Y1	
	Ta/Li = 1.1	450	300	10 K	37.7	8.2	3.84			2.7	0.71		I1, G6	
$PbTiO_3$	470 (492)	25	200	(Probably 1-10K)	~66	~6	3.23	7.78		3	0.93		Y4; S11, B8, S12, S13	Transmits 0.6 to 6μ. Generally doped 0.1% UO_3 Constant responsivity -20° to 60°C.
PZT 5A (Clevite)	365	25	1900	1 K	38	4.0	3.1	7.75	4.7 x 10^7	0.21	0.068	0.89	L1, C1	
PZT 4 (Clevite)	328	25	1400	1 K	30	3.7	3.0	7.5	3.2 x 10^8	0.26	0.087	2.2	L1, C1	
PZT HST-41 (Gulton)	270	25	1800	1 K	23	2	3.0	7.6	4.5 x 10^7	0.11	0.037	0.45	L2, G8	
$5PbO \cdot 3GeO_2$	177	50	60	10 K	4.5	1				1.7			I2	
PLZT 6.5/65/35 (Honeywell)	~164	27	1400	1 K		10	2.6	7.83	5.1 x 10^7	0.71	0.27	2.76	L4, H6	Transmits 0.4 to ~9μ.
$Ge_2(MoO_4)_3$	161±2	25	9-12	(Probably 1-10 K)	0.2			4.6						
		100	10		0.15	0.1	2.1			1.0	0.48		K1, R1	Does not exhibit dielectric anomaly at Curie temp. Operates as a laser with Nd^{+3} doping. Ferroelastic.
		143	9.8	"	0.1	0.14	2.1			1.4	0.67		U1, U2	
		151	10.0	"	0.01	0.25	2.1			2.5	1.2		C2, F1	
		159	9.7	"		4.9	8.7			50	5.8			
$NaNO_2$	160	25	8	1 K	7	0.4	2.0	2.1	>10^{11}	5	2.5	>6.3	S2, P1	ϵ practically constant to 140°C.

TABLE A-1. PYROELECTRIC MATERIALS CHARACTERISTICS (CONTINUED)

MATERIAL	Curie Temperature T_c °C	Temperature of Measurement T °C	Dielectric Constant ϵ	Frequency of ϵ Measurement F Hz	Spontaneous Polarization P_s C cm^{-2} x 10^{-6}	Pyroelectric Constant dP_s/dT C cm^{-2} °K^{-1} x 10^{-8}	Specific Heat c J cm^{-3} °K^{-1}	Density s g cm^{-3}	A.C. Resistivity (1 KHz) ρ Ω - cm	$(dP_s/dT)\,\epsilon^{-1}$ x 10^{-10}	$(dP_s/dT)\,(\epsilon c)^{-1}$ x 10^{-10}	$(dP_s/dT)\,\rho^{1/2} c^{-1}$ x 10^{-4}	Reference	COMMENTS
$BaTiO_3$ (single crystal)	120	23			26	5							P1, H1	Absorbs 0.7 to 2μ (I3)
		30			25.5	2							C_3	Cannot be fully poled (S3)
		60	200	1 K	24	7	3.0	6	6×10^6	3.5	1.2	0.57		
		100			20	20								
SBN, x = 0.52[A]	115	25	380	1 K	29.2	6.5	2.1	5.2	1.6×10^8	1.7	0.81	4.0	G3, G4	Transmits 0.5-6.0μ (B5)
SBN, x = 0.33	62	25	1800	1 K	23.3	11			1.2×10^8	0.61	0.29	5.8	B1	
SBN, x= 0.25	47	25	5000	1 K	18	31			7.1×10^6	0.62	0.29	3.9		
NH_4IO_3	85	26	30	1 K	0.7	0.3		3.3	2.9×10^8	1			C4, K4	Transmits 0.35 to 2μ. Explodes above 180° C.
TGFB[B]	73	25	11	10 K	3.7	1.3	2.6	1.66		12	4.6		W1, S4	
		50	20	10 K	3.1	4.5	3.1			22	7.1		H2	
DTGS[C]	62.9	25	20	1 K	2.6	2.5	(2.5)	(1.7)	5×10^{10}	12	4.8	22	S5, B3	T_c depends on D_2 substitution for H_2. Only a maximum of 64.8% possible.
		50	80	1 K	1.8	7.5				9.4	3.8		B4	
$TGS_{0.67}\,TGFB_{0.33}$	58.9	25	(35)	1 K	2.9	3.0	(2.5)	(1.66)		9	3.4		B6	TGS:TGFB ratio can be varied to vary T_c
		50			1.75	8.2								
KTN[D]	54	25	900	800	9.3	2				0.22			A1	Transmits out to 6μ. $KTaO_3$ and $KNbO_3$ form solid solution. Parameters depend on composition (C6, T1)
		40	2500	800	8.4	20				1.3				
TGS[E]	49	10	35	1 K	3.0	1.5	2.4			4.4	1.8		P1, D1	Absorbs below 0.24μ (S9) and between 2 to > 400μ (M2). Transmits 0.25-1.8μ. Loss tan. increases below ambient with decreasing temp. (I4). Doping, Xray, and U. V. irradiation affect parameters (Z1, He, W6, C8, Y2, Y3, S9).
		25	50	1 K	2.75	3.5	2.5	1.65-1.68	1.8×10^{10}	7.0	2.8	19	S6, C5	
		40	150	1 K	2.0	11	2.8			7.3	2.6		K2	

TABLE A-1. PYROELECTRIC MATERIALS CHARACTERISTICS (CONTINUED)

MATERIAL	Curie Temperature T_c °C	Temperature of Measurement T °C	Dielectric Constant ϵ	Frequency of ϵ Measurement F Hz	Spontaneous Polarization P_s C cm^{-2} x 10^{-6}	Pyroelectric Constant dP_s/dT C cm^{-2} °K^{-1} x 10^{-8}	Specific Heat c J cm^{-3} °K^{-1}	Density s g cm^{-3}	A.C. Resistivity (1 KHz) ρ Ω - cm	$(dP_s/dT)\ \epsilon^{-1}$ x 10^{-10}	$(dP_s/dT)\ (\epsilon\ c)^{-1}$ x 10^{-10}	$(dP_s/dT)\ \rho^{1/2}\ c^{-1}$ x 10^{-4}	Reference	COMMENTS
TGS/Se(~15%Se) + additive	49	25	28	10 K		5	2.5		4×10^9	17.8	7.1	12.7	P2	Mullard (U.K.) Development; Material does not depole.
TGS/Se(~5%Se)	47	25	26	10 K		4.1	2.5		5×10^9	15.8	6.3	11.7	P2	Mullard (U. K.) Development; Material does not depole.
DTGSe(F)	34.5	25	(100)		3.2	7.5	(2.3)			7.5	3.3		M3	
TGSe(G)	22.2	0			3.0		2.1						H2, M3,	
		15	(100)		2.6	13	2.3			13	5.7		S7, S8, G7	
$Li_2SO_4 \cdot H_2O$	(M)	25	10.3	1 K	0.8	0.82	2.06			7.8	9.5		L1, A2, L3, W2	Will operate up to 95% relative humidity (C1). Has rather flat response over a wide temp. range (B1, N3).
		50	(10)		1					(10)	(12)			
$Li_2SeO_4 \cdot H_2O$		20				0.57							A2	
		79				0.65								
Polyvinylidene fluoride $(CH_2\ CF_2)_n$	not known, softens at 150°C melts at 177°C	25	11		2	0.24			6.7×10^9	2.2	0.9	0.82	B2, G5	Transmits 0.4-2μ absorbs 3-300μ. T_c (if it exists) may be near the melting point (N2)

TABLE A-1. PYROELECTRIC MATERIALS CHARACTERISTICS (CONTINUED)

MATERIAL	Curie Temperature T_c °C	Temperature of Measurement T °C	Dielectric Constant ϵ	Frequency of ϵ Measurement F Hz	Spontaneous Polarization P_s C cm^{-2} x 10^{-6}	Pyroelectric Constant dP_s/dT C cm^{-2} °K^{-1} x 10^{-8}	Specific Heat c J cm^{-3} °K^{-1}	Density s g cm^{-3}	A.C. Resistivity (1 KHz) ρ Ω - cm	$(dP_s/dT)\ \epsilon^{-1}$ x 10^{-10}	$(dP_s/dT)\ (\epsilon\ c)^{-1}$ x 10^{-10}	$(dP_s/dT)\ \rho^{1/2}\ c^{-1}$ x 10^{-4}	Reference	COMMENTS
SbSi	22	0	2200		22								F2	Also photoconductive (U3)
		10	2500		15	60	2.38	8.2		2.4	1.0		W2	
		15	3000		12	100				3.3	1.4			
GASH[H]	(M)	25	6	1 K	0.35	0.15	~ 1		9 x 10^{10}	2.5	2.5	4.5	H4,P1, N3	Ge isomorph (for Al) SeO_4 isomorph (for SO_4) (Ge and SeO_4) isomorph (for Al and SO_4). Similar performance (H4).
GUL[I]		25	4.6	1 K		0.62	~1.5		4 x 10^{11}	13.5	9	26	P1	
EDT[I]		25	7.0	1 K		0.2	~1		>10^{11}	3	3	>6	P1	dP_s/dT is constant from 20° to 80°C (N3)
Colemanite[K]	-7	-10	60	1 K	0.29	5.4	0.58	2.42		9	15.5		W3, C7	Depending on purity, T_c of 2.5°C is also reported (D2). Synthetic strontium isomorphs (polycrystalline) have been grown (W4, W5).
		-20	12	1 K	0.46	1.2				10	17			
KDDP[L]	-50±2	-60	50	1 K	4.0	10		2.36	8.6 x 10^7	20			M4, A3	Transmits 0.2 to 2μ.
$(NH_2CH_2COOH)\cdot HNO_3$	-67	-77	50	10 K	0.6	5	2.0	1.58		10	5		P3	
		-190	15	10 K	1.5	0.13				0.87				
$CS(NH_2)_2$ (Thiourea)	-104	-178	400		3.4	1		1.40		0.25			G9	
KH_2PO_4 (KDP)	-150	-178	2500	1K	4.8	3.3	0.94	2.34	7.2 x 10^6	0.13	0.14	1	B7, A3, D3, K3, S10	Transmits 0.2 to 2μ.

TABLE A-I. PYROELECTRIC MATERIALS CHARACTERISTICS (CONTINUED)

NOTES

Values in parentheses are based on assumptions.

A	SBN = $Sr_{1-x}Ba_xNb_2O_6$
B	TGFB = $(NH_2CH_2COOH)_3H_2BeF_4$
C	DTGS = $(ND_2CH_2COOD)_3D_2SO_4$
D	KTN = $KTa_{0.57}Nb_{0.43}O_3$
E	TGS = $(NH_2CH_2COOH)_3H_2SO_4$
F	DTGSe = $(ND_2CH_2COOH)_3D_2SeO_4$
G	TGSe = $(NH_2CH_2COOH)_3H_2SeO_4$
H	GASH = $(CN_3H_6)Al(SO_4)_2 \cdot 6H_2O$
I	GUL = Glucuronolactone = $CO \cdot (CHOH)_2 \cdot CH(O) \cdot CHOH \cdot CHO$
J	EDT = $C_2H_4(NH_3)_2C_4H_4O_6$
K	Colemanite = $2CaO \cdot 3B_2O_3 \cdot 5H_2O$
L	KDDP = KD_2PO_4 (~90%D_2)
M	Decomposes before T_c can be measured.

APPENDIX B - MEASURED DATA ON SELECTED PYROELECTRIC MATERIALS - OPTICAL TRANSMISSION - OPTICAL REFLECTANCE

DTGS	0.1 mm
TGS	0.1 mm
$Li_2SO_4 \cdot H_2O$	0.1 mm
Polyvinyl Fluoride	15 μm
$Se_{0.75}\ Ba_{0.25}\ Nb_2O_6$	1.5 mm
$LiTa_2O_3$	1.0 mm

Printed in U.S.A. 69TW740 910

Beckman DK-2 CHART

WHEN REORDERING SPECIFY CHART NO 566402 BECKMAN INSTRUMENTS INC., FULLERTON, CALIF., U.S.A.

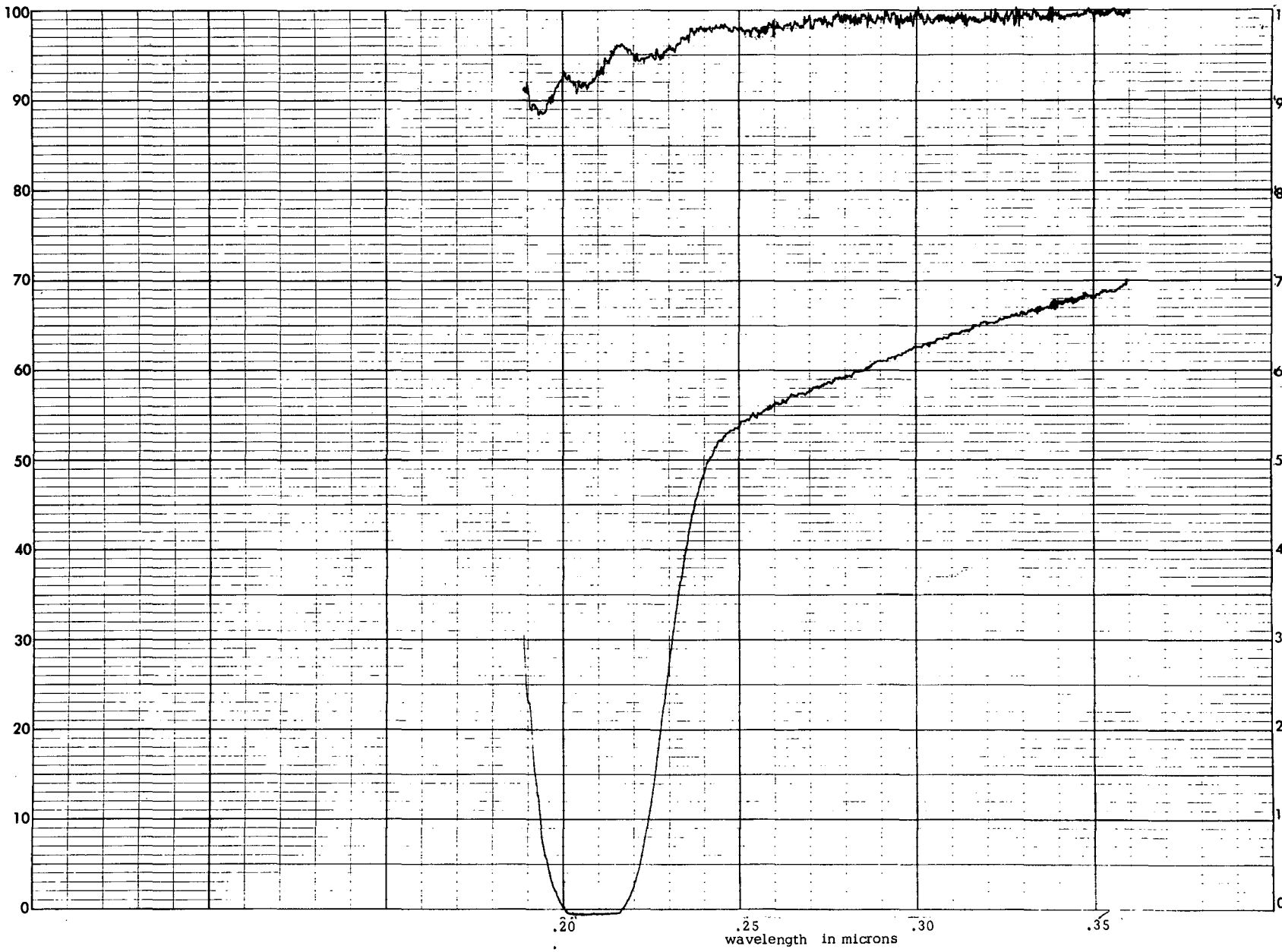

SAMPLE DTGS

PATH 1×10^{-2} cm

ORIGIN BEC

SOLVENT

Trans. at normal incidence

REF Air

SPEED: 5 nm/min

SCALE 0-100%T

SENS 100

PERIOD 0.2 sec.

SOURCE: W

H_2

D_2

DETECTOR: PM ✓

PbS

ANALYST JB

DATE 1/25/72

Printed in U.S.A. 69TW740 910

Beckman DK-2 CHART

WHEN REORDERING SPECIFY CHART NO. 566402 BECKMAN INSTRUMENTS INC., FULLERTON, CALIF., U.S.A.

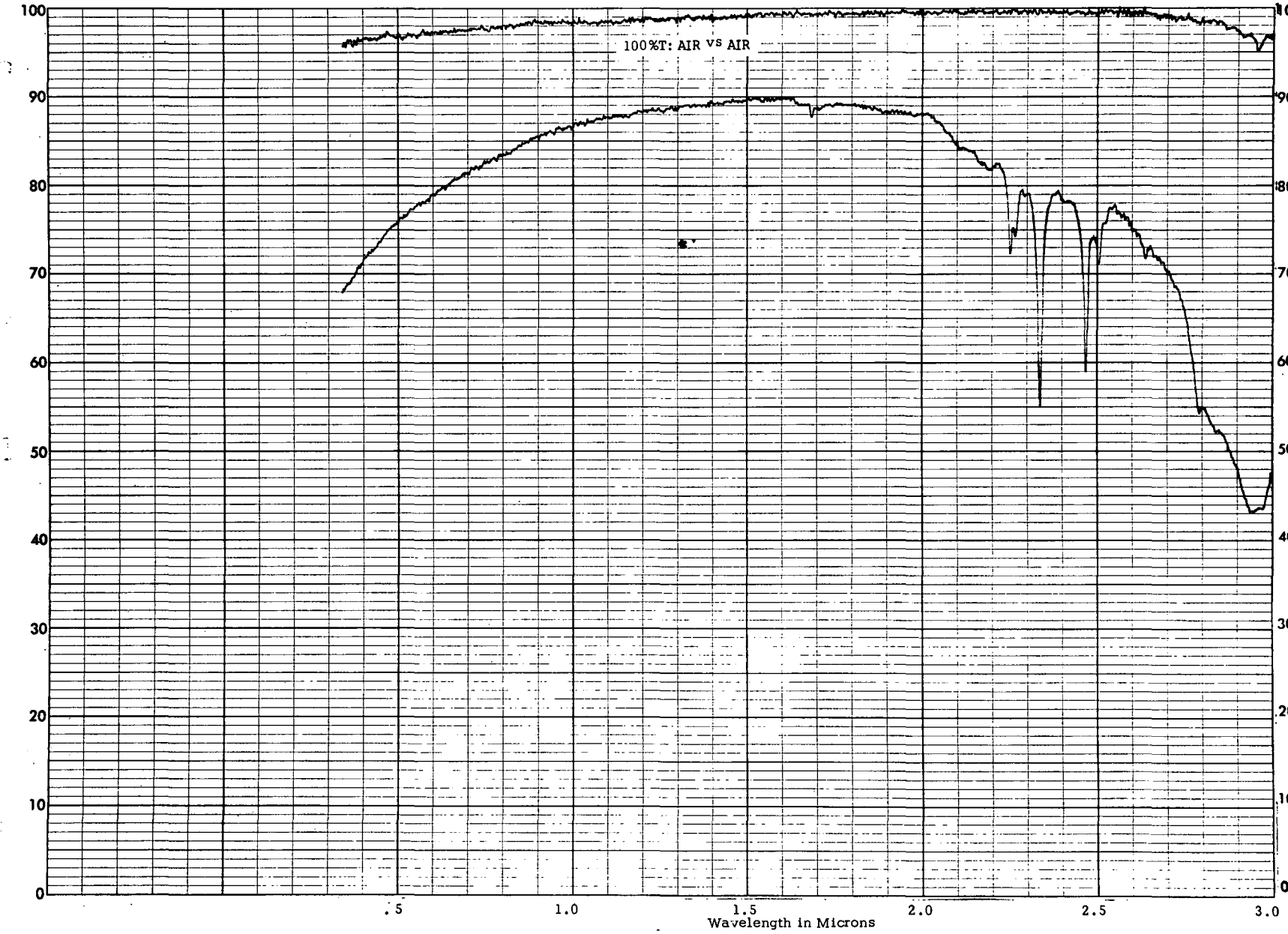

SAMPLE DTGS

PATH 1×10^{-2} cm

ORIGIN BEC

SOLVENT

DK-2 Transmission at Normal Incidence

REF AIR

SPEED: 5 Div/ nm/min

SCALE 0-100% T

SENS 100

PERIOD 0.2 Sec.

SOURCE: W ✓

H_2

D_2

DETECTOR: PM

PbS ✓

ANALYST JB

DATE 1/18/72

B2

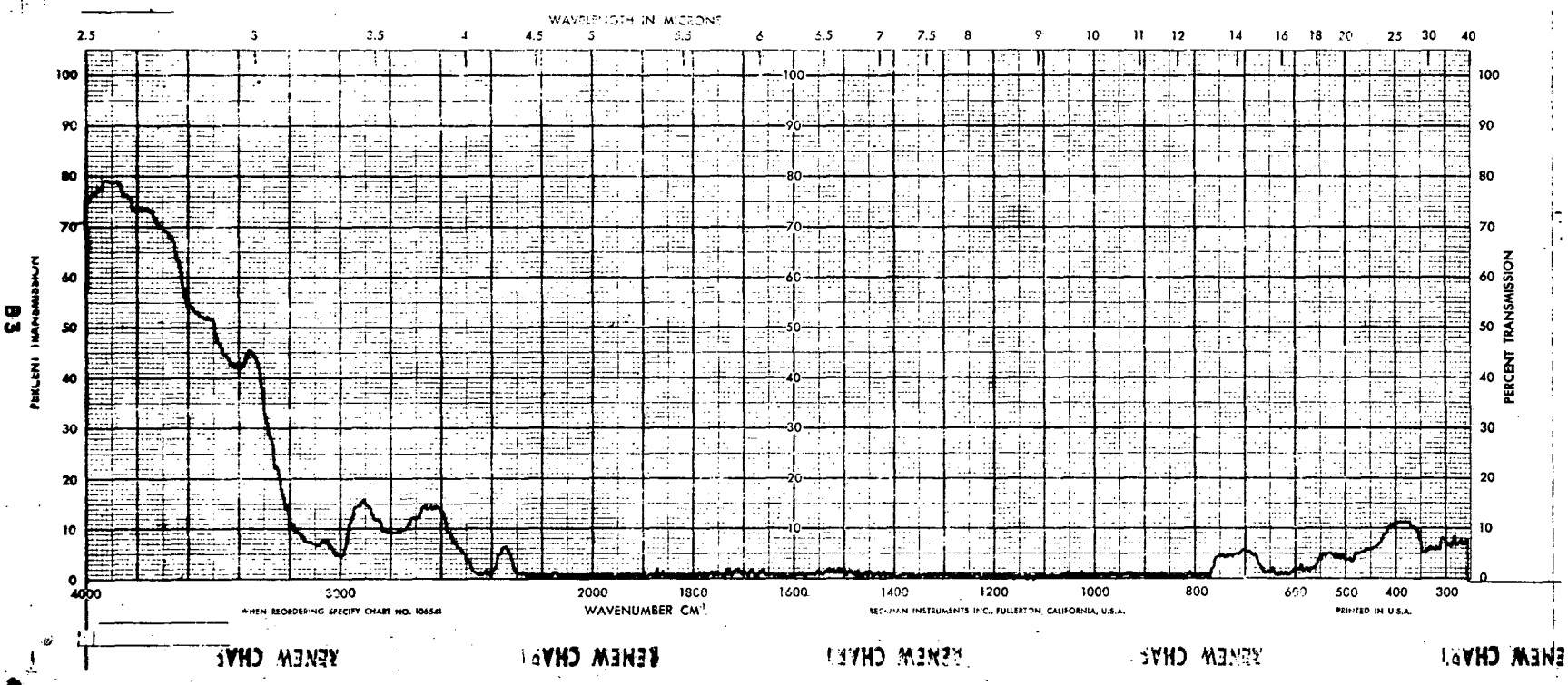

SPECTRUM NO. Jan. 25, 1972
DATE
SAMPLE DTGS
SOURCE BEC
STRUCTURE
IR-20 Transmission at Normal Incidence
PATH 0.1 mm
SOLVENT
CONCENTRATION
PHASE
COMMENTS
ANALYST AWB

Beckman
INFRARED
SPECTROPHOTOMETER

Printed in U.S.A. 69TW740

Beckman DK-2 CHART

566402

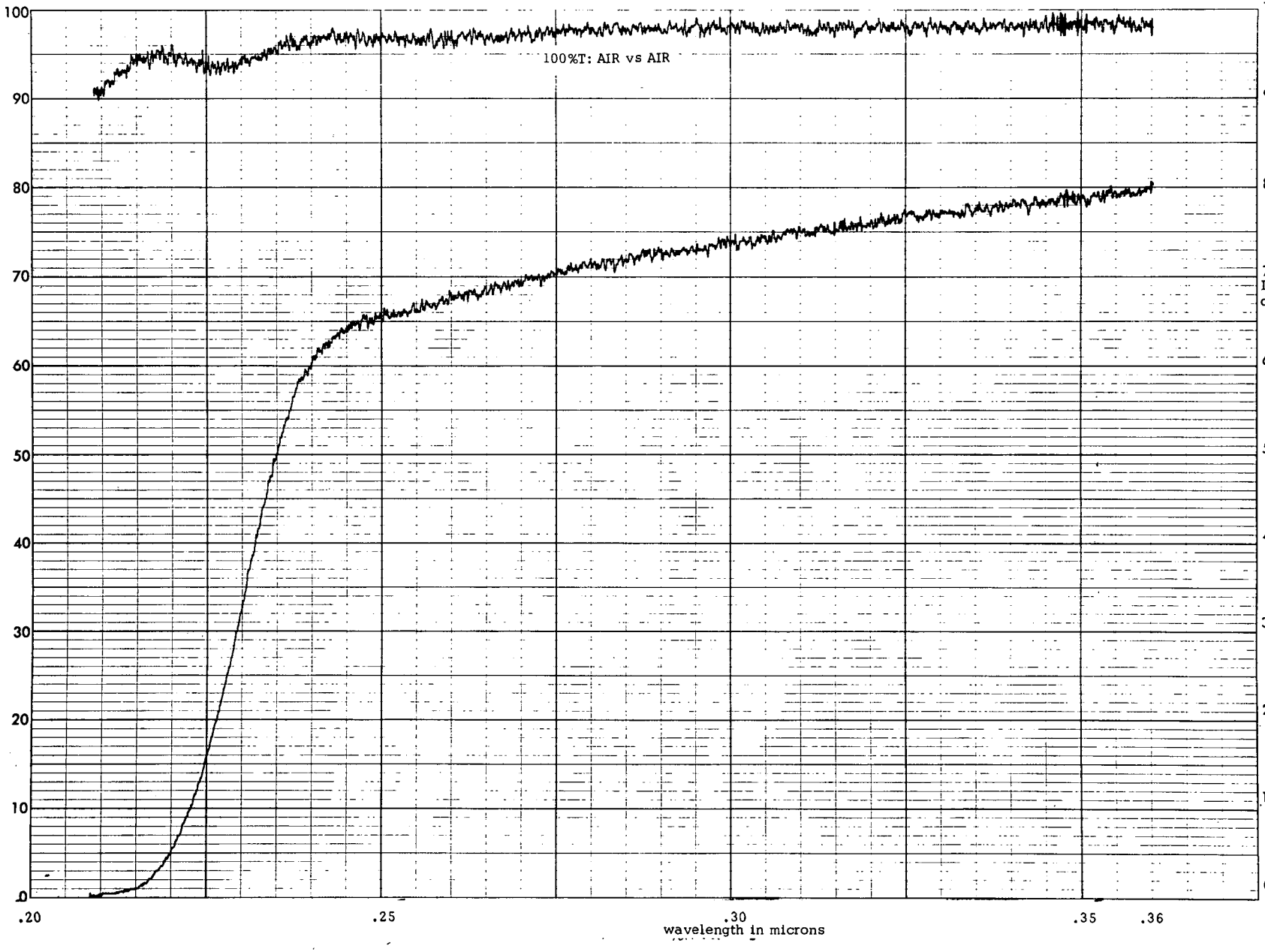

SAMPLE

TGS

PATH 1×10^{-2} cm

ORIGIN BEC

SOLVENT

DK-2 Transmission at Normal Incidence

REF AIR

SPEED: 5 Div / nm/min

SCALE 0-100% T

SENS 100

PERIOD 0.2 Sec

SOURCE: W

H_2

D_2 ✓

DETECTOR: PM

PbS ✓

ANALYST AWB

DATE 12-21-71

B4

Printed in U.S.A. 69TW740 910

Beckman DK-2 CHART

WHEN REORDERING SPECIFY CHART NO. 566402 BECKMAN INSTRUMENTS INC., FULLERTON, CALIF., U.S.A.

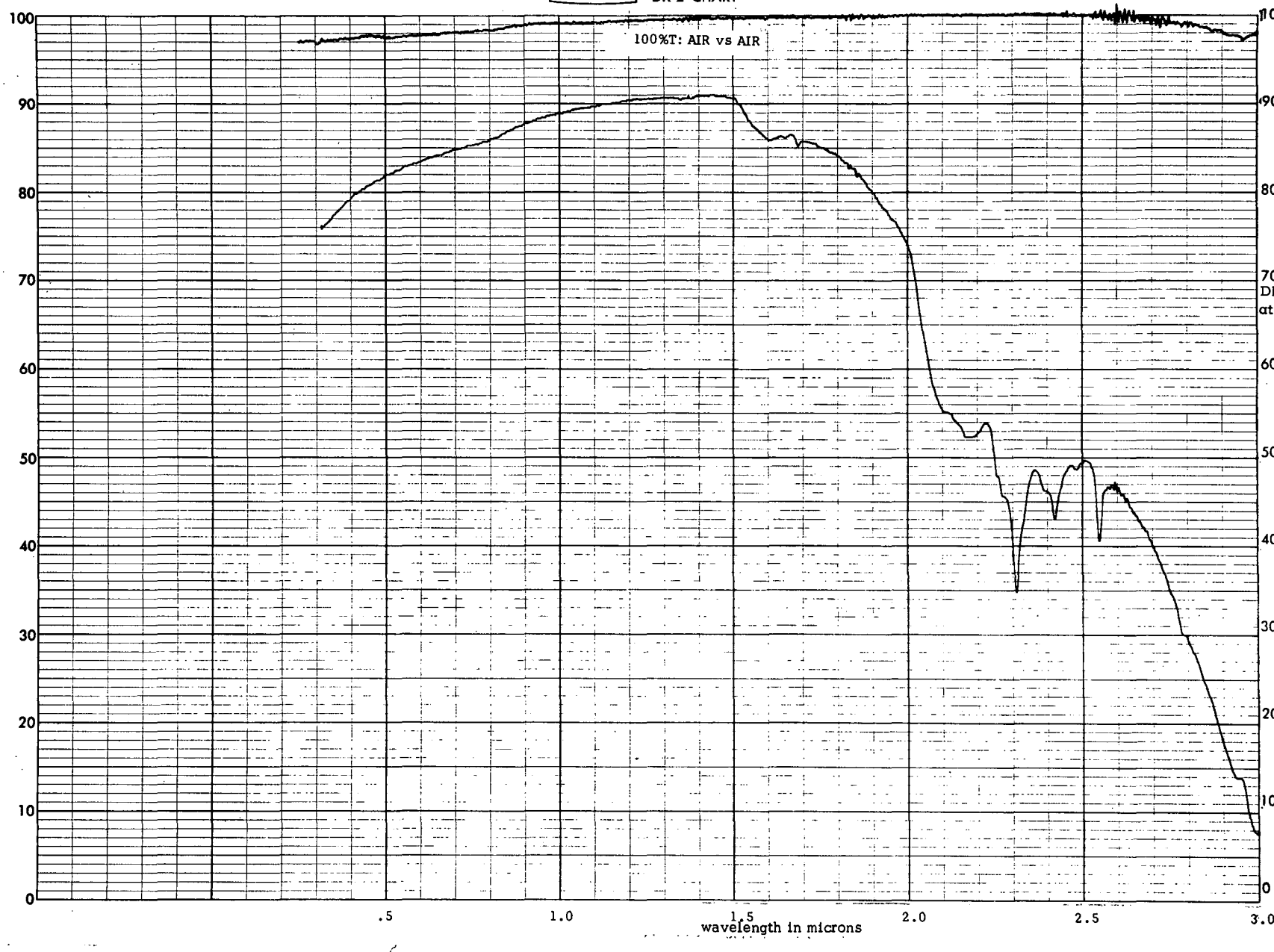

SAMPLE

TGS

PATH 1×10^{-2} cm

ORIGIN BEC

SOLVENT

DK-2 Transmission at Normal Incidence

REF AIR

SPEED: 5 Div / nm/min

SCALE 0-100% T

SENS 70

PERIOD 0.2 Sec

SOURCE: W ✓

H_2

D_2

DETECTOR: PM

PbS ✓

ANALYST AWB

DATE 12-29-71

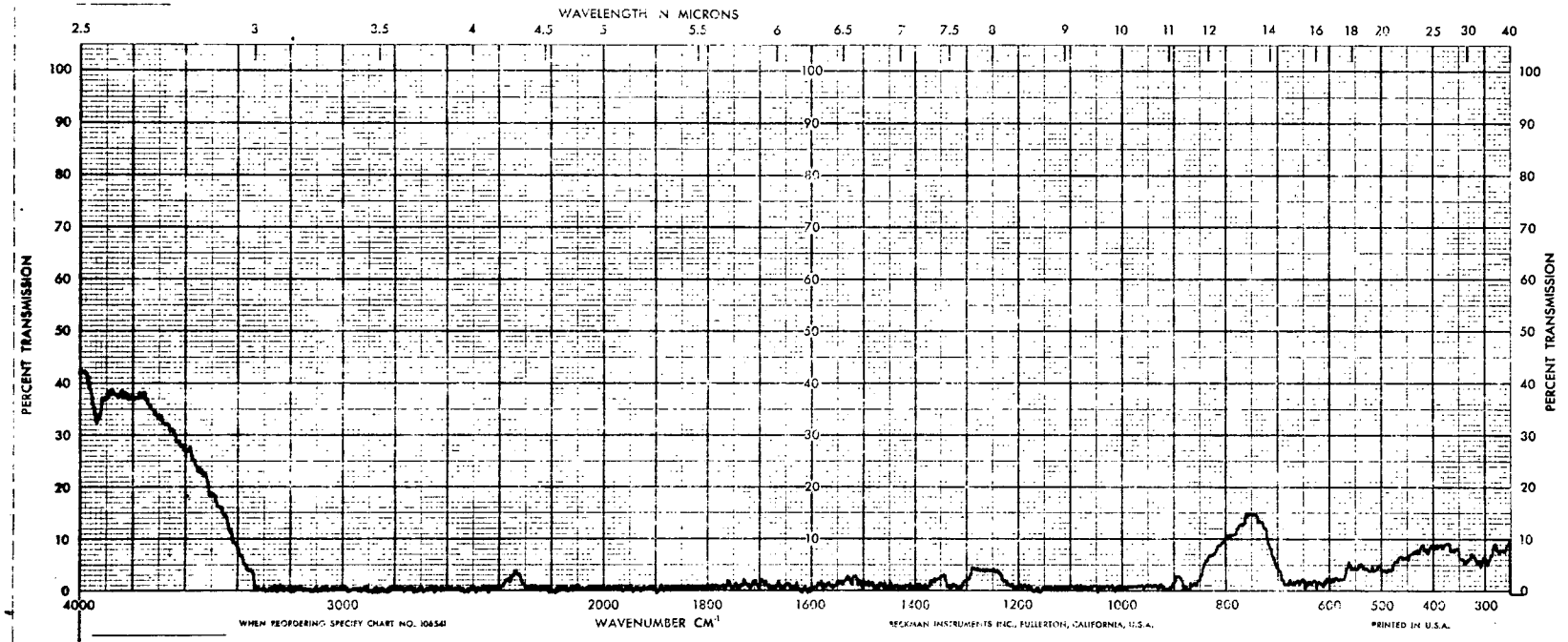

SPECTRUM NO. _____

DATE 12/20/71

SAMPLE TGS - 0.1 mm

SOURCE BEC

STRUCTURE

IR-20, T 1 incidence

PATH 0.1 mm

SOLVENT _____

CONCENTRATION _____

PHASE _____

COMMENTS _____

ANALYST AWB

Beckman

INFRARED

SPECTROPHOTOMETER

Printed in U.S.A. 69TW740 910

Beckman DK-2 CHART

566402 BECKMAN INSTRUMENTS, INC., FULLERTON, CALIF., U.S.A.

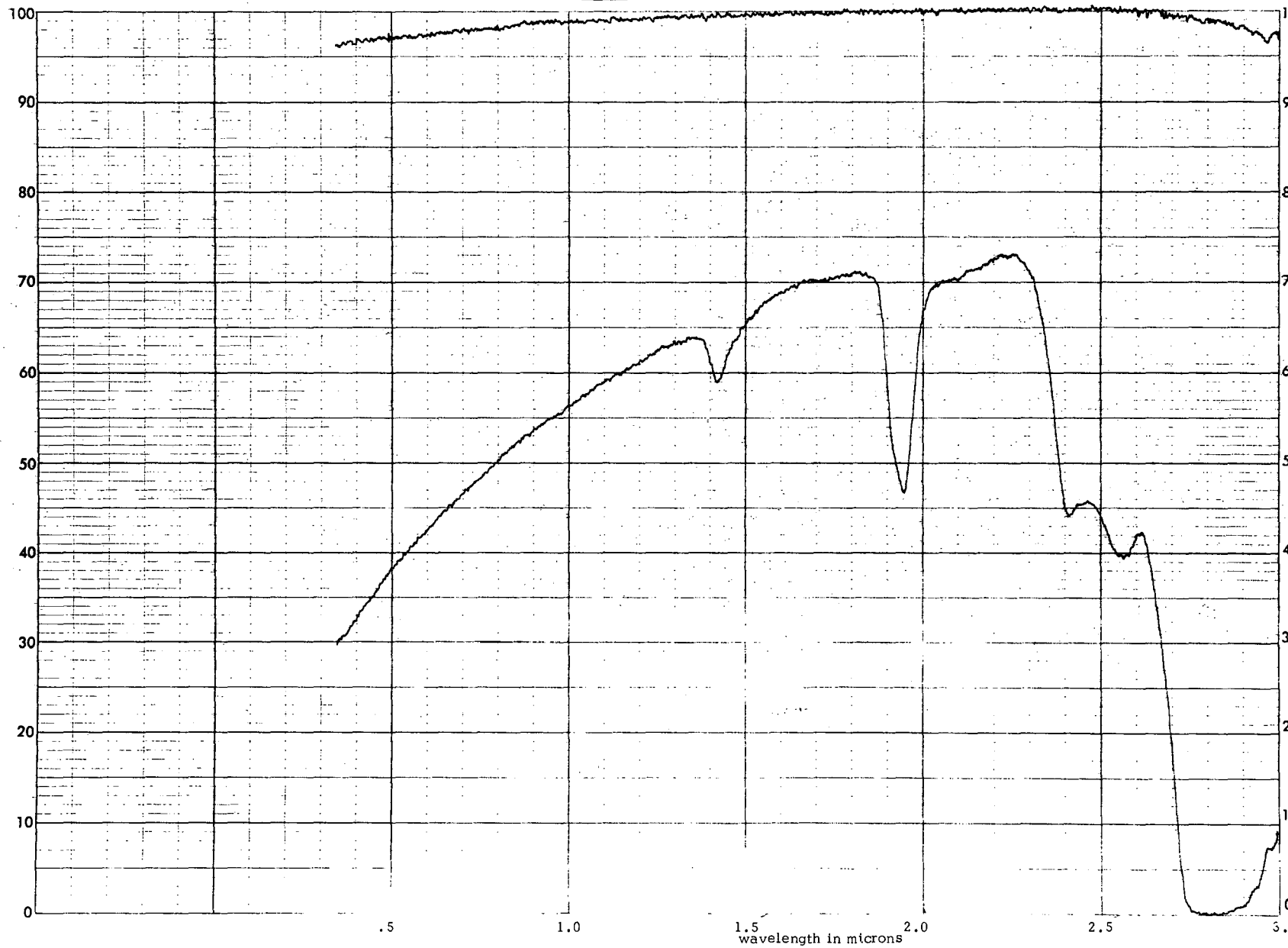

SAMPLE $Li_2SO_4 \cdot H_2O$

PATH 0.01 cm

ORIGIN Clevite

SOLVENT

REF AIR

SPEED: 5 nm/min

SCALE 0-100% T

SENS 100

PERIOD 0.2

SOURCE: W x

H_2

D_2

DETECTOR: PM

PbS

ANALYST JB

DATE 1/31/72

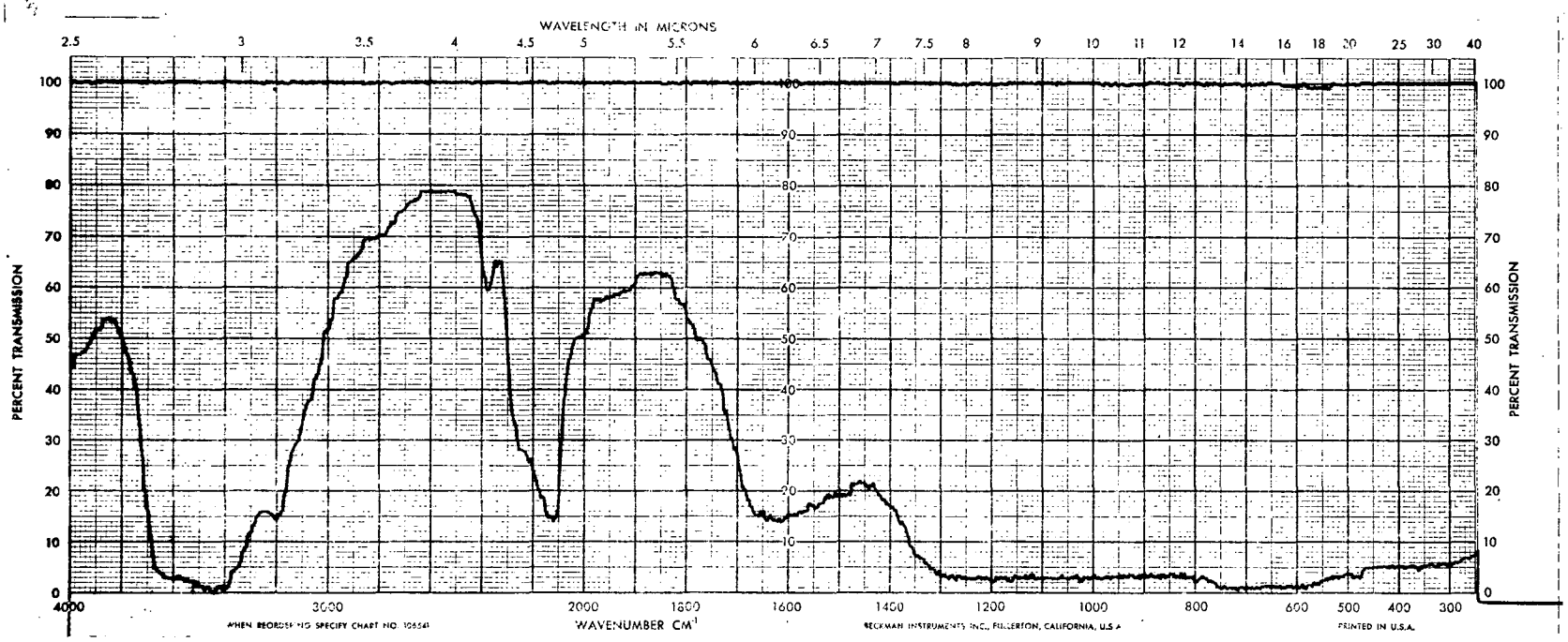

SPECTRUM NO. _____

DATE 1/31/72

SAMPLE $Li_2SO_4H_2O$

SOURCE Clevite

STRUCTURE

PATH 0.1 mm

SOLVENT _____

CONCENTRATION _____

PHASE _____

COMMENTS _____

ANALYST JB

Beckman

INFRARED

SPECTROPHOTOMETER

Printed in U.S.A. 68TW740 910

Beckman DK-2 CHART

WHEN REORDERING SPECIFY CHART NO. 566402 BECKMAN INSTRUMENTS INC., FULLERTON, CALIF., U.S.A.

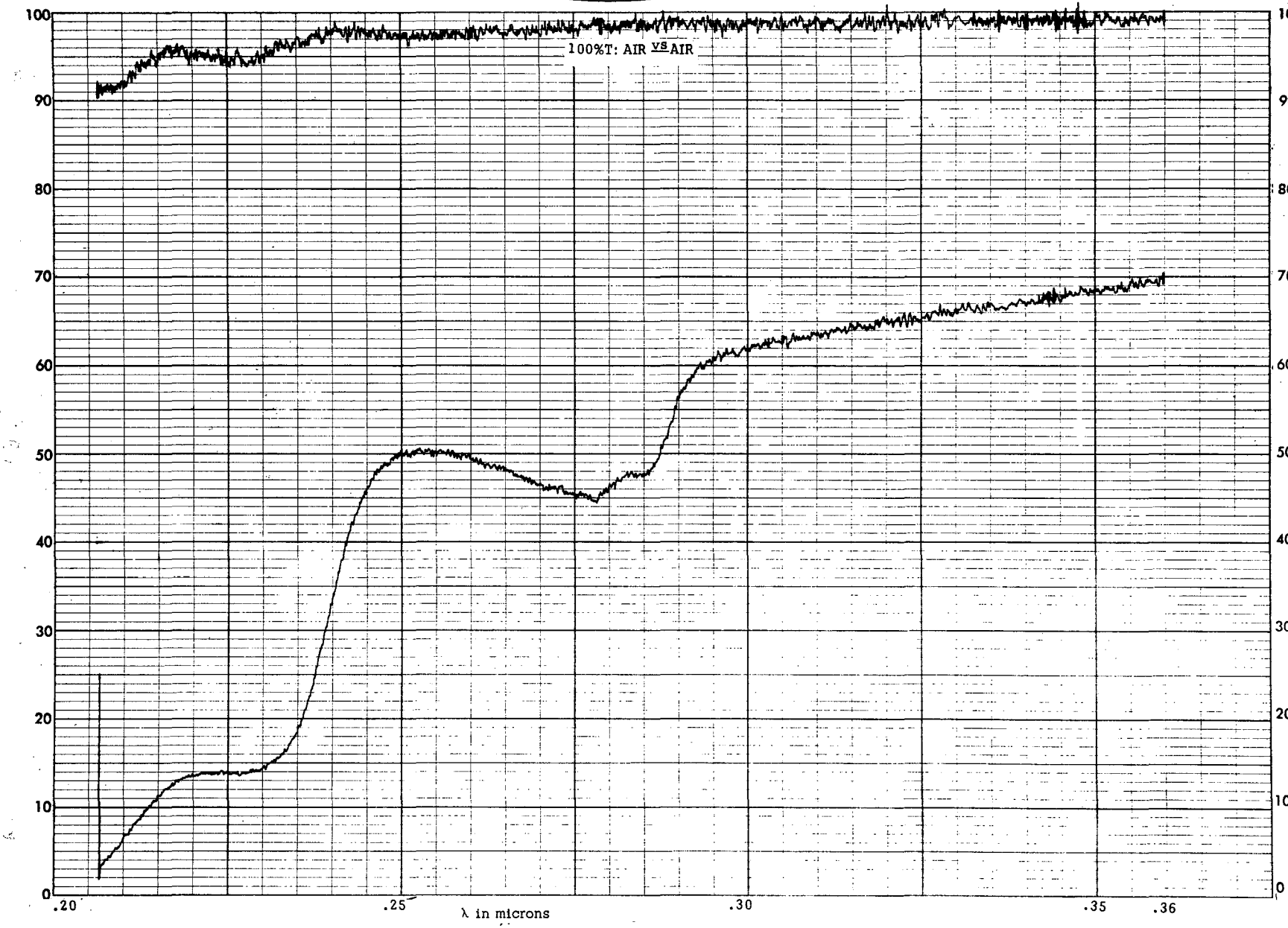

SAMPLE "Tedlar" PVF Films 50AG207R

PATH 15 x 10^{-4} cm

ORIGIN Dupont

SOLVENT

DK-2 Transmission at normal incidence

REF AIR

SPEED: 5 Div / nm/min

SCALE 0-100%T

SENS 100

PERIOD 0.2 Sec

SOURCE: W

H_2

D_2 ✓

DETECTOR: PM ✓

PbS

ANALYST AWB

DATE 12-21-71

69

Printed in U.S.A. 69TW740

Beckman DK-2 CHART 566402

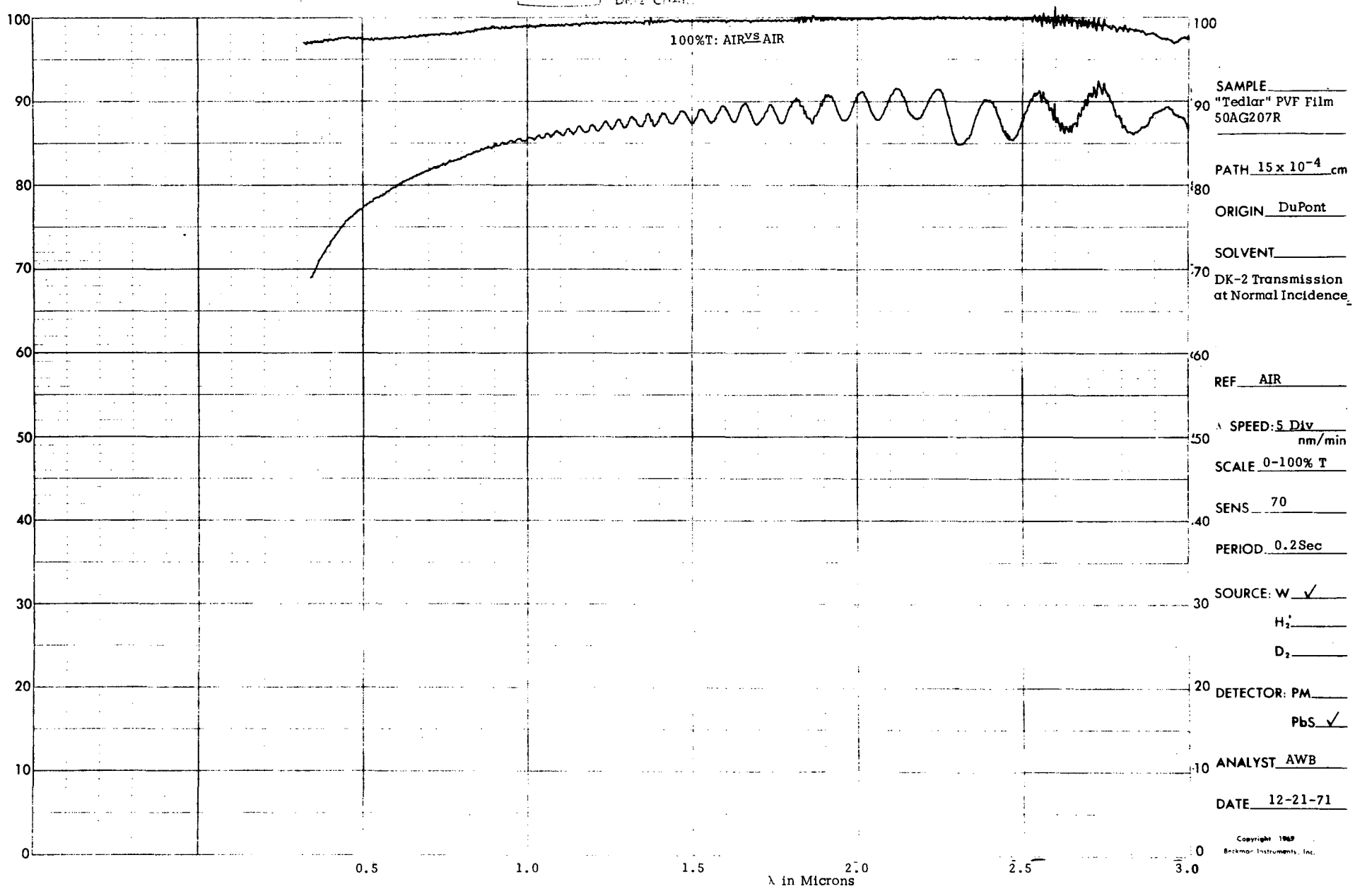

SAMPLE "Tedlar" PVF Film 50AG207R

PATH 15×10^{-4} cm

ORIGIN DuPont

SOLVENT

DK-2 Transmission at Normal Incidence

REF AIR

λ SPEED: 5 Div nm/min

SCALE 0-100% T

SENS 70

PERIOD 0.2Sec

SOURCE: W ✓

H_2

D_2

DETECTOR: PM

PbS ✓

ANALYST AWB

DATE 12-21-71

B10

Printed in U.S.A. 69TW740 910

Beckman DK-2 CHART

WHEN REORDERING SPECIFY CHART NO. 566402 BECKMAN INSTRUMENTS INC., FULLERTON, CALIF., U.S.A.

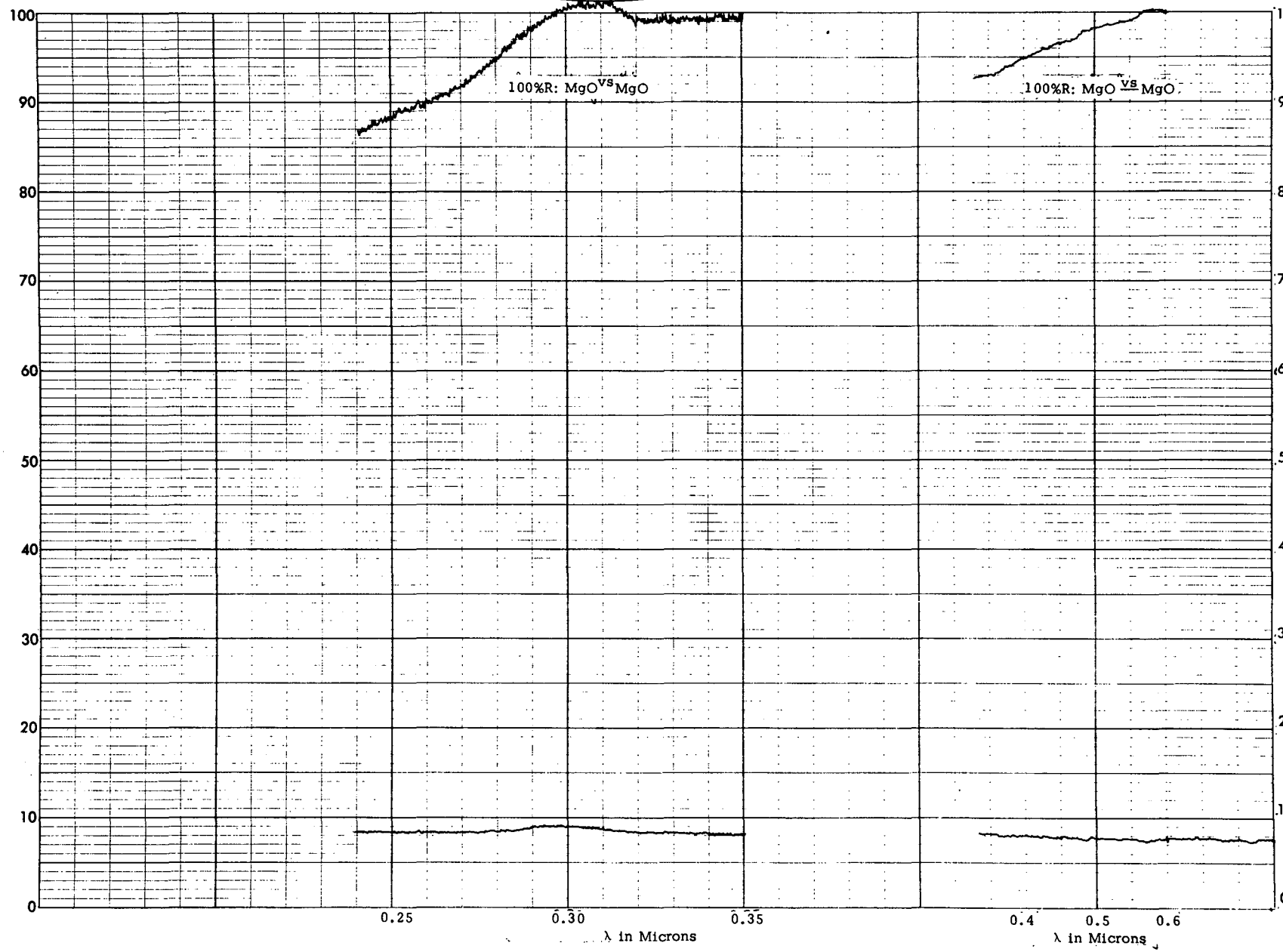

SAMPLE Tedlar PVP Film 50AG207R

PATH 15×10^{-4} cm

ORIGIN DuPont

SOLVENT DK-2 Reflectance at 5° Incidence

REF MgO

λ SPEED: 5 Div/Min, nm/min

SCALE 0-100%R

SENS 100

PERIOD 0.2Sec

SOURCE: W

H_2

D_2 ✓

DETECTOR: PM ✓

PbS

ANALYST AWB

DATE 12-29-71

B 11

Printed in U.S.A. 69TW740 910

Beckman DK-2 CHART

WHEN REORDERING SPECIFY CHART NO. 566402 BECKMAN INSTRUMENTS INC., FULLERTON, CALIF., U.S.A.

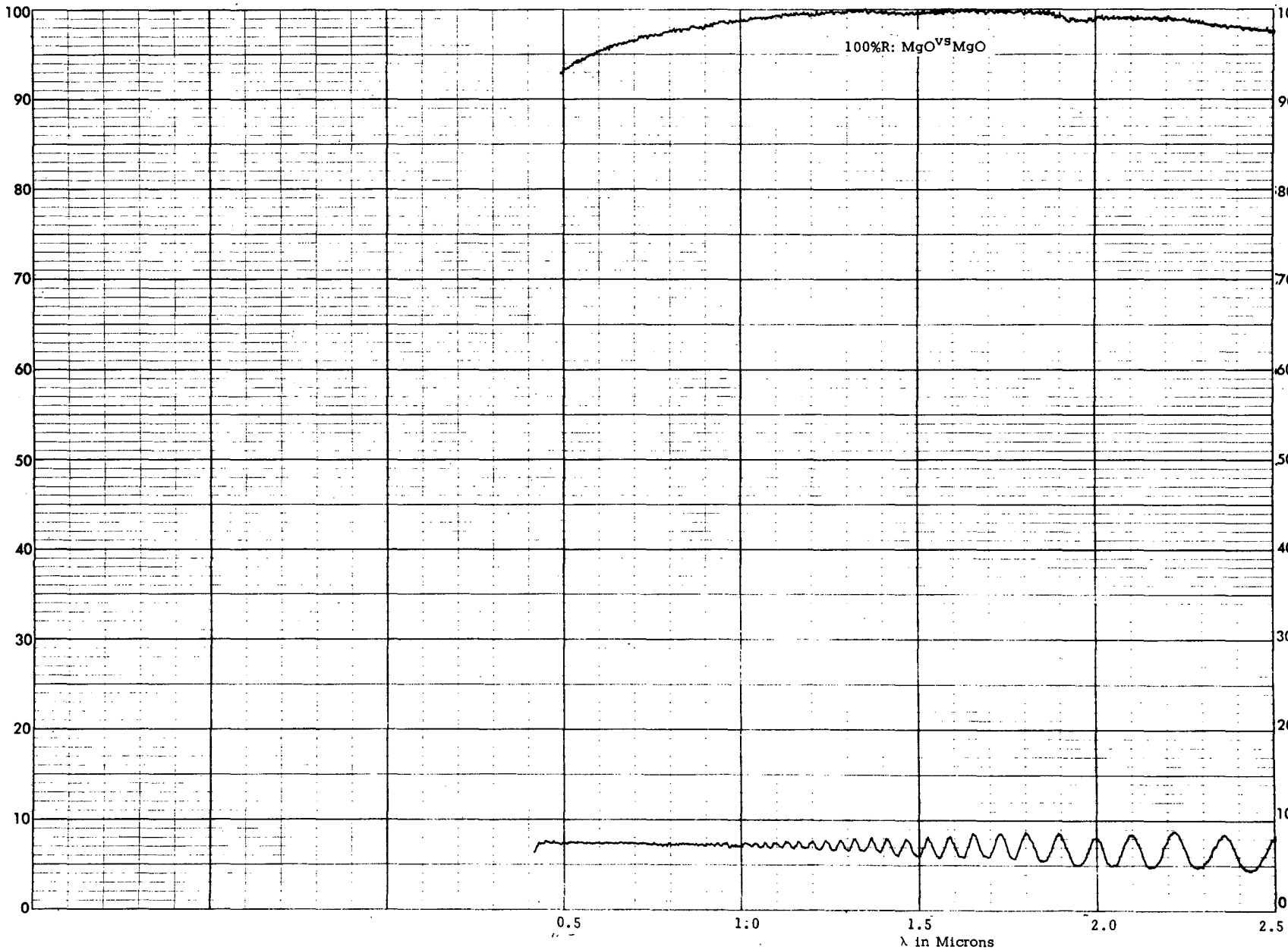

SAMPLE Tedlar PVF Film 50AG207R

PATH 15×10^{-4} cm

ORIGIN DuPont

SOLVENT DK-2 Reflectance at 5° Incidence

REF MgO

λ SPEED: 5 Div nm/min

SCALE 0-100%R

SENS 100

PERIOD 0.25 Sec.

SOURCE: W ✓

H_2

D_2

DETECTOR: PM

PbS ✓

ANALYST AWB

DATE 12-29-71

B12

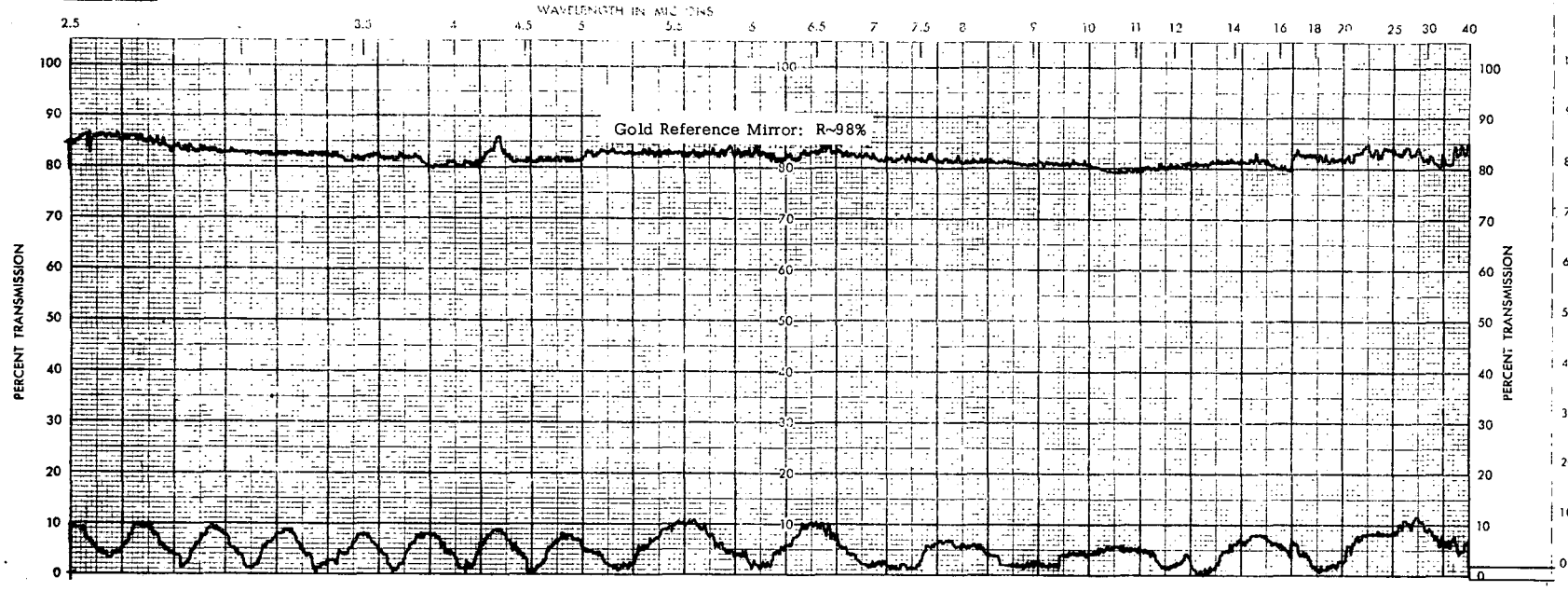

SPECTRUM NO. _____
DATE 12-21-71
SAMPLE "Tedlar" PVF Films
50AG207R
SOURCE DuPont
STRUCTURE
IR-20 Reflectance at 30° Incidence
PATH ____ mm
SOLVENT _____
CONCENTRATION _____
PHASE _____
COMMENTS _____
ANALYST AWB

Beckman

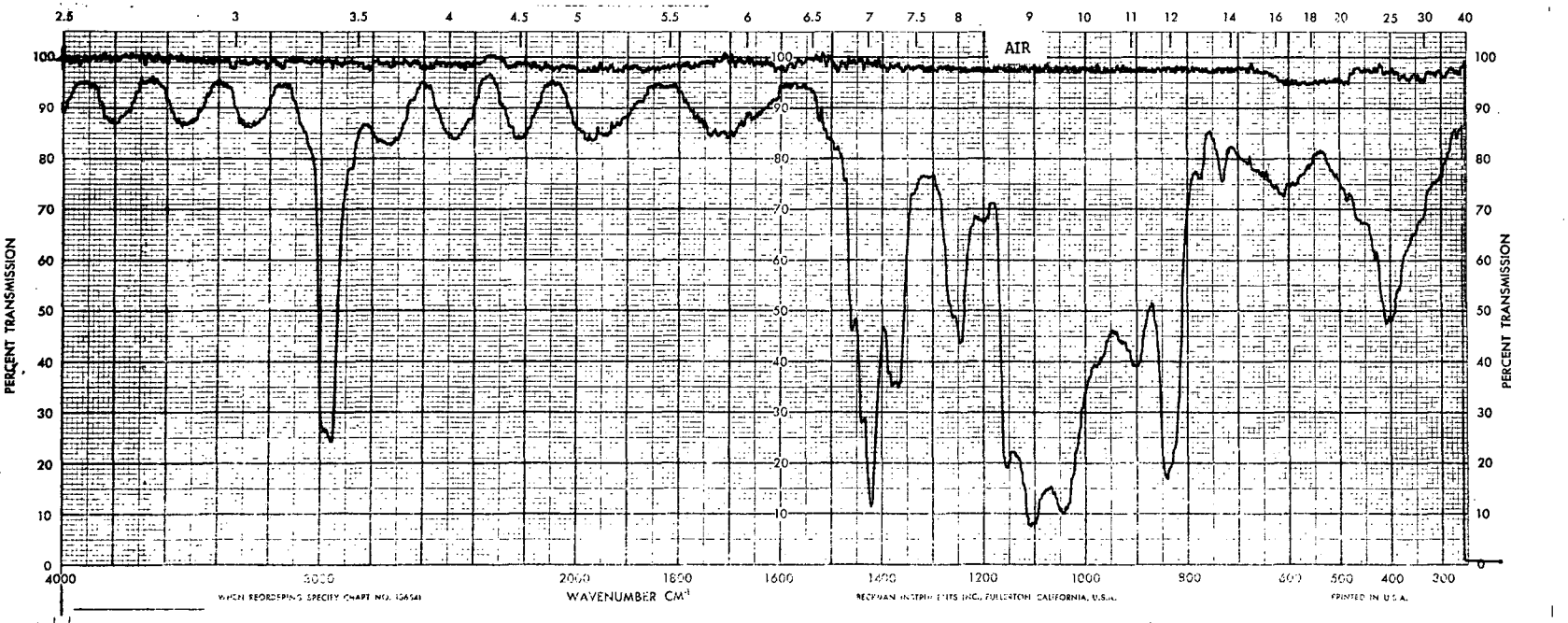

SPECTRUM NO. _____
DATE 12-21-71
SAMPLE "Tedlar" PVF Films
50AG207R
SOURCE Dupont
STRUCTURE
IR-20 Transmission at Normal Incidence
15×10^{-3}
PATH ____ mm
SOLVENT _____
CONCENTRATION _____
PHASE _____
COMMENTS _____
ANALYST AWB

Beckman
INFRARED
SPECTROPHOTOMETER

B13

Printed in U.S.A. 69TW740 910

Beckman DK-2 CHART

WHEN REORDERING SPECIFY CHART NO. 566402 BECKMAN INSTRUMENTS INC., FULLERTON, CALIF., U.S.A.

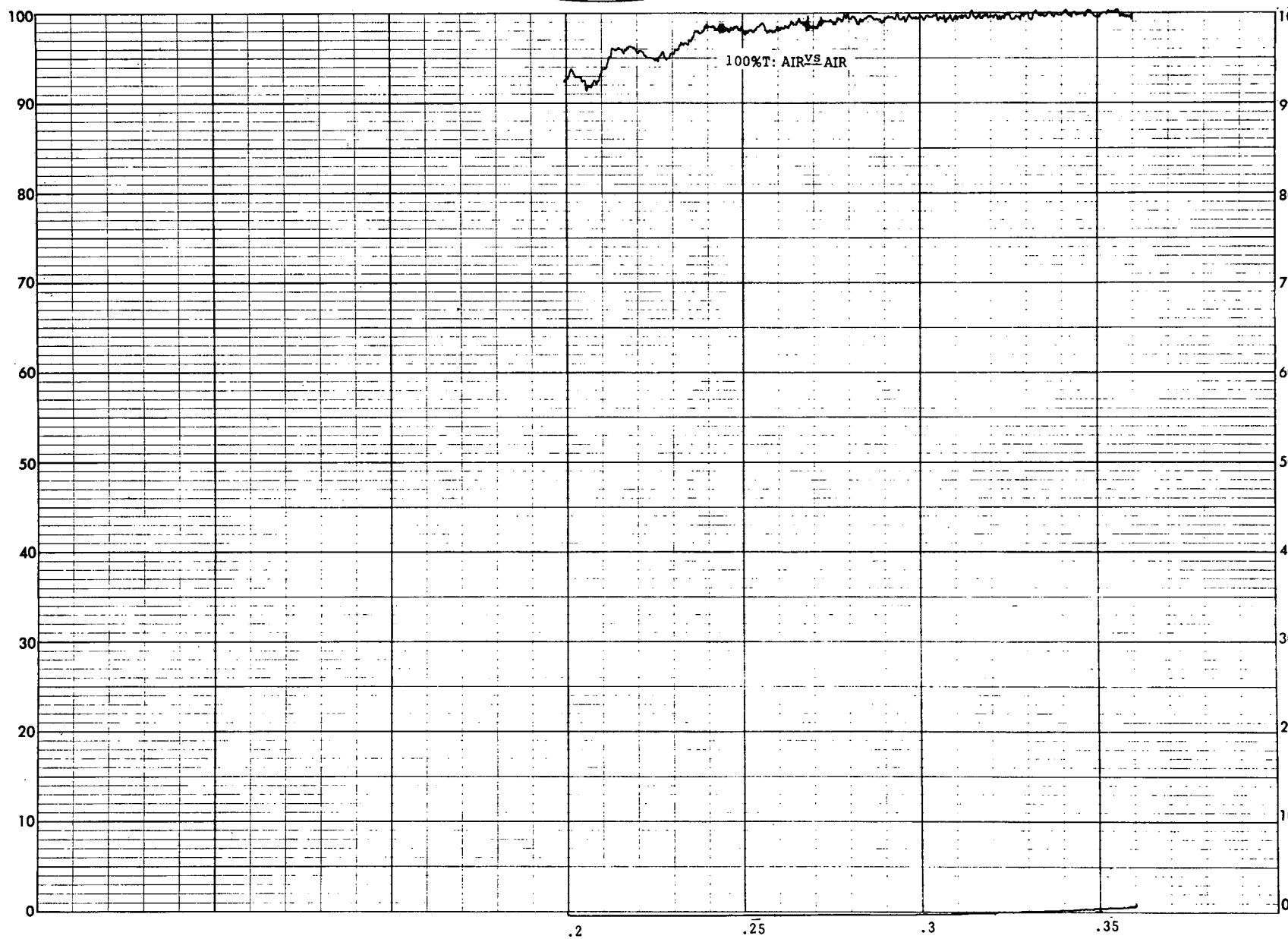

SAMPLE $Se_{0.75}Ba_{0.25}Nb_2O_6$

PATH 0.15 cm

ORIGIN Crystal Tech.

SOLVENT

Transmission at Normal Incidence

REF Air

λ SPEED: 5 nm/min

SCALE 0-100%T

SENS 100

PERIOD 0.25 Sec

SOURCE: W ✓

H_2

D_2

DETECTOR: PM

PbS ✓

ANALYST JB

DATE 12-16-71

B14

Printed in U.S.A. 69TW740 910

Beckman DK-2 CHART

WHEN REORDERING SPECIFY CHART NO. 566402 BECKMAN INSTRUMENTS INC., FULLERTON, CALIF., U.S.A.

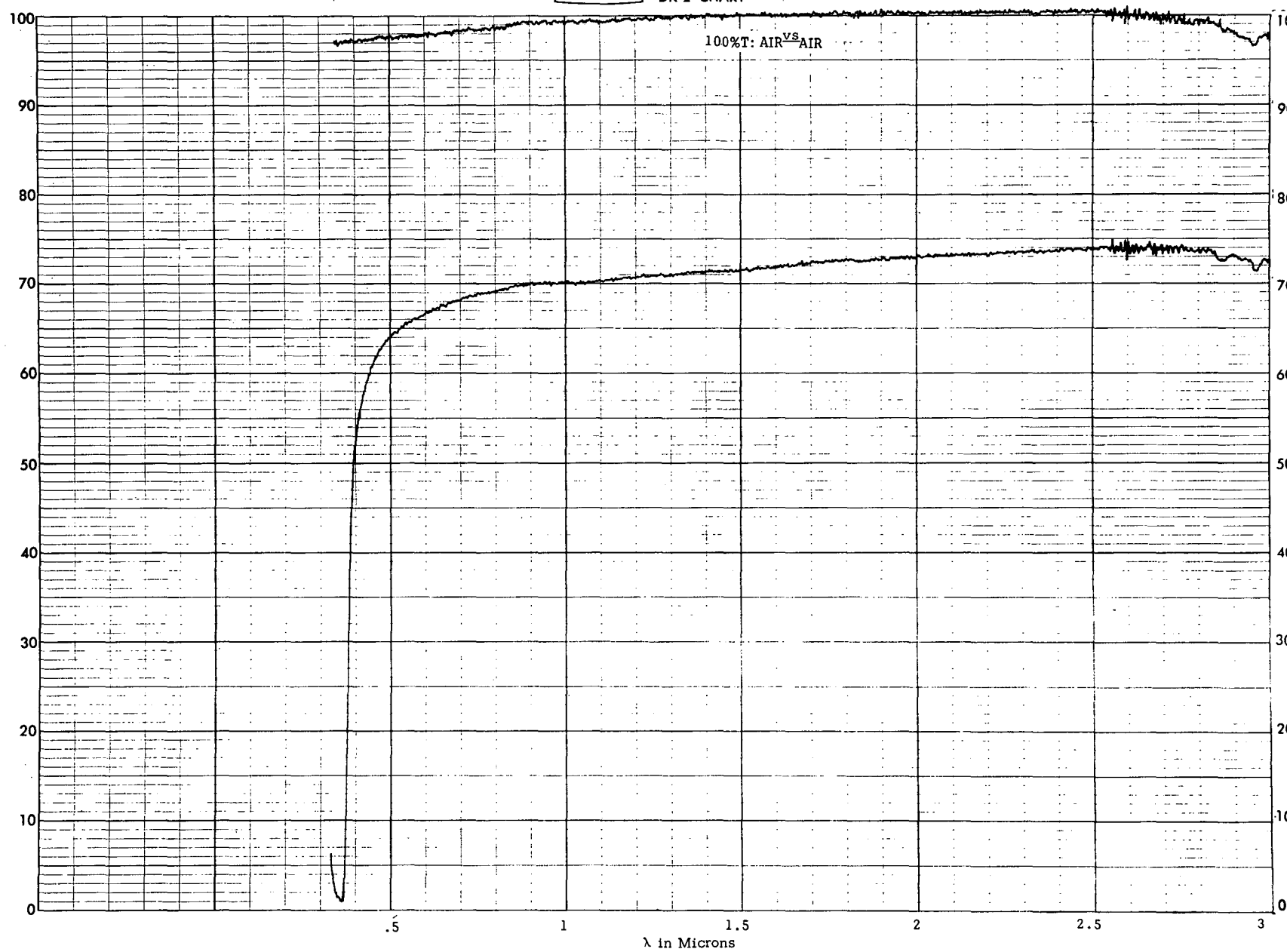

SAMPLE $Se_{0.75}Ba_{0.25}NbO_6$

PATH 0.15 cm

ORIGIN Crystal Tech

SOLVENT

Transmission at Normal Incidence

REF AIR

λ SPEED: 5 nm/min

SCALE 0-100%T

SENS 100

PERIOD 0.2 Sec

SOURCE: W ✓

H_2

D_2

DETECTOR: PM

PbS ✓

ANALYST JB

DATE 12-16-71

B 15

Printed in U.S.A. 69TW740 910 Beckman DK-2 CHART WHEN REORDERING SPECIFY CHART NO 566402 BECKMAN INSTRUMENTS INC., FULLERTON, CALIF., U.S.A.

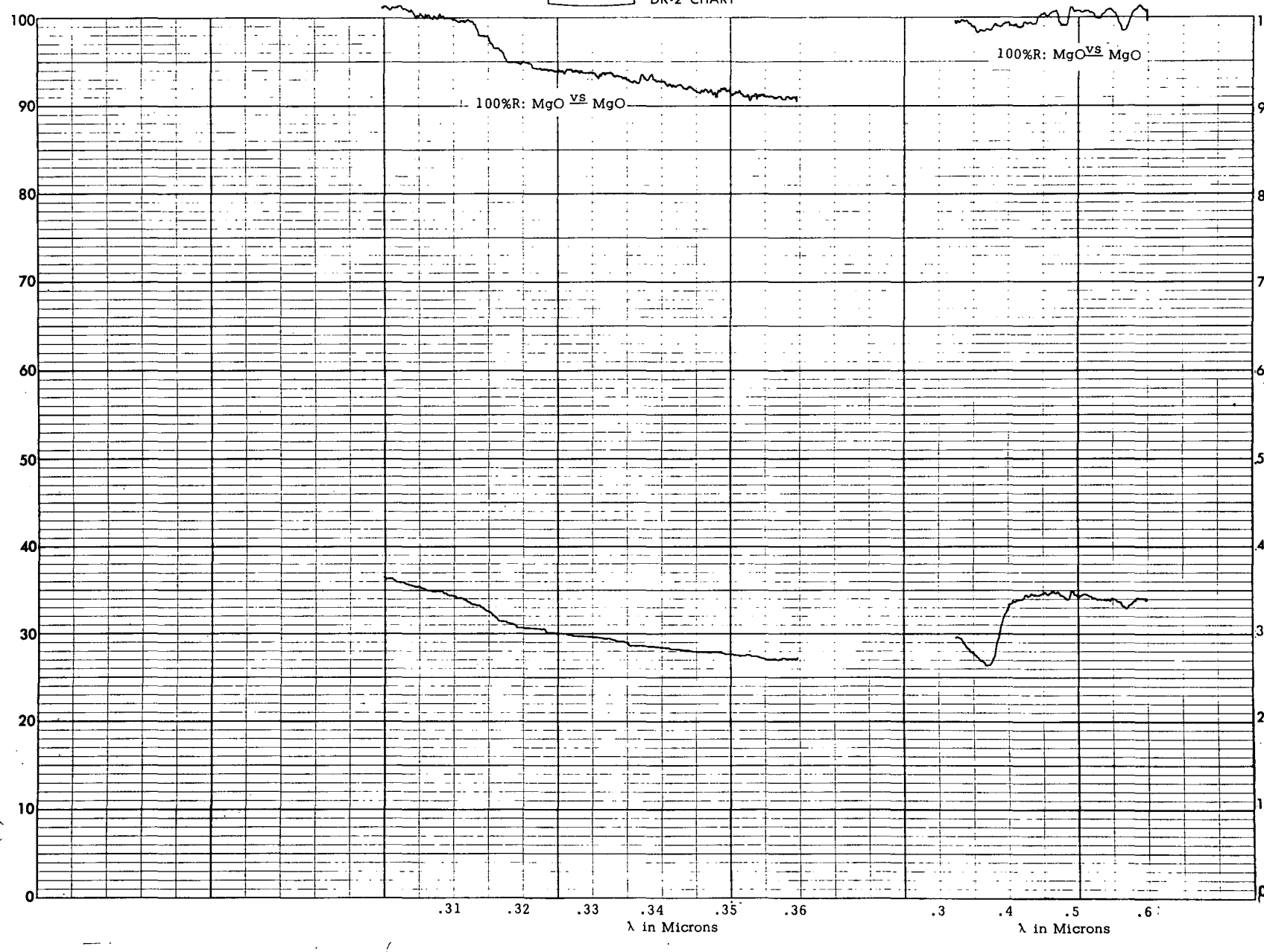

SAMPLE $Se_{0.75}Ba_{0.25}Nb_2O_6$

PATH _____ cm

ORIGIN Crystal Tech'

SOLVENT _____

DK-2 Reflectance at 5° Incidence

REF MgO

λ SPEED: 5 nm/min

SCALE 0-100%R

SENS 150

PERIOD 0.25 Sec

SOURCE: W _____

H_2 _____

D_2 ✓

DETECTOR: PM ✓

PbS _____

ANALYST IB

DATE 12-16-71

Printed in U.S.A. 69TW740 910

Beckman DK-2 CHART

WHEN REORDERING SPECIFY CHART NO. 566402 BECKMAN INSTRUMENTS, INC. FULLERTON, CALIF., U.S.A.

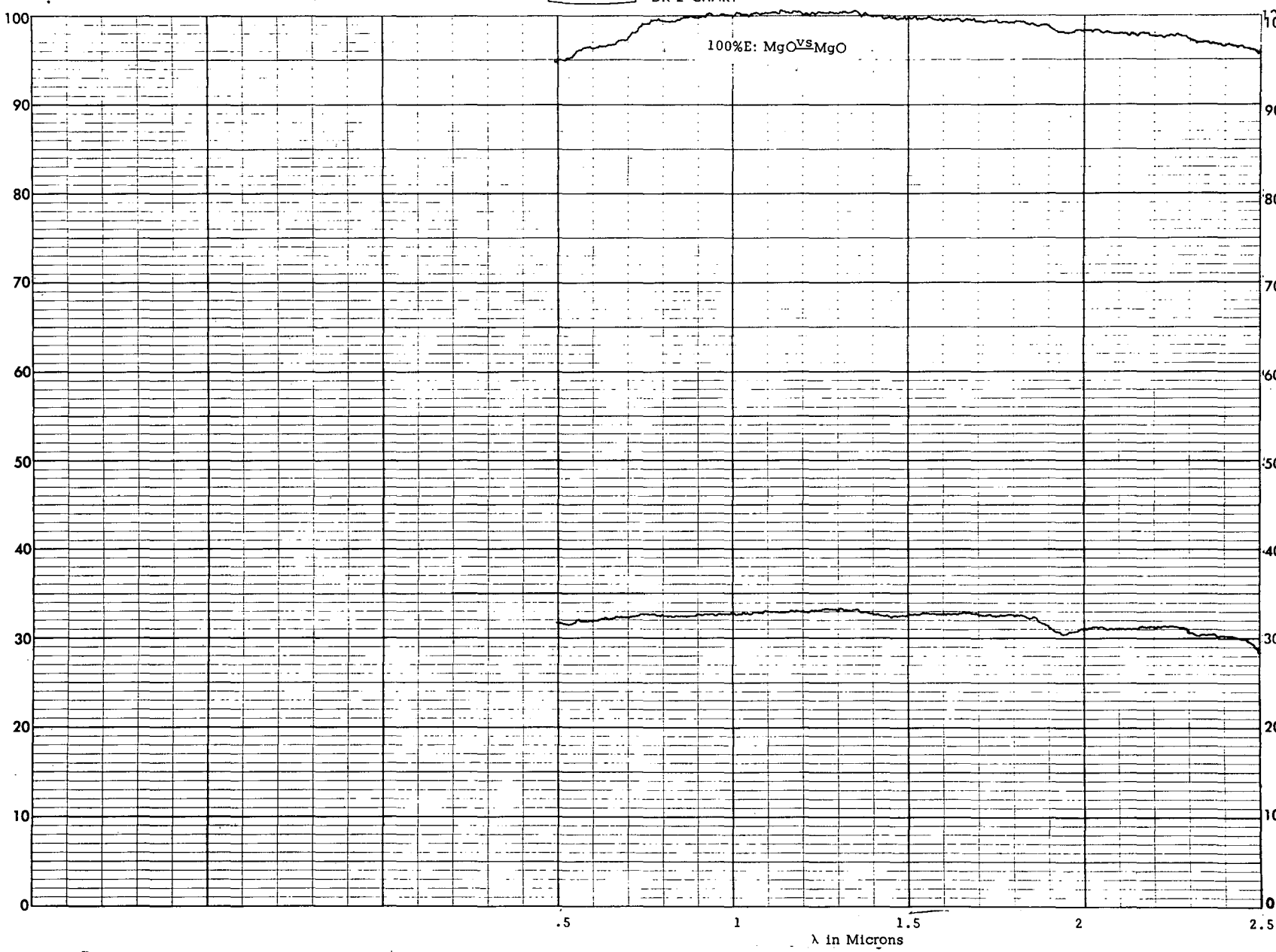

SAMPLE $Se_{0.75}Ba_{0.25}Nb_2O_6$

PATH _____ cm

ORIGIN Crystal Tech

SOLVENT _____

DK-2 Reflectance at 5° Incidence

REF MgO

λ SPEED: _____ nm/min

SCALE 0-100% R

SENS 150

PERIOD 0.25 Sec

SOURCE: W x

H_2 _____

D_2 _____

DETECTOR: PM _____

PbS x

ANALYST JB

DATE 12-16-71

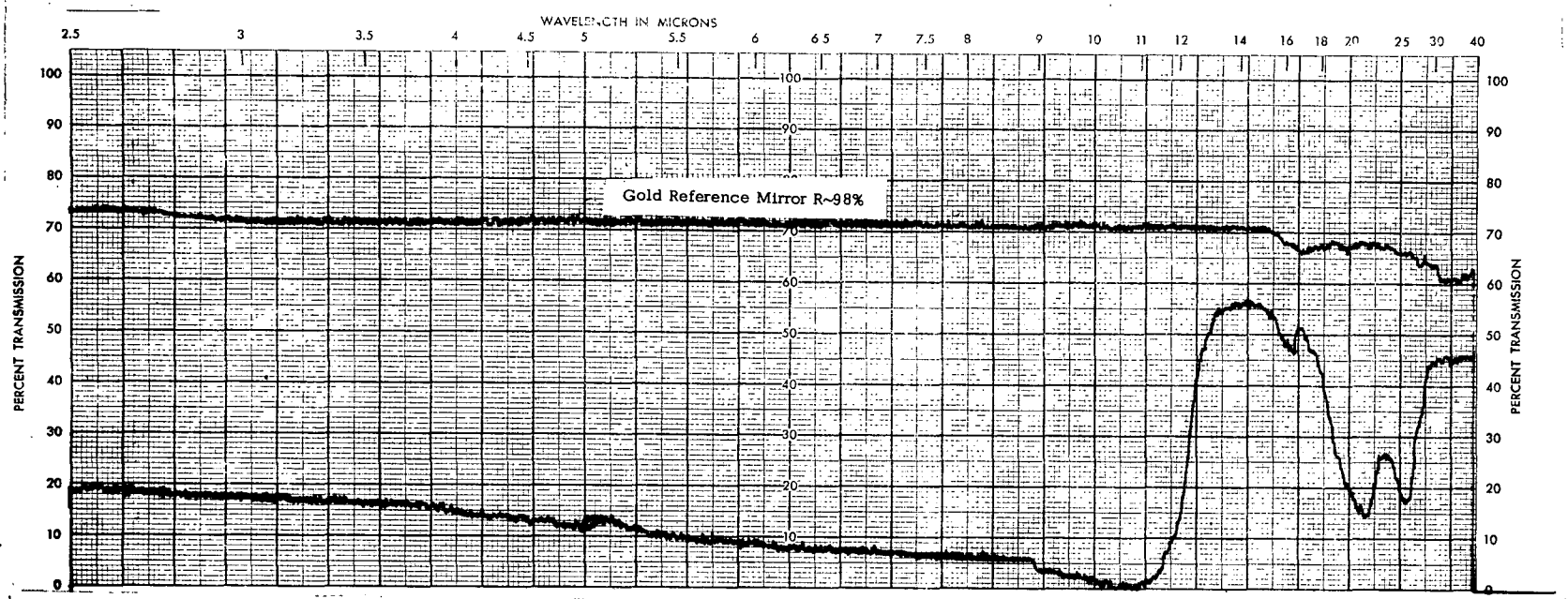

SPECTRUM NO. _____
DATE 12-16-71
SAMPLE _____
$Se_{0.75}Ba_{0.25}Nb_2O_6$
SOURCE _____
STRUCTURE
I.R.-20 Specular Reflectance at 30° Incidence
PATH ___ mm
SOLVENT _____
CONCENTRATION _____
PHASE _____
COMMENTS _____
ANALYST AWB
Beckman

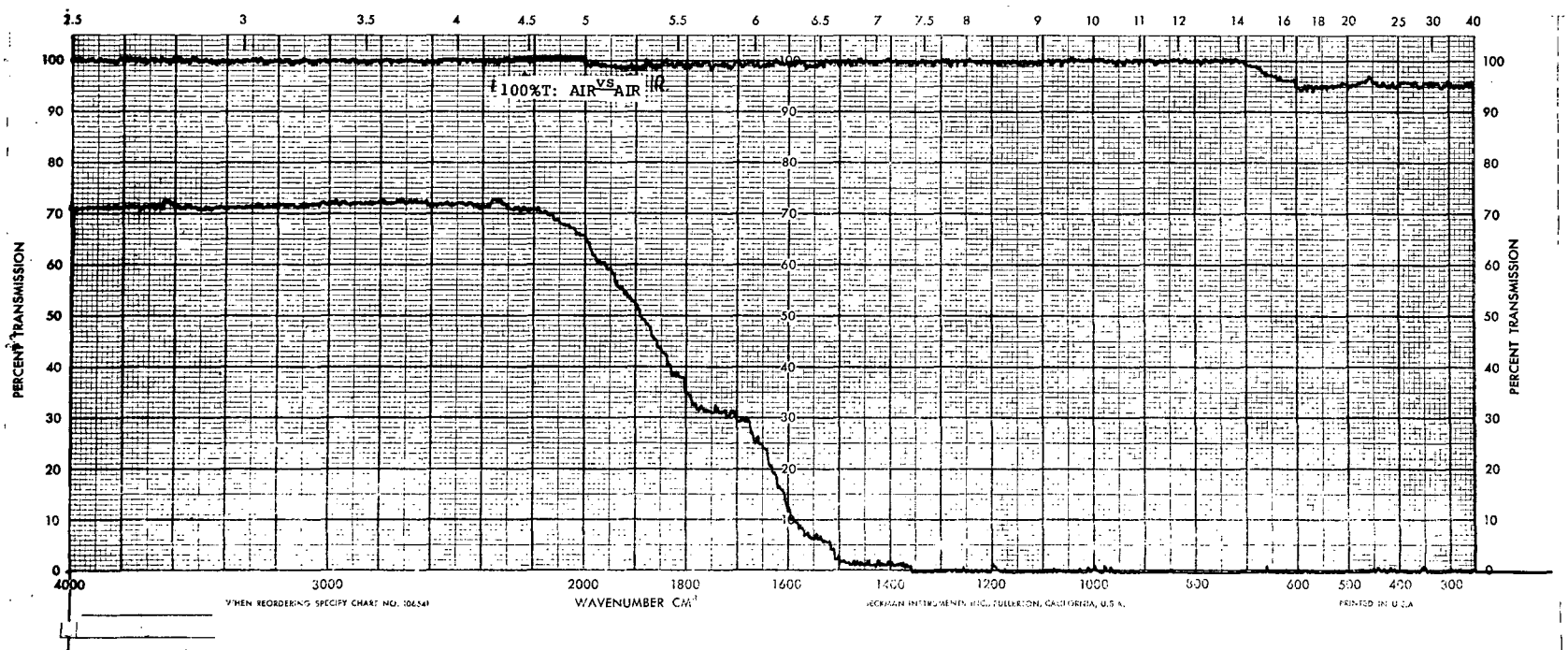

SPECTRUM NO. _____
DATE 12-16-71
SAMPLE _____
$Se_{0.75}Ba_{0.25}Nb_2O_6$
SOURCE Crystal Tech, Inc.
STRUCTURE
I.R. 20 Transmission at Normal Incidence
PATH 1.5 mm
SOLVENT _____
CONCENTRATION _____
PHASE _____
COMMENTS _____
ANALYST AWB
Beckman
INFRARED SPECTROPHOTOMETER

Printed in U.S.A. 69TW740

Beckman DK-2 CHART

566402

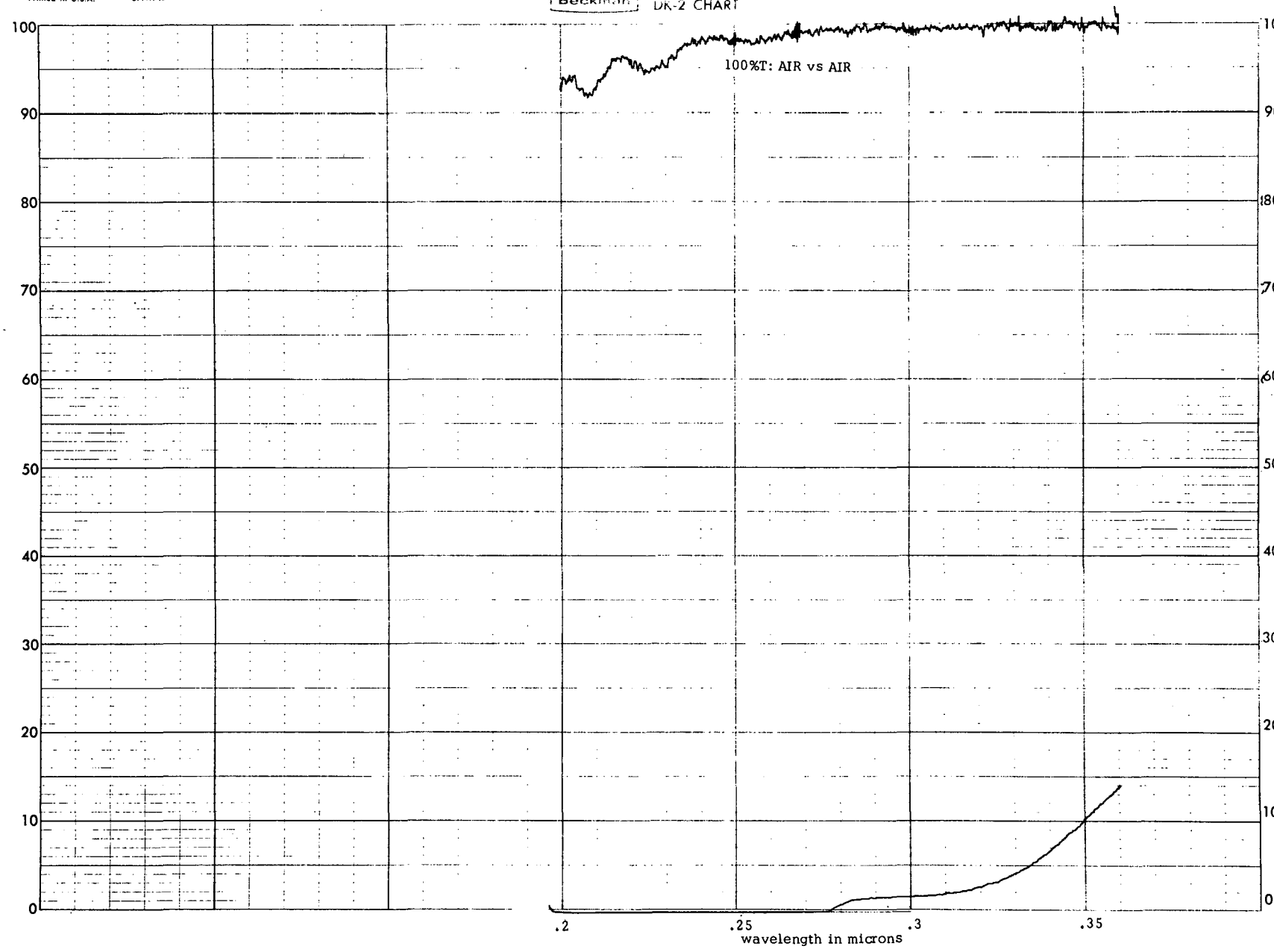

SAMPLE $Li_2O.\ Ta_2O_5$

PATH 0.1 cm

ORIGIN Crystal Tech.

SOLVENT

Transmission at Normal Incidence

REF Air

λ SPEED: 5 nm/min

SCALE 0-100 %T

SENS 100

PERIOD 0.2 Sec

SOURCE: W ✓

H_2

D_2

DETECTOR: PM

PbS ✓

ANALYST JB

DATE 12-16-71

Printed in U.S.A. 69TW740 910

Beckman DK-2 CHART

WHEN REORDERING SPECIFY CHART NO. 566402 BECKMAN INSTRUMENTS INC., FULLERTON, CALIF., U.S.A.

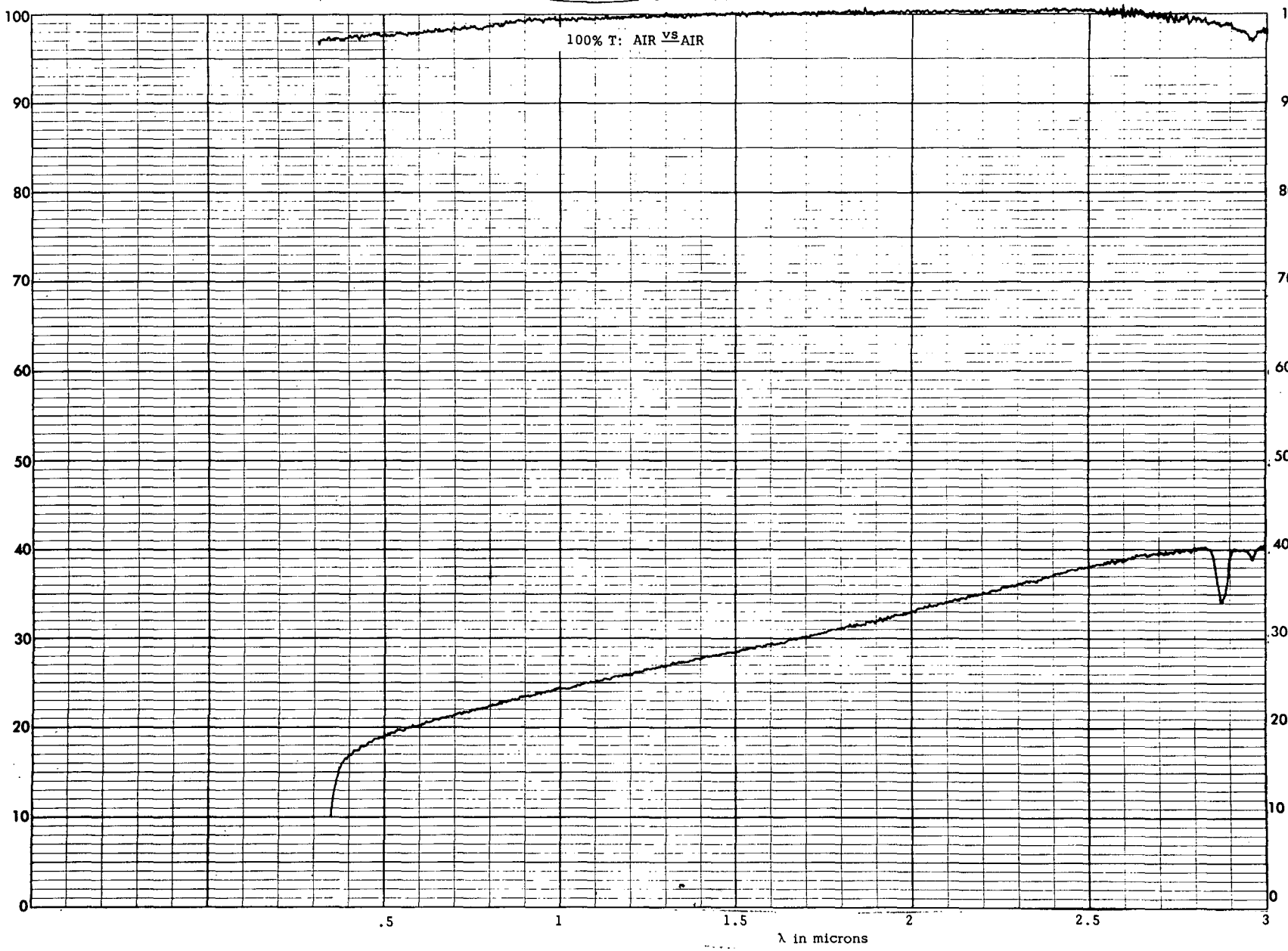

SAMPLE $Li_2O \cdot Ta_2O_5$

PATH 0.1 cm

ORIGIN Crystal Tech,

SOLVENT

Transmission at Normal Incidence

REF Air

λ SPEED: 5 nm/min

SCALE 0-100%T

SENS 100

PERIOD 0.2 Sec

SOURCE: W x

H_2

D_2

DETECTOR: PM

PbS x

ANALYST JB

DATE 12-16-71

B 20

Printed in U.S.A. 69TW740

Beckman DK-2 CHART

WHEN REORDERING SPECIFY CHART NO. 566402 BECKMAN INSTRUMENTS INC., FULLERTON, CALIF., U.S.A.

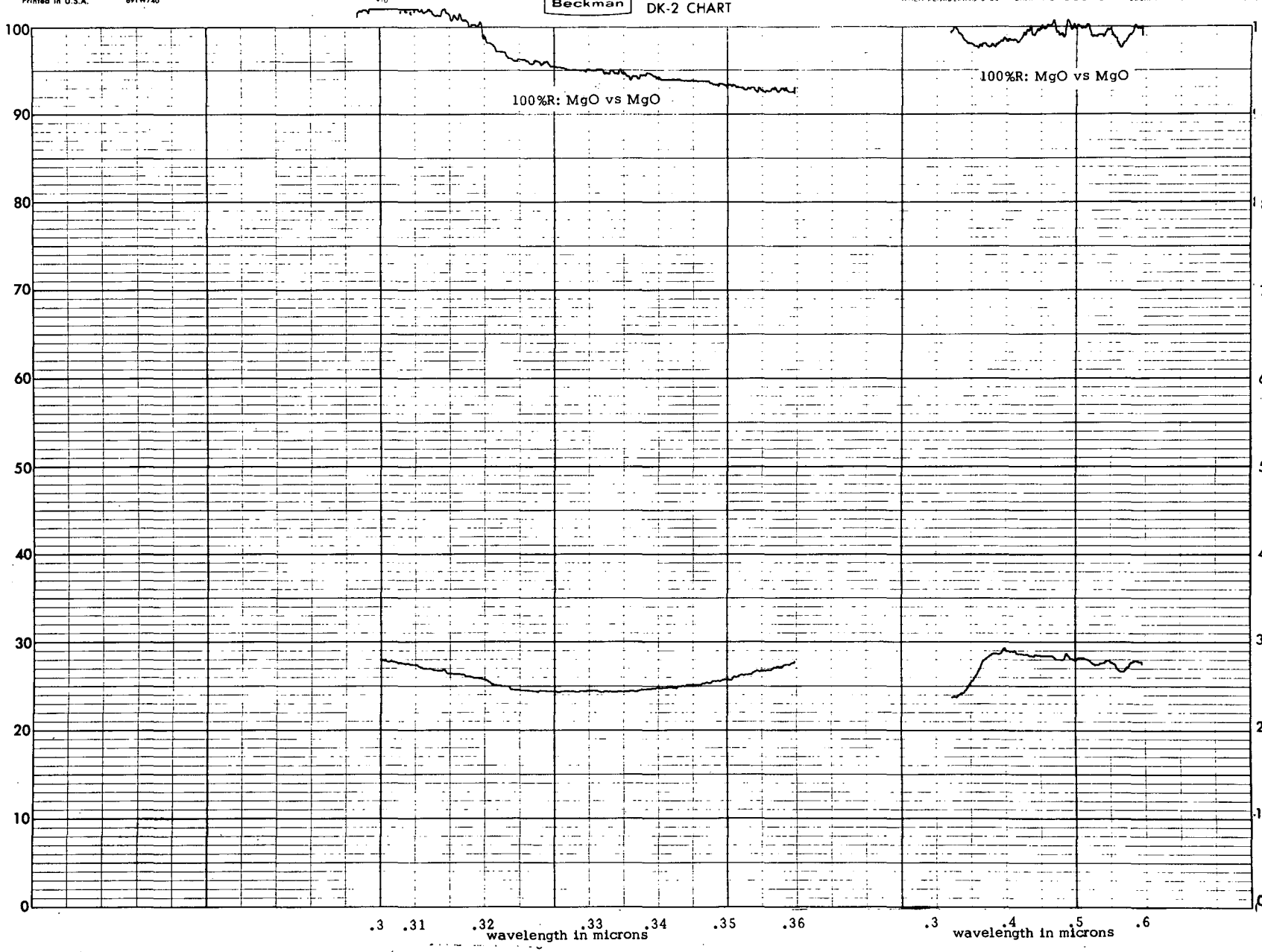

SAMPLE $Li_2O \cdot Ta_2O_5$

PATH _____ cm

ORIGIN Crystal Tech

SOLVENT _____

DK-2 Reflectance at 5° Incidence

REF MgO

SPEED: 5 nm/min

SCALE 0 - 100%R

SENS 150

PERIOD 0.2 Sec

SOURCE: W _____

H_2 _____

D_2 ✓

DETECTOR: PM ✓

PbS _____

ANALYST JB

DATE 12-16-71

B 21

Printed in U.S.A. 69TW740

Beckman DK-2 CHART 566402

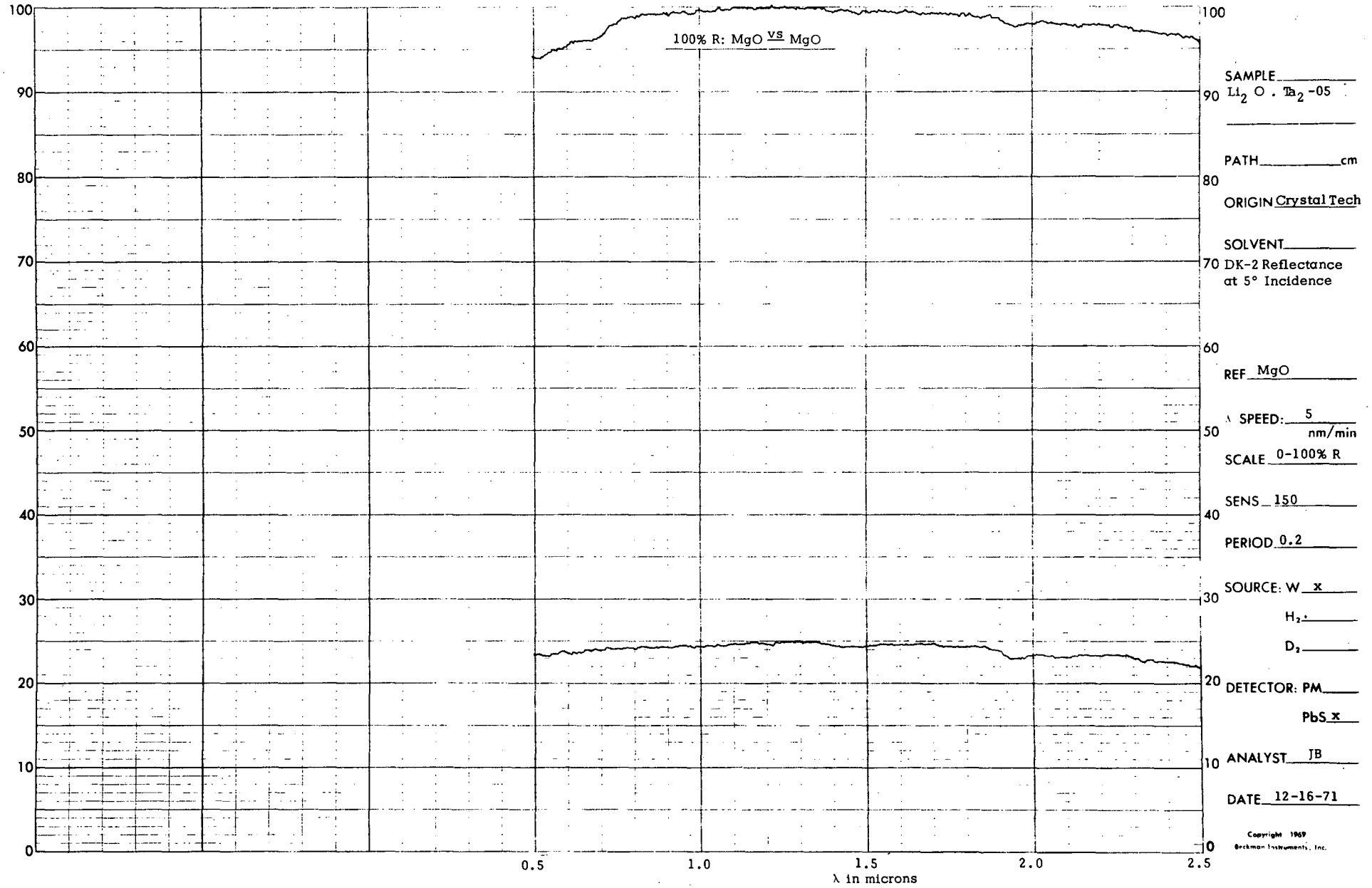

SAMPLE $Li_2O \cdot Ta_2$ -05

PATH _____ cm

ORIGIN Crystal Tech

SOLVENT _____

DK-2 Reflectance at 5° Incidence

REF MgO

λ SPEED: 5 nm/min

SCALE 0-100% R

SENS 150

PERIOD 0.2

SOURCE: W x

H_2 _____

D_2 _____

DETECTOR: PM _____

PbS x

ANALYST JB

DATE 12-16-71

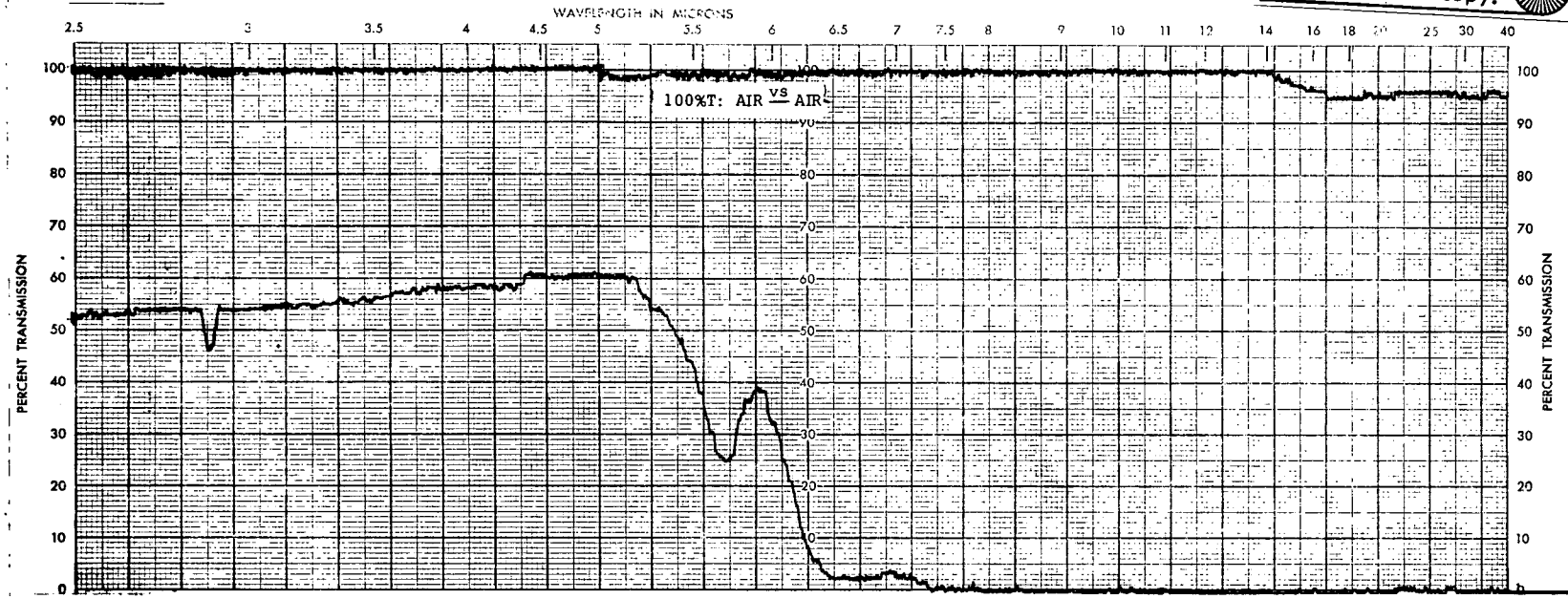

SPECTRUM NO. _____
DATE 12-16-72
SAMPLE $Li_2O \cdot Ta_2O_5$
SOURCE Crystal Tech. Inc.
STRUCTURE
I.R. -20 Transmission at Normal Incidence
PATH 1 mm
SOLVENT _____
CONCENTRATION _____
PHASE _____
COMMENTS _____
ANALYST AWB

Beckman
INFRARED
SPECTROPHOTOMETER

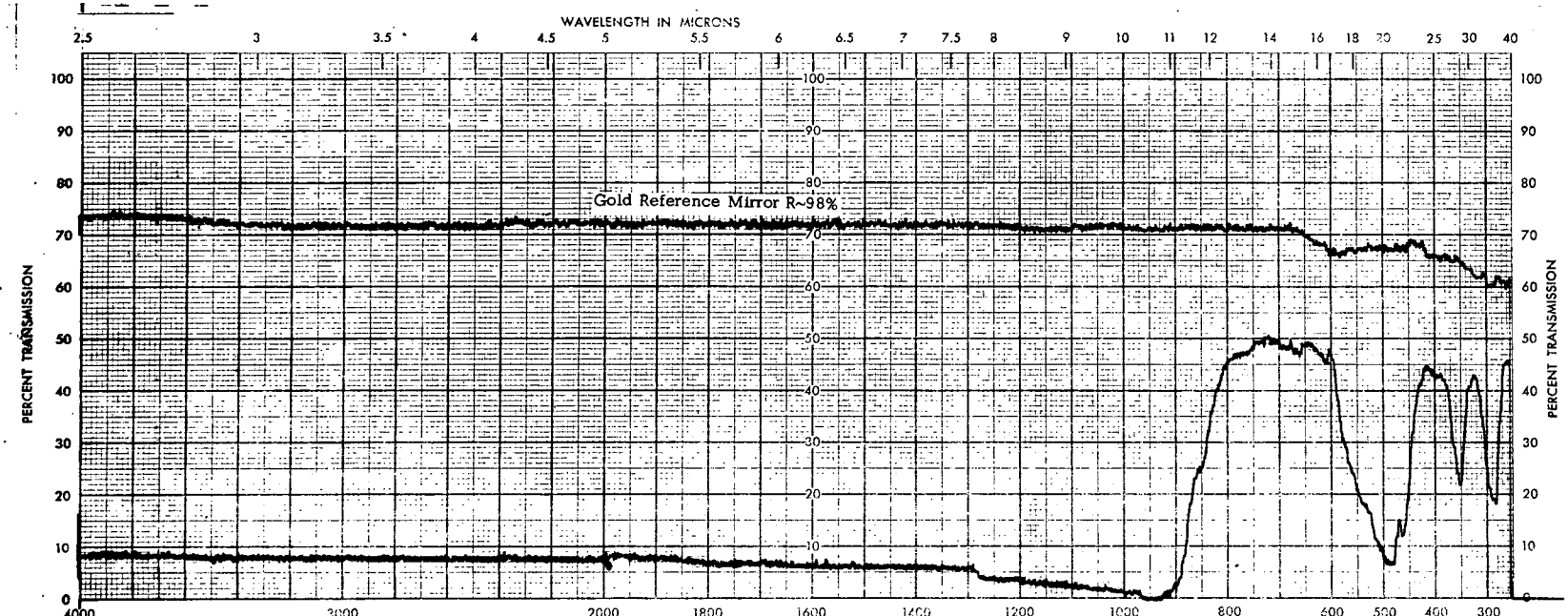

SPECTRUM NO. _____
DATE 12-16-71
SAMPLE $Li_2O \cdot Ta_2O_5$
SOURCE Crystal Tech, Inc.
STRUCTURE
I.R.-20 Specular Reference at 30° Incidence
PATH ____ mm
SOLVENT _____
CONCENTRATION _____
PHASE _____
COMMENTS _____
ANALYST AWB

Beckman
INFRARED
SPECTROPHOTOMETER

WHEN REORDERING SPECIFY CHART NO. 106541
BECKMAN INSTRUMENTS INC., FULLERTON, CALIFORNIA, U.S.A.
PRINTED IN U.S.A.

REFERENCES

(A 1) ANISTRATOV, A.T., Trans. 6th Int, Conf. Ferroelectricity, Riga, 1014 (May 1968).

(A 2) ACKERMANN, W., Ann. Physik, 46, 197 (1915)

(A 3) AZOULAY, J., GRINBERG, Y., PELAH, I., WIENER, E., J. Phys. Chem. Solids, 29, 843 (1968).

(B 1) BEERMAN, H.P., Ferroelectrics, 2, 123 (1971).

(B 2) BERGMAN, J.G., McFEE, J.H., CRANE, G.R., Appl. Phys. Letters, 18, 203 (1971)

(B 3) BŘEZINA, B., STMUTNÝ, B., Czech. J. Phys., B 18, 393 (1968).

(B 4) BEERMAN, H.P., Measurement of ϵ and ρ at Barnes Engr. Co.

(B 5) BRICE, J.C., HILL, O.F., WHIFFIN, P.A.C., WILKINSON, J.A., J. Crystal Growth, 10, 133 (1971).

(B 6) BŘEZINA, B., ŠAFRÁNKOVÁ, M., KVAPIL, J., Phys. Stat. Sol., 15, 451 (1966).

(B 7) BUSCH, G., Helv. Phys. Acta, 11, 269 (1938).

(B 8) BHIDE, V.G., HEDGE, M.S., DESHMUKH, K.G., J. Am. Ceramic Soc., 51, 565, (1968).

(C 1) Clevite Corp Data (1965).

(C 2) CUMMINS, S.E., Ferroelectrics, 1, 11 (1970).

(C 3) CHYNOWETH, A.G., J. Appl. Phys., 27, 78 (1956).

(C 4) CRANE, G.R., BERGMAN, J.G., GLASS, A.M., presented 71 st Annual meeting, Am. Ceramic Soc. (May 3-8, 1969).

(C 5) CHYNOWETH, A.G., Phys. Rev., 117, 1235 (1960).

(C 6) CHEN, F.S., GEUSIC, J.E., KURTZ, S.K., SKINNER, J.G., WEMPLE, S.H., J. Appl. Phys., 37, 388 (1966).

(C 7) CHYNOWETH, A.G., Acta Crys., 10, 511 (1957).

(C 8) CHYNOWETH A.G., U.S. Pat. 3, 005, 096, Oct. 17, 1961.

(D 1) DIMAROVA, E.N., POPLAVKO, Yu.M., Trans. 6th Int. Conf. Ferroelectricity, Riga, 332 (May 1968).

(D 2) DAVISSON, J.W., Acta Cryst., 9, 9 (1956).

(D 3) DeQUERVAIN, M., Helv. Phys. Acta, 17, 509 (1944).

(F 1) FOUSKOVA, A., J. Phys. Soc. Japan, 27, 1699 (1969).

(F 2) FATUZZO, E., HARBECKE, G., MERZ, W.J., NITSCHE, R., ROETSCH, H., RUPPEL, W., Phys. Rev., 127, 2036 (1962).

(F 3) FURUKAWA T., VEMETSU Y., ASAKAWA K., WADA Y., J. Appl. Polymer Sci., 12, 2675, (1968).

(G 1) GLASS, A.M., Phys. Rev., 172, 564 (1968).

(G 2) GLASS, A.M., ABRAMS, R.L., J. Appl. Phys., 41, 4455 (1970).

(G 3) GLASS, A.M., J. Appl. Phys., 40, 4699 (1969).

(G 4) GLASS, A.M., Appl. Phys. Letters, 13, 147 (1968).

(G 5) GLASS, A.M., McFEE, J.H., BERGMAN, J.G., J. Appl. Phys.- to be published.

(G 6) GLASS, A.M., Private Communication of Value ρ.

(G 7) GAVRILOVA, N.D., NOVIK, V.K., KOPTSIK, V.A., Sov. Phys.- Cryst., 13, 949 (1969).

(G 8) GULTON INDUSTRIES, INC., (Metuchen, N.J.) - Glennite Piezoceramics data.

(G 9) GOLDSMITH, G.J., WHITE, J.G., J. Chem. Phys., 31, 1175 (1959).

(H 1) HADNI, A., Optics Comm., 1, 251 (1969).

(H 2) HOSHINO, S., MITSUI, T., JONA, F., PEPINSKY, R., Phys, Rev. 107, 1255 (1957).

(H 3) HILCZER, B., Trans. 6th Int. Conf. Ferroelectricity, (Riga 1968), 1023.

(H 4) HOLDEN, A.N., MERZ, W.J., REMEIKA, J.P., MATHIAS, B.T., Phys. Rev., 101, 962 (1956).

(H 5) HAERTLING G.H., LAND, C.E., J. Am. Ceramic Soc., 54, 1, (1971).

(I 1) IWASAKI, H., UCHIDA, N., YAMADA, T., Japan. J. Appl. Phys. 6, 1336 (1967).

(I 2) IWASAKI, H., SUGII, K., YAMADA, T., NIIZEKI, N., Appl. Phys. Letters, 18, 444 (1971).

(I 3) IWASAKI, H., J. Radio Research Lab., Japan, 17, 147 (1970).

(I 4) ITOH, K., MITSUI, T., J. Phys. Soc. Japan, 23, 334 (1967).

(K 1) KUMATA, A., YUMOTO, H., ASHIDA, S., J. Phys. Soc. Japan, 28, 351 (1970 Supplement).

(K 2) KREMENCHUGSKII, L.S., SAMOILOV, V.B., Sov. Phys.-Cryst., 12, 940 (1968).

(K 3) KAMYSHEVA, L.N., et al., Acad. Sci., USSR, Bull. Phys. Ser. 31, 1202 (1967).

(K 4) KEVE, E.T., ABRAHAMS, S.C., BERNSTEIN, J.L., J. Chem. Phys., 54, 2556, (1971).

(L 1) LANG, S.B., NBS Report #9289, (7-28-1967).

(L 2) LACHAMBRE, J.L., Rev. Sci. Inst., 42, 74 (1971).

(L 3) LANG, S., Phys. Rev. B., 4, 3603, (1971).

(L 4) LIU, S.T., HEAPS, J.D., TUFTE, O.N., Paper G-2 IEEE Symp. Application of Ferroelectricity, I.B.M. Yorktown Height, N.Y., (June 7-8, 1971).

(L 5) LOCK, P.J., Appl. Phys. Letters, 19, 390, (1971).

(M 1) MATTHIAS, B.T., Science 113, 591 (1951).

(M 2) MÖLLER, K., FARLEIGH DICKINSON U., private communication.

(M 3) MÁLEK, Z., ŠTRAJBLOVÁ, J., NOVOTNÝ, J., MAREČEK, V., Czech. J. Phys. B 18, 1226 (1968).

(M 4) MILEK, J.T., WELLES, S.J., Linear Electrooptics Modulator Materials., Air Force Materials Lab, Air Force Systems Command Contract F33615-68C-1225 to Hughes Aircraft Co., S-14, 143 (Jan. 1970).

(N 1) NASSAU, K., LEVINSTEIN, H.J., LOIACONO, G.M., J. Phys. Chem. Solids, 27, 989 (1966).

(N 2) NAKAMURA, K., WADA, Y., J. Polymer Sc; part A-2, 9, 161 (1971).

(N 3) NOVIK, V.K., Sov. Phys.-Cryst., 10, 89 (1965).

(P 1) PUTLEY, E.H., Proc. Symp. Submillimeter Waves, (N.Y. 1970), 267.

(P 2) PUTLEY, E.H., "Pyroelectric Detectors and their Application in Thermal Imaging Systems", R.R.E. Malvern, Worcs, U.K. - to be published.

(P 3) PEPINSKY, R., VEDAM, K., HOSHINO, S., OKAYA, Y., Phys. Rev. 111, 430 (1958).

(P 4) PHELAN, R.J., MAHLER, R.J., COOK, A.R., Appl. Phys. Letters, 19, 337, (1971).

(R 1) RABINOVICH, A.Z., ROITBERG, M.B., Sov. Phys.-Cryst., 15, 1023 (May-June 1971).

(S 1) SAVAGE,A., J. Appl. Phys., 37, 3071 (1966).

(S 2) SAWADA, S., NOMURA, S., FUGII, S., YOSHIDA, I., Phys. Rev. Letters, 1, 320 (1958).

(S 3) SANDERS ASSOC.-private communications.

(S 4) STRUKOV, B.A., Proc. Int. Meeting Ferroelectricity, Prague, 1, 191 (1966).

(S 5) SILVESTROVA, I.M., Sov. Phys.-Cryst., 6, 466 (1962).

(S 6) STRUKOV, B.A., Sov. Phys.-Sol. State, 6, 2278 (1965).

(S 7) STRUKOV, B.A., TARASKIN, S.A., KOPTSIK, V.A., VARIKASH, V.M., Sov. Phys.-Cryst., 13, 447 (1968).

(S 8) STRUKOV, B.A.,TARASKIN, S.A., VARIKASH, V.M., Sov. Phys.-Solid State, 10, 1445 (1968).

(S 9) SIL'VESTROVA, I.M., ROMANYUK, N.A., Sov. Phys.-Cryst., 5, 138 (1960).

(S 10) STEPHENSON, C.C., HOOLEY, J.G., J. Am. Chem. Soc., 66, 1397 (1944).

(S 11) SINGH, S., REMEIKA, J.P., POTOPOWITZ, J.R., Appl. Phys. Letters, 20, 135, (1972).

(S 12) SEKIDO, T., MITSUI, T., J. Phys. Chem. Solids, 28, 967, (1967).

(S 13) SHIRANE, A., HOSHINO, S., SUZUKI, K., Phys. Rev. 80, 1105, (1950).

(S 14) SMOLENSKII, G.A., DOKLADY, A.K., Nauk SSSR, 70, 405, (1950).

(T 1) TRIEBWASSER, S., Phys. Rev., 114, 63 (1959).

(U 1) ULLMAN, F.G., GANGULY, B.N., ZEIDLER, J.R., Conf. Electronics Materials Comm. of AIME, S. Francisco (August 29-Sept 1, 1971). To be published J. Electronics Mat.

(U 2) ULLMAN, F.G., GANGULY, B.N., HARDY, J.R., Ferroelectrics, 2, (1971) in press.

(U 3) UEDA, S., TATSUZAKI, I., SHINDO, Y., Phys. Rev. Letters, 18, 453 (1967).

(W 1) WIEDER, H.H., PARKERSON, C.R., J. Phys. Chem. Solids, 27, 247 (1966).

(W 2) WILLARDSON, R.K., BEER, A.C., Ed., Semiconductors and Semimetals, 5, Academic Press, (N.Y. & London 1970), 260.

(W 3) WIEDER, H.H., J. Appl. Phys., 30, 1010 (1959).

(W 4) WIEDER, H.H., CLAWSON, A.R., PARKERSON, C.R., J. Appl. Phys., 33, 1720 (1962).

(W 5) WIEDER, H.H., CLAWSON, A.R., PARKERSON, C.R., U.S. Patent #3,337,293.

(W 6) WIEDER, H.H., PARKERSON, C.R., J. Phys. Chem. Solids, 25, 241 (1964).

(Y 1) YAMADA, T., NIIZEKI, N., TOYODA, H., Japan, J. Appl. Phys., 7, 298 (1968).

(Y 2) YURIN, V.A., SILVESTROVA, I.M., ZHELUDEV, I.S., Sov. Phys.-Cryst., 7, 312 (1962)

(Y 3) YURIN, V.A., ZHELUDEV, I.S., Bull. Aca. Science USSR, 28, 633 (1964).

(Y 4) YAMAKA, E., HAYASHI, T., MATSUMOTO, M., Infrared Phys., 11, 347 (1971).

(Z 1) ZHELUDEV, I.S., Zh. Ludupov Ts., Ak. Nauk SSSR, Bull. Phys. Ser. 31, 1207 (1967).

DISTRIBUTION LIST

No. of Copies	Addressee	Code
1	Systems Reliability Directorate	300
1	T & DS Directorate	500
1	Patent Counsel	204
1	Documentation Branch	256
1	GSFC Library	252
1	Contracting Officer	245
1	Space Sciences Directorate	600
3	Technical Officer	652